Hashemite Kingdom of Jordan

Scientific Research Support Fund

Hashemite University

Jordan Journal of Earth and Environmental Sciences

JJEES

An International Peer-Reviewed Scientific Journal

Financed by the Scientific Research Support Fund

http://jjees.hu.edu.jo/

Volume (8) Number (1) ISSN 1995-6681 September 2017 / Dhu al-Hijjah 1438

Jordan Journal of Earth and Environmental Sciences (JJEES)

JJEES is an International Peer-Reviewed Research Journal, Issued by Deanship of Scientific Research, The Hashemite University, in corporation with, the Jordanian Scientific Research Support Fund, the Ministry of Higher Education and Scientific Research.

Editorial Board:

Editor –in-Chief:

- **Professor Issa Makhlouf**
  (The Hashemite University, Jordan)

Assistant Editor:

- **Professor. Nezar Hammouri**
  (The Hashemite University, Jordan)

Editorial Board:

- **Professor Najib Abu Karaki**
  University of Jordan
- **Professor Nizar Abu-Jaber**
  German-Jordan University
- **Professor Mohammad Atallah**
  Yarmouk University
- **Professor Anwar Jiries**
  Mu'tah University
- **Professor Atef Al-Kharabsheh**
  Al Balqa Applied University
- **Professor Khaled Al Tarawneh**
  Al-Hussein Bin Talal University
- **Professor Fayez Ahmad**
  The Hashemite University
- **Professor Abdullah Al-Diabat**
  Al al-Bayt University

The International Advisory Board:

- **Prof. Sayed Abdul Rahman,**
  Cairo University, Egypt
- **Prof. Abdullah Al-Amri,**
  King Saud University, Saudi Arabia
- **Prof. Waleed Al-Zubair,**
  Arabian Gulf University, Bahrain
- **Prof. Ute Austermann-Haun,**
  Fachhochschule und Lipp, Germany
- **Prof. Ibrahim Banat,**
  University of Ulster, UK
- **Prof. Matthias Barjenbruch,**
  Technisch Universitat Berlin, Germany
- **Prof. Mohamed Boukhary,**
  Ain Shams University, Egypt
- **Prof. Mohammad El-Sharkawy,**
  Cairo University, Egypt
- **Prof. Venugopalan Ittekkot,**
  Center for Tropical Marine Ecology, Bremn, Germany
- **Prof. Christopher Kendall,**
  University of North Carolina, U.S.A.
- **Prof. Elias Salameh,**
  University of Jordan, Jordan.
- **Prof. V. Subramanian,**
  Jawaharlal Nehru University, India.
- **Prof. Omar Rimawy,**
  University of Jordan, Jordan.
- **Prof. Hakam Mustafa,**
  Yarmouk University, Jordan.
- **Dr. Michael Crosby,**
  The National Science Board, National Science Foundation, Virginia, U.S.A.
- **Dr. Brian Turner,**
  Durham University, U.K..
- **Dr. Friedhelm Krupp,**
  Senckenberg Research Institute and Natural History Museum, Germany.
- **Dr. Richard Lim,**
  University of Technology, Australia.

Editorial Board Support Team:

Language Editor

- **Dr. Qusai Al-Debyan**

Publishing Layout

- **Obada Al-Smadi**

Submission address:

Manuscripts should be submitted electronically to the following e-mail:

jjees@hu.edu.jo

For more information and previous issues:

www.jjees.hu.edu.jo

Hashemite Kingdom of Jordan

Scientific Research Support Fund

Hashemite University

Jordan Journal of Earth and Environmental Sciences

JJEES

An International Peer-Reviewed Scientific Journal

Financed by the Scientific Research Support Fund

Volume 8 Number (1)

http:// jjees.hu.edu.jo/

ISSN 1995-6681

المجلة الأردنية لعلوم الأرض والبيئة
Jordan Journal of Earth and Environmental Sciences (JJEES)
http://jjees.hu.edu.jo

Hashemite University

Deanship of Scientific Research

TRANSFER OF COPYRIGHT AGREEMENT

Journal publishers and authors share a common interest in the protection of copyright: authors principally because they want their creative works to be protected from plagiarism and other unlawful uses, publishers because they need to protect their work and investment in the production, marketing and distribution of the published version of the article. In order to do so effectively, publishers request a formal written transfer of copyright from the author(s) for each article published. Publishers and authors are also concerned that the integrity of the official record of publication of an article (once refereed and published) be maintained, and in order to protect that reference value and validation process, we ask that authors recognize that distribution (including through the Internet/WWW or other on-line means) of the authoritative version of the article as published is best administered by the Publisher.

To avoid any delay in the publication of your article, please read the terms of this agreement, sign in the space provided and return the complete form to us at the address below as quickly as possible.

Article entitled:----------

Corresponding author: ----------

To be published in the journal: Jordan Journal of Earth & Environmental Sciences (JJEES)

I hereby assign to the Hashemite University the copyright in the manuscript identified above and any supplemental tables, illustrations or other information submitted therewith (the "article") in all forms and media (whether now known or hereafter developed), throughout the world, in all languages, for the full term of copyright and all extensions and renewals thereof, effective when and if the article is accepted for publication. This transfer includes the right to adapt the presentation of the article for use in conjunction with computer systems and programs, including reproduction or publication in machine-readable form and incorporation in electronic retrieval systems.
Authors retain or are hereby granted (without the need to obtain further permission) rights to use the article for traditional scholarship communications, for teaching, and for distribution within their institution.

☐ **I am the sole author of the manuscript**

☐ **I am signing on behalf of all co-authors of the manuscript**

☐ **The article is a 'work made for hire' and I am signing as an authorized representative of the employing company/institution**

Please mark one or more of the above boxes (as appropriate) and then sign and date the document in black ink.

Signed:_____ **Name printed:** _____

Title and Company (if employer representative) : _____

Date: _____

Data Protection: By submitting this form you are consenting that the personal information provided herein may be used by the Hashemite University and its affiliated institutions worldwide to contact you concerning the publishing of your article.

Please return the completed and signed original of this form by mail or fax, or a scanned copy of the signed original by e-mail, retaining a copy for your files, to:

Deanship of Scientific Research
The Hashemite University P.O. Box 150458, P.C.13115, Zarqa, Jordan
Tel.: 00962 53903333/ Ext. 4235
Fax: 00962 53826823
E-mail: jjees@hu.edu.jo

Subscription

Jordan Journal of Earth & Environmental Sciences (ISSN 1995-6681)
An International Peer- Reviewed Research Journal
Published by the Deanship of Scientific Research - The Hashemite University

Name:	الاســـــــــــم:
Specialty:.....	التخصـــــــــص:
Address:.....	العنـــــــــوان:
P.O. Box:.....	صنـــدوق البريـــــد:
City & Postal Code:	المدينة: الرمز البريدي:
Country:.....	الـــــــــــدولة:
Phone:.....	رقـــم الهاتـــــف:
Fax No:.....	رقـــم الفاكـــــس:
E-mail:.....	البريـــد الإلكترونـــي:
Method of payment:	طريقـــــة الدفـــع:
Amount Enclosed:.....	المبلـــغ المرفـــق:
Signature:.....	التوقيـــــــــع:

Cheques should be paid to Deanship of Research - The Hashemite University

I would like to subscribe to the Journal:

For

- ☐ One year
- ☐ Two years
- ☐ Three years

One year Subscription Rates		
	Inside Jordan	Outside Jordan
Individuals	10JD	70$
Students	5JD	35$
Institutions	20JD	90$

Correspondence

Subscriptions and sales:

Professor Issa Makhlouf
Deanship of Scientific Research
The Hashemite University P.O. Box 150458, P.C.13115, Zarqa, Jordan
Tel.: 00962 53903333/ Ext. 4235
Fax: 00962 53826823
E-mail: jjees@hu.edu.jo

JJEES
Jordan Journal of Earth and Environmental Sciences

JJEES

Volume 8, (Number 1), Sept, 2017
ISSN 1995-6681
Pages 1 - 10

Jordan Journal of Earth and Environmental Sciences

Air Pollution Impact of Medical Waste Incineration in Semi-Arid Areas

Walaa I. Matalqah[1], Bashar M. Al Smadi[2] and Kamel K. Al-Zboon[3]*

[1] Civil Engineering Department, The University of Jordan Amman, Jordan
[2] Associate Professors, Water and Environmental Engineering, Civil Engineering Department, The University of Jordan, Amman, Jordan
[3] Environmental Engineering Department, Al-Huson University College, Al-Balqa Applied University, Irbid, Jordan

Received 10 November, 2016; Accepted 24 August, 2017

Abstract

Breeze AERMOD software is used to predict the impacts of medical waste incineration on ambient air quality in a semi-arid region of Jordan. The air quality impact is evaluated based on the predicted concentrations of sulfur dioxide, nitrogen dioxide, and carbon monoxide. Procured results reveal that the maximum average predicted concentrations of the three oxides are below their corresponding national and international standards and are expected to occur at a short distance of about 200m downwind from the incinerator main stack. The screening option in the model is used to calculate the hourly concentration at worst conditions for each month. Most of the maximum concentrations occur at nighttime hours (18:00 and 00:00 GMT), where stable conditions dominate the tropospheric boundary layer. The adequacy of AERMOD is also evaluated by comparing the predicted concentrations against measured values of the three criteria oxides. The findings demonstrated great deal of agreement between predicted and measured concentrations of nitrogen dioxide (R^2= 0.94), and carbon monoxide (R^2 = 0.98). However, predicted sulfur dioxide showed a lower correlation with the measured data (R^2 = 0.49).

© 2017 Jordan Journal of Earth and Environmental Sciences. All rights reserved

Keywords: Air pollution, Dispersion, Incineration, Medical Waste, AERMOD, Modeling.

1. Introduction

Medical Waste (MW) is one of the most sensitive issues relating to the environment, so the threat extends to be one of the most serious sources of environmental pollution to the citizens surrounding the incinerators (Cole and Mickey, 2011).

Ministry of Health (MoH) is the government agency responsible of MW disposal and has regulations issued in 2011 deals with the management of MW. The regulations define the MW as all the waste, solid, liquid and gaseous wastes resulting from health care establishments, medical laboratories, medical research centers, pharmaceutical factories, human and veterinary medicines, veterinary clinics and institutions home nursing (MoH, 2014).

MW in Jordan has a witnessed rapid development as a result of rapid growth of population and the migration from neighboring countries. Populations were 5.6 million in 2006 and increased to 9.5 million in 2015 with 6.9 % average growth rate (DoS, 2015).

The number of hospitals increased from 101 hospitals with 11,049 total numbers of beds and an average occupancy rate of 60.9 % in 2006 to 104 with total number of beds of 12407 and an average occupancy rate of 50.3 % in 2014. In addition to that, the number of Health Care Centers (HCCs) was 671 in 2006 and has increased to 677 in 2014 (MoH, 2012). In Jordan, hazardous waste divided to industrial hazardous waste with 25,600 tons in 2002, and estimated to increase to 52,780 tons by 2015; and medical hazardous waste with the amount of 3,470 tons in 2002, and estimated in 2015 to 5,100 tons [METAP, 2005].

Incineration has been the most widely used treatment technology for MW disposal. The primary purposes for Medical Waste Incineration (MWI) are to transform the waste into non-hazardous residues and to reduce the volume (about 90 %) and mass (about 70 %) of the waste. These objectives are achieved by burning the waste at high temperatures over a sufficiently long period of time to sanitize infectious and contagious pathogenesis and burn the combustible portion of the waste (El-Hamouz, 2002; USEPA, 1993).

From environmental perspectives, incineration is not considered a clean process because toxic air pollutants emanated from incinerators unless properly operated and managed, because medical waste typically contains a variety of plastic materials, such as Polyvinyl Chloride (PVC) (Jang et al., 2006).

The present paper aims to investigate air emissions from the MW incinerators at the campus of Jordan University of Science and Technology (JUST) and to assess their impact on local air quality by applying BREEZE AERMOD Pro Plus version 7.0 for air dispersion modeling.

* Corresponding author. e-mail: kalzboon@yahoo.com

2. Methods and Materials

2.1. Study Area

JUST incinerator is located within JUST campus at Latitude 34.48 N and Longitude of 35.89 E. The incinerator is located on a rural flat land with an elevation of approximately 590 meters above mean sea level. It is located about 20 km to the east of Irbid city. JUST incinerator is surrounded by agricultural areas in east, south and west directions. The west side is near the main road and JUST buildings are located in the north of incinerator.

A Hoval pyrolysis incinerator is used to incinerate MW generated from various Health Care Establishments (HCEs), including King Abdullah University Hospital (KAUH), 13 hospitals of the MoH and 8 private hospitals in northern governorates and other hospitals and centers in Amman and Zarqa. The incinerator was established in 1983 and occupies an area of 900 m^2 with a capacity of 2800 kg/hr. The temperature of combustion is sustained in the range of 800-900 °C with a residence time of the waste at least one hour. The hot gases released from the combustion process are flowing up into the secondary chamber in which further combustion of these gases occur at a temperature in the range of 1100-1200 °C with a minimum residence time of two seconds and 100 % excess air.

2.2. Description of Dispersion Model

The dispersion model used in the present study was BREEZE AERMOD Pro plus Version 7.0, developed by the Trinity Consultants.

AERMOD model is a steady-state plume model, calculates the spread of a plume from planetary boundary layer structure and scaling concepts, including treatment of both surface and elevated sources and both simple and complex terrain (USEPA, 2004). It assumes that the concentrations at all distances during modeled hour are governed by the set of hourly meteorological inputs.

AERMOD is a recommended model by USEPA and it is an updated version of the Industrial Source Complex Short Term (ISCST) model. This model is used to estimate the dispersion from industrial source points, flares, lines, areas, or volumes. AERMOD generates daily, monthly and annually concentrations in the ambient air and unlimited number of point sources, source groups, receptors, and short- and long-term averages can be modeled.

In general, AERMOD modeling system consists of the dispersion model (AERMOD) and two pre-processors (AERMET and AERMAP). AERMET is a meteorological preprocessor which can accept a range of inputs including surface characteristics in the form of Albedo, surface roughness, Bowen Ratio, and standard meteorological data; wind speed and direction, temperature and cloud cover (USEPA, 2004). AERMET then calculates the planetary boundary layer parameters including friction velocity, Monin-Obukhov length, convective velocity scale, temperature scale, mixing height, and surface heat flux. These parameters are used to calculate vertical profiles for wind speed, lateral and vertical turbulent fluctuations, potential temperature gradient and potential temperature.

During the present study, AERMOD was run using hourly surface data from the nearest station; Ar Ramtha station and the upper air data from the only station in the Jordan; Al Mafraq station.

AERMAP is a terrain preprocessor that calculates terrain and critical hill height values for each receptor for input into AERMOD. During the study, AERMAP was not used because the area is flat.

2.3. Meteorological Data

Meteorological data include hourly surface data and upper air data for the year 2010. Hourly surface data were obtained for Ar Ramtha station in the SCRAM format and upper air data for Al Mafraq station were used. Upper air data include pressure; height; temperature; dew point; wind speed; and wind direction in FSL format and can be downloaded from National Oceanic and Atmospheric Administration (NOAA) website http://www.esrl.noaa.gov/raobs/.

Wind rose (Figure 1) showed that the prevailing winds blow from the northwest much of the time and comprise about 38 % of all hourly wind directions. The frequency distribution of wind speeds of 5.7 – 8.8 m/s, 3.6 – 5.7 m/s and calms wind equal to 18.6 %, 20.2 % and 40.6 %, respectively. Wind speeds up to and including 0.514 m/s (1 knot) are considered to be calm (USEPA, 2012).

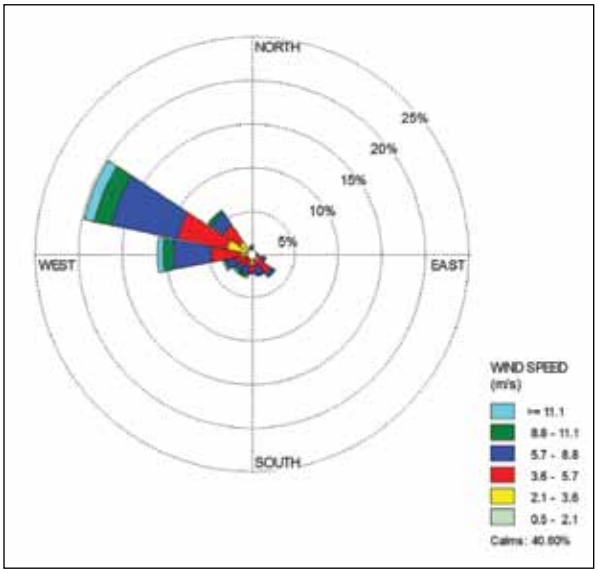

Figure 1. Wind rose for meteorological data of year 2010.

2.4. Emission Data

Real-time stack emissions measurements from the incinerators were conducted for 2-weeks. The capacity, technology and other specifications of the incinerators are shown in Table 1.

Table 1. Description of Medical Waste Incinerators

Capacity (Kg/hr)	Technology	Fuel	No. of Stacks per Incinerator	Stack Height (m)	Stack Diameter (m)
2800	Hoval Pyrolysis	Diesel	1	7	0.54

The stack emissions were measured for the following pollutants; Carbon Monoxide, Nitrogen Oxides, and Sulfur Dioxide. The sampling and analysis of flue gases from the stacks of incinerators were conducted using an electrochemical cells analyzer and this method is approved in the Jordanian Standard JS1189/2006.

The measurement of gaseous pollutants was carried out using a MRU VARIO plus Industrial stack gas analyzer which compiles with US EPA CTM methods 030 and 034. The MRU analyzer is equipped with electrochemical and NDIR sensors. The measurement range of the gas sensors were carbon Monoxide, 0 – 4,000 ppm; Nitrogen Oxide, 0 – 5,000 ppm; Nitrogen Dioxide, 0 – 1,000 ppm; and Sulfur Dioxide, 0 – 5,000 ppm. The pollutants measured in the present study were SO_2, NO_2, and CO and the emissions were compared with the Jordanian standard JS 1189/2006 of air pollutants emitted from the stationary source.

The pollutants concentrations and stacks data obtained from each incinerator over a 2-weeks period were statistically averaged and are presented in Table 2.

Table 2. Stack Emissions Data of MW Incinerators

#	Parameter	Stack 1	Stack 2
1	Average flue gas temperature (°C)	750.95	823.45
2	Flue gas velocity (m/s)	4.6	4.6
3	Volumetric flow rate of flue gas (m^3/s)	1.05	1.05
4	Average concentration of Carbon Monoxide in flue gas (mg/m^3)	19.98	20.88
5	Emission rate of Carbon Monoxide (g/s)	0.021	0.022
6	Average concentration of Nitrogen Dioxide in flue gas (mg/m^3)	116.75	159.47
7	Emission rate of Nitrogen Dioxide (g/s)	0.123	0.168
8	Average concentration of Sulfur Dioxide in flue gas (mg/m^3)	122.45	140.48
9	Emission rate of Sulfur Dioxide (g/s)	0.129	0.148

The MRU analyzer, used for the measurements, was new and the sensors were factory-calibrated; in addition to that, the analyzer was calibrated at the site. The MRU analyzer has a program for auto zero calibration using an integrated solenoid valve. A solenoid valve allowing the analyzer air to be discharged into the in-situ cell, forcing out the flue gas, and enabling the analyzer to check zero. So, zero calibration was done with respect to the Oxygen present in the atmosphere at 20.9%.

All of the experimental work was carried out by implementing the following quality control and quality assurance protocols. The MRU analyzer was zero calibrated before each measurement, calibration was carried out at the stack base, so the possibility of mixing the flue gas with the breathable atmosphere expected to be nil. It can, therefore, be assumed that the calibration of the analyzer with reference to the atmospheric Oxygen was acceptable.

Measurements were also taken by repeatedly using another analyzer; Testo 350 xl Portable Emissions Analyzer. This analyzer is used by the Queen Rania Al-Abdullah Center for Environmental Science & Technology to assure that the incinerators emissions are within JS 1189/2006 limits.

Testo 350 xl analyzer is equipped with electrochemical cells to measure flue gases and it has a program for self-calibration, and once the equipment is switched on, it automatically initiates fresh air and zeroing phase for 1-minute.A real-time EVM-7 ambient gas analyzer was used to measure the hourly concentration of the pollutants at 22 receptors in the study area for model evaluation purposes. EMV-7 analyzer is an electrochemical cell analyzer used to simultaneously measure toxic gases, such as Sulfur Dioxide, Nitrogen Dioxide, and Carbon Monoxide.

The monitoring sites are situated mainly at the north direction where the JUST buildings and other service facilities were located. 1.6 meter receptor height was used based on the height of the average human nose (Al Smadi et al., 2009). The analyzer was factory calibrated and the measured concentrations were compared with the ambient air quality standards 1140/2006 in Jordan, Ministry of Health (MoH) standards and National Ambient Air Quality Standards (NAAQS).

2.5. Model Performance Evaluation

Model performance evaluation was tested by comparing the predicted pollutants concentrations with those measured actual concentrations (hourly concentrations) at 22 discrete receptors.

Several measures used to evaluate model performance. Hanna et al. (1991; 1993) recommend the use of the following statistical performance measures; Fractional Bias (FB), Geometric Mean (MG), Normalized Mean Square Error (NMSE), Geometric Variance (VG), Correlation Coefficient (R), and the Factor of 2 (FAC2).

During the present study, the following statistical measures were used to evaluate the model performance; fractional Bias (FB), Normalized Mean Square Error (NMSE), Factor of 2 (FAC2), and Correlation Coefficient (R).

Fractional Bias (FB) is the mean error that defines the residual of the observed and the predicted concentrations. In this evaluation, it has been selected because it is a dimensionless number which is convenient for comparing the results from studies involving different concentration levels or even different pollutants and because it is symmetrical and bounded from -2 (extreme under-prediction) to 2 (extreme

over-prediction).

It has the value of zero for an ideal model and express as (Chang and Hanna, 2004):

$$B = 2\times\left(\frac{\overline{C_o}-\overline{C_p}}{\overline{C_o}+\overline{C_p}}\right) \quad \text{..... 1}$$

where $\overline{C_o}$: Average observed concentration

$\overline{C_p}$: Average predicted concentration

Values of the FB that are equal to -0.67 are equivalent to over-predictions by a factor of 2; while values that are equal to +0.67 are equivalent to under-predictions by a factor of 2.

Normalized Mean Square Error (NMSE) emphasizes the scatter in the entire set and it is an estimator of the overall deviations between the observed and predicted values. The normalization by the product C_o*C_p assures that the NMSE will not be biased towards models that over predict or under predict. It is expressed as (Chang and Hanna, 2004):

$$NMSE = \frac{\overline{(C_o-C_p)^2}}{\overline{C_o}\times\overline{C_p}} \quad \text{..... 2}$$

where C_o: observed concentration

C_p: Predicted concentration

Normalized mean square error measures the mean relative scatter and reflects both the systematic ($NMSE_s$) and unsystematic ($NMSE_u$) errors. The lower the NMSE; the better the model ability to provide accurate predictions. For an ideal model performance, NMSE value is zero indicating no scatter between observed and predicted concentrations. For NMSE values less than 1.0; the magnitude of the scatter is less than the mean concentration and a value of 1.0 indicates that a typical difference between predictions and observations is approximately equal to the mean.

Factor of Two (FAC2) gives the fraction of the predictions that are within a factor of two of observations that satisfy $0.5 \leq FAC \leq 2.0$. The FAC2 is the most robust performance measure because it is not affected by the low and high outliers. It is expressed as (Chang and Hanna, 2004):

$$FAC2 = \frac{C_p}{C_o} \quad \text{.....(3)}$$

The ability of the model to predict at least 50% of the concentrations within a FAC2 of the observed concentrations is a fundamental requirement to accept the model (Derwen et al., 2010). In general, for an ideal or perfect model, both FB and NMSE equal zero and FAC2 equals one, and due to the random atmospheric processes, there is no such a thing. Hence, the acceptable limits according to the study of Kumar et al. (1993) are taken into consideration:

$-0.5 \leq FB \leq +0.5$

$NMSE \leq 0.5$

$FAC2 \geq 0.8$

The correlation coefficient (R) represents the strength of a linear relationship between two variables on a scatter plot; it is expressed as (Chang and Hanna, 2004):

$$R = \frac{\overline{(c_o-\overline{c_o})\times(c_p-\overline{c_p})}}{\delta_{Cp}\times\delta_{Co}} \quad \text{.....(4)}$$

where δ_C is the standard deviation over the data set.

A correlation coefficient of 1.0 indicates a perfect linear relationship; whereas a correlation coefficient of 0.0 means that there is no linear relationship between the variables.

3. Results and Discussion

3.1. Emissions from Source

Uniform Cartesian grid receptors network of 10 km x 10 km cover the study area with 2601 receptors was studied. The region within this field is mostly cultivated land, with other facilities scattered intermittently throughout the entire study area.

The stack emissions data were reported on a 3 % O_2 basis; the results were normalized to 8 % oxygen according to the Jordanian standard JS1189/2006 as presented in (Table 3)

Table 3. The sources parameters used as input to AERMOD

Parameter	Stack 1	Stack 2
UTM Coordinates (m)	3597783.595 Northing 779674.604 Easting	3597786.974 Northing 779668.394 Easting
Elevation (m asl)	590	590
Fuel Type	Diesel	Diesel
SO_2 emission rate (g/s)	0.129	0.148
NO_2 emission rate (g/s)	0.123	0.168
CO emission rate (g/s)	0.021	0.022
Velocity (m/s)	4.6	4.6
Temperature (°K)	750.95	823.45
Stack Inside Diameter (m)	0.54	0.54
Stack Height (m)	7	7

Normalization was done using the following equation:

$$C_{8\%} = C_{3\%}\times\left(\frac{20.9\%-8\%}{20.9\%-3\%}\right) \quad \text{.....(5)}$$

where $C_{8\%}$: pollutants concentrations at 8% O_2

$C_{3\%}$: pollutants concentrations at 3% O_2

20.9 %: the percent of O_2 in the air.

The stack exit concentrations were compared with the Jordanian standards (JS 1189/2006) and there are no exceedances occurred (Table 4).

Table 4. Concentrations of gases from the stacks

Stack ID	Concentration measured at 3% (mg/m^3)			Concentration normalized to 8 % (mg/m^3)		
	SO_2	NO_2	CO	SO_2	NO_2	CO
Stack 1	122.4	116.7	19.9	88.3	84.1	14.3
Stack 2	140.4	159.4	20.9	101.2	114.9	15.1
Jordanian standards				6500	200	---

3.2. Ambient air Quality

AERMOD was run using meteorological data for a whole year (2010) to identify the highest expected ground level concentrations (GLCs) during that year. AERMOD results are summarized in (Table 5).

Table 5. Concentrations of gases from the stacks

Pollutant	Maximum Predicted Concentration (µg/m³)			
	Hourly	8-hours	Daily	Annual
SO_2	28.86	-	4.25	3.63
Jordanian standards	779	--	363.7	104
NO_2	30.29	-	4.46	3.81
Jordanian standards	392	--	149	93
CO	4.48	1.31	-	-
Jordanian standards	29556	10231	-	-

The maximum 1 hr, 24 hr and annual SO_2 levels were 28.86µg/m³, 4.25µg/m³ and 3.63µg/m³ respectively (Figure 2).

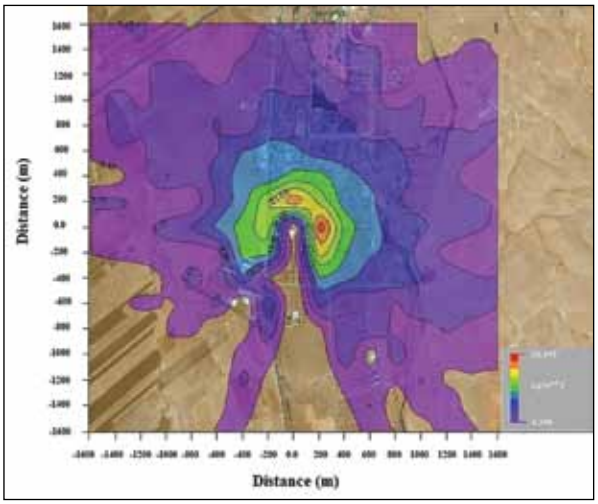

Figure 2a. Hourly concentration

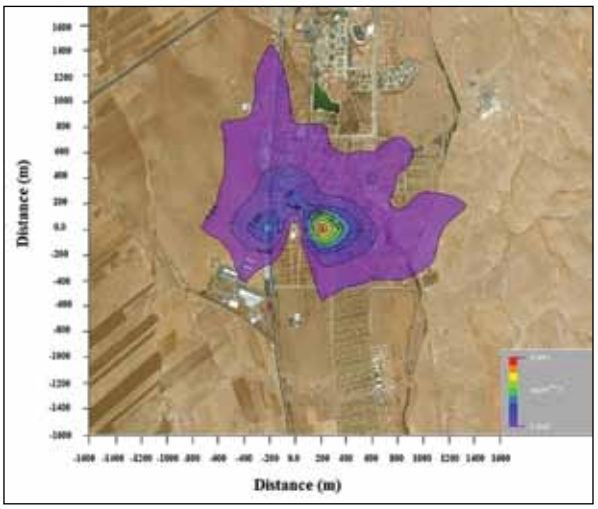

Figure 2b. Daily concentration

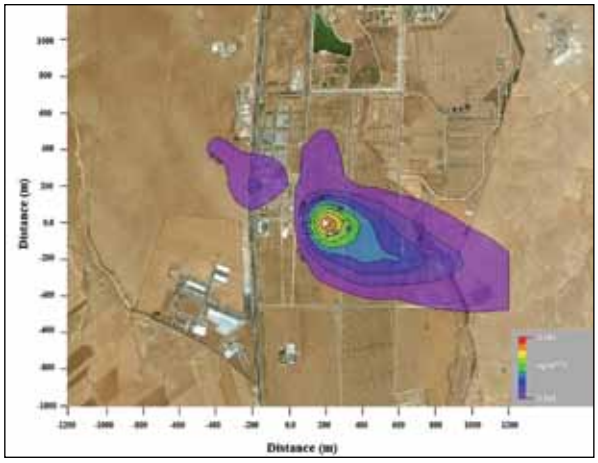

Figure 2c. Annual concentration

Figure 2. The average GLC of SO_2 in µg/m³

The concentrations of pollutant were very high at a downwind distance of about 200 m from the sources in the north direction for 1hr averaging period and in the east direction for daily and yearly. The higher 1 hr concentration is predicted to have occurred on the 15th of January/2010 at 06:00 while it is in October for 24 hr averaging period. The maximum 1hr, 24 hr and annual SO_2 concentrations predicted were comply with Jordan standards for these averaging periods.

The maximum levels of NO_2 predicted were 30.29 µg/m³ for 1 hr, 4.46 µg/m³ for 24 hr and 3.81 µg/m³, for annual averaging period (Figure 3). The max concentration is located at a downwind distance of 200 m in the north direction for 1hr averaging period and in the east direction for daily and yearly periods. The higher 1 hr concentration was found in 15th January at 06:00 (calm wind = 44.35%) while it is in October (calm wind = 51.61%) for 24 hr averaging period.

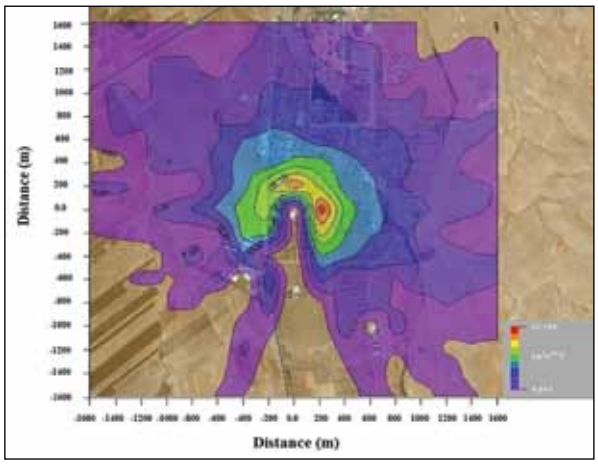

Figure 3a. Hourly concentration

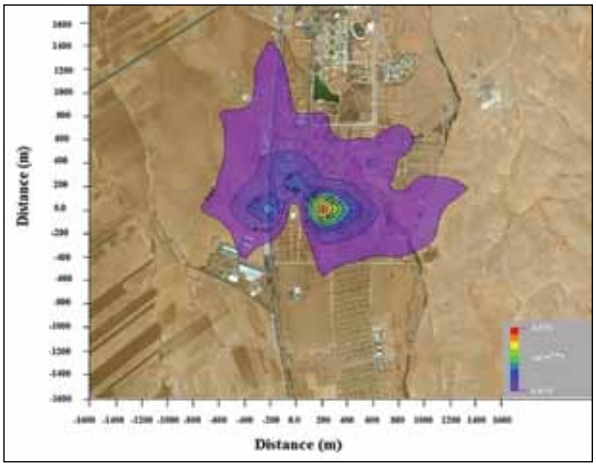

Figure 3b. Daily concentration

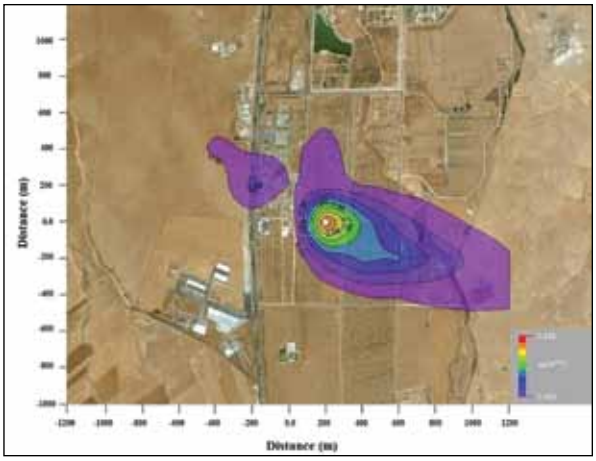

Figure 3c. Annual concentration

Figure 3 The average GLC of NO_2 in µg/m^3

The maximum 1hr, 24 hr and annual NO_2 concentrations predicted comply with Jordan standards for these averaging periods as well as NAAQS.

The maximum 1 hr and 8 hr levels of CO were 4.48µg/m^3 and 1.31µg/m^3, respectively (Figure 4). These concentrations were found at a downwind distance of 200 m in the east direction from the sources. The max concentrations for these averaging periods were founded in October (30th October at 00:00 am) and there is no exceedance of the national and international ambient air quality standard.

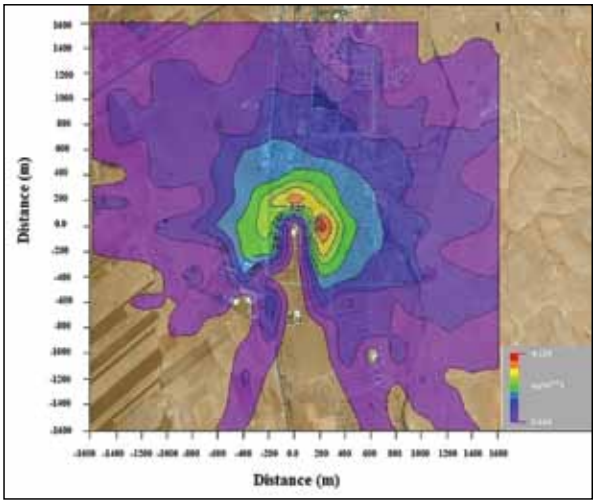

Figure 4a. Hourly concentration

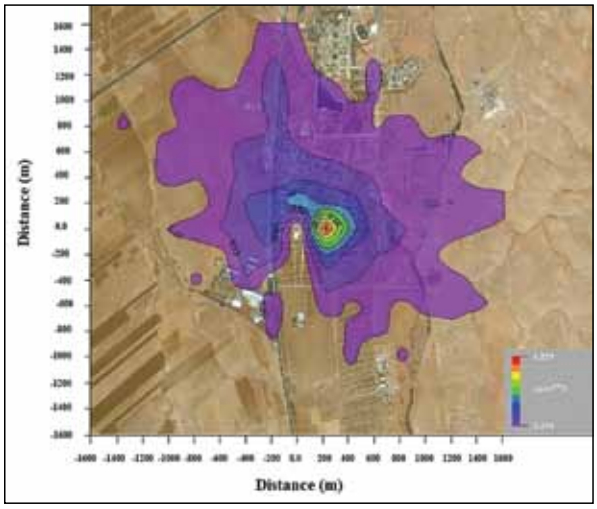

Figure 4b. 8-hours concentration

Figure 4. The average GLC of CO in µg/m^3

The maximum concentrations occur in cold months (January and October) due to emissions from stoves and other heating sources in addition to higher emission rates from motor vehicles during cold start ignition [Al-zboon, 2017]. Another important reason for higher concentrations of air pollutants is the frequent thermal inversion that which becomes more frequent in winter months. Thermal inversion is a natural phenomenon results during the night and early morning hours due to cooling of Earth surface and adjacent air at rates faster than air aloft. It could lead to poor air quality at urban areas because it obstructs the dilution of air pollution.

3.3. Worst Case Results

An initial screening analysis was conducted to identify the worst case for each month. The meteorological condition that yields the highest concentration was considered as the worst case. The screening procedure utilizes the Gaussian dispersion equation to estimate the maximum 1-hour GLC. The impact of other averaging periods is provided using the scaling factors presented in (Table 6).

Table 6. Recommended Factors to Convert Maximum 1-hour Average Concentrations to Other Averaging Periods (California EPA, 2003)

Averaging Time	Range	Recommended Multiplying Factor
3-hours	0.8 – 1.0	0.9
8-hours	0.5 – 0.9	0.7
24-hours	0.2 – 0.6	0.4
30-days	0.2 – 0.3	0.3
Annual	0.06 – 0.10	0.08

Tables 7 and 8 show the worst meteorological conditions and the maximum concentrations for each month, respectively except for November because no data is available for that month.

Table 7. Worst Meteorological Conditions for Each Month

Month	Hour	Ws (m/s)	Wd (degree)	T (°C)	H (w/m^2)	L (m)	Mixing Height (m)
Jan	18	7.2	100	20	-22.5	325.3	677
Feb	18	7.2	260	18.4	-22.6	323.4	677
Mar	18	5.14	200	23.2	-18	247	528
Apr	18	5.14	290	26.8	-2.7	1725.6	544
May	18	5.14	300	20	-2.4	1931.2	545
Jun	00	5.14	280	20	-29.8	573.7	1036
Jul	00	3.09	310	18.8	-17.7	199.5	471
Aug	06	3.09	300	24.8	-12	308.1	482
Sep	18	5.14	300	28	-20.5	295.4	616
Oct	18	5.14	160	11	-20.6	294	616
Nov	NA	NA	NA	NA	NA	NA	NA
Dec	18	7.2	260	12.4	-23.1	316.4	677
W_s: Wind Speed, W_d: Wind Direction, NA: Not Available							

Most of the worst cases shown in (Table 7) were in the nighttime at 18:00 GMT and 00:00 GMT where the stable boundary layers occur and once a daytime at 06:00 GMT. At night, the air is too stable and does not allow the plume to lift, whereas the measured wind speed may appear sufficient to move it.

Stability conditions can be identified form the values of sensible heat (H) and Monin-Obukhov Length (L) calculated by AERMET. AERMET define stable conditions if $H < 0$ and $L > 0$ and convective conditions if $H > 0$ and $L < 0$. Atmospheric stability is a primary influence on plume dispersion and it is most stable at nighttime hours and the least at daytime hours. In the presence of stable air; convective and turbulence are inhibited, while they are enhanced in unstable conditions.

From mixing height values in Table 7, it can be shown that the highest mixing height was 1036 m in June, that means a larger volume is available to dilute pollutant emissions. The lowest value was 471 m in July month but it can be noticed that the concentration in this month was not the highest and this violates the fact that the lower mixing height lead to higher concentration. In such a case, cold temperature in this month may have an opposite influence on the plume dispersion. Heat is responsible for the upward movement of the air. At high temperatures, pollutants will not hang at the ground level, but will disperse quickly. This would not happen at cold temperatures.

The maximum GLCs occurred at 200 m from source in the north and east directions and this distance is very close to the source. This may due to short stack height (7m). This condition has allowed the building downwash phenomena to occur which drawing the plume to the ground near the source.

Table 8. Maximum Concentrations for each month at the worst meteorological conditions

Month	CO Concentration (µg/m^3)		SO_2 Concentration (µg/m^3)			NO_2 Concentration (µg/m^3)		
	1 hr	8 hr*	1 hr	24 hr**	Annual***	1 hr	24 hr**	Annual***
Jan	4.639	4.175	29.868	17.921	2.987	31.354	18.812	3.135
Feb	4.633	4.170	29.829	17.897	2.983	31.314	18.788	3.131
Mar	4.489	4.040	28.892	17.335	2.889	30.316	18.190	3.032
Apr	4.663	4.197	30.017	18.010	3.002	31.506	18.904	3.151
May	4.641	4.177	29.874	17.924	2.987	31.358	18.815	3.136
Jun	2.867	2.580	18.466	11.080	1.847	19.398	11.639	1.940
Jul	3.933	3.540	25.308	15.185	2.531	26.553	15.932	2.655
Aug	3.983	3.585	25.633	15.380	2.563	26.899	16.139	2.690
Sep	4.508	4.057	29.021	17.413	2.902	30.465	18.279	3.047
Oct	4.506	4.055	29.011	17.407	2.901	30.455	18.273	3.046
Dec	4.611	4.150	29.693	17.816	2.969	31.171	18.703	3.117
* Multiplied by 0.9, ** Multiplied by 0.6, *** Multiplied by 0.01								

3.4. Model Performance Evaluation

To evaluate the performance of the model; predicted and observed concentrations at 22 receptors (Figure 5) were compared using statistical measures as presented in (Table 9).

Figure 5. Locations of the receptors

FB values have both positive and negative values, the majority of which (91%) lie between -0.5 and +0.5 for NO_2 and CO, indicating predicted results are close approximations of the observed data but 41% of SO_2 results fall out of the recommended range. The positive values of FB indicate that the model has a tendency towards under-prediction as compared to observed values (Khare et al., 2012).

NMSE is an indicator of variance and its values are > 0.5 for 36% of SO_2 predicted values indicating that the observed and predicted results are not in a good agreement with each other. For NO_2 and CO, NMSE values are within the acceptable range (NMSE ≤ 0.5) except for NO_2 at R1 and R15 and for CO at R1. Most of the predictions (68.2%, 72.7%, 60% for SO2, NO2, CO, respectively), FAC2 values are > 0.8 that means a good model performance.

Table 9. Model performance evaluation results

Receptor ID	SO_2			NO2			CO		
	FB	NMSE	FAC2	FB	NMSE	FAC2	FB	NMSE	FAC2
R1	0.831	0.835	0.413	0.803	0.770	0.427	0.790	0.740	0.434
R2	0.541	0.316	0.574	0.612	0.414	0.531	0.495	0.261	0.603
R3	-0.147	0.022	1.158	-0.180	0.033	1.198	-0.196	0.039	1.217
R4	0.030	0.001	0.971	-0.473	0.237	1.620	-0.024	0.001	1.024
R5	-1.613	7.444	9.337	-0.389	0.158	1.484	0.252	0.065	0.776
R6	-0.474	0.238	1.621	-0.466	0.230	1.608	0.378	0.149	0.682
R7	0.013	0.000	0.987	0.497	0.263	0.602	-0.036	0.001	1.036
R8	0.465	0.229	0.623	0.434	0.197	0.644	0.419	0.184	0.654
R9	0.058	0.003	0.944	0.025	0.001	0.975	0.009	0.000	0.991
R10	-0.077	0.006	1.080	-0.110	0.012	1.116	-0.126	0.016	1.135
R11	-0.088	0.008	1.093	-0.122	0.015	1.130	-0.139	0.019	1.149
R12	-0.484	0.248	1.638	-0.159	0.026	1.173	0.539	0.313	0.576
R13	-1.264	2.663	4.437	0.085	0.007	0.919	0.058	0.003	0.944
R14	-0.780	0.718	2.279	-0.164	0.027	1.179	-0.185	0.035	1.204
R15	1.656	8.710	0.094	1.645	8.367	0.097	0.294	0.088	0.744
R16	0.683	0.528	0.491	-0.015	0.000	1.015	-0.030	0.001	1.030
R17	0.172	0.030	0.842	0.139	0.019	0.870	0.125	0.016	0.882
R18	-0.023	0.001	1.023	-0.056	0.003	1.058	-0.070	0.005	1.073
R19	-0.369	0.141	1.452	-0.001	0.000	1.001	-0.413	0.178	1.521
R20	0.105	0.011	0.901	0.072	0.005	0.931	0.456	0.219	0.629
R21	0.791	0.741	0.433	0.110	0.012	0.896	0.094	0.009	0.910
R22	0.999	1.331	0.334	0.367	0.140	0.690	0.352	0.128	0.701

The correlation coefficient (R^2) reflects the linear relationship between the predicted and observed concentrations. Scatter plots and correlation coefficients indicate that the relation between the observed and predicted data for NO_2 and CO are linear and that the correlation coefficient was high while there is lower correlation in the case of SO_2 (Figure 6) Putter (2000) found poor agreement between the model and the raw measurement of SO2. USEPA, reported that the AERMOD predicted to observed ratio for annual averages SO2 concentration ranges from 0.30 to 1.64, with a geometric mean of 0.73 (USEPA, 1989).

Kho et al. (2007) evaluated the performance of AERMOD for NO_2 and SO_2 and found that the results are within FB acceptable ranges (-0.5- 0.5) except for NO_2 at one location, and 90% of the hourly average values within a factor of two (with ≥0.8).

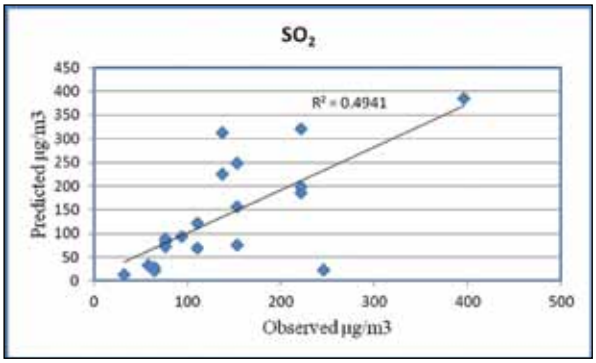

Figure 6a. SO_2 Concentration

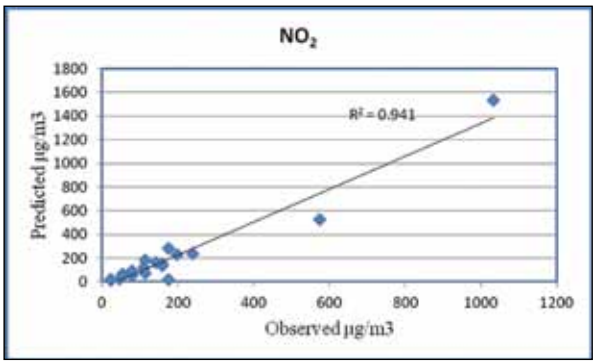

Figure 6b. NO_2 Concentration

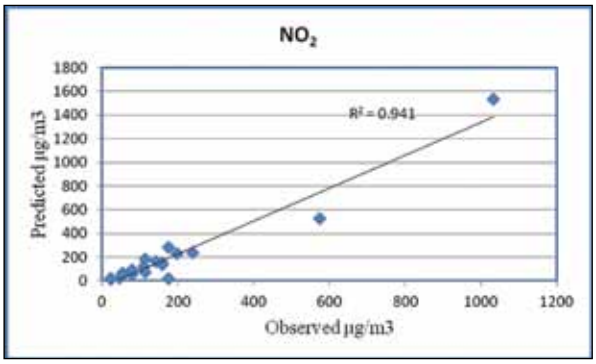

Figure 6c. CO Concentration

Figure 6. Scatter Plots of Observed and Predicted Concentrations

4. Conclusions and Recommendations

Stacks exit concentrations are within the allowable limits set by the Jordanian standards for stationary sources. Most of the time, pollutants are dispersed near the incinerators within 200 m in the downwind distances (north and east directions). The worst-case concentrations were found at nighttime hours where the more stability conditions occurred.

Predicted results from AERMOD show a good agreement with the observed results and better to the NO_2 and CO more than for SO_2. It is recommended that the stacks height be increased to reduce the maximum GLC and increase dispersion of pollutants. The decision makers should consider air modeling in Environment Impact Assessment (EIA) studies in order to asses proposed project›s impact on air quality. Conduct periodic monitoring program of emissions to detect any exceedances and to take the necessary preventive measures.

References

[1] Al Smadi B., Al-Zboon K., and Shatnawi K., 2009. Assessment of Air Pollutants Emissions from a Cement Plant: A Case Study in Jordan. Jordan Journal of Civil Engineering, 3 (3): 265-282.

[2] Al-zboon K., 2017, Indoor air pollution due to household use of olive cake as a source of energy, International Journal of Environment and Waste Management, 19(3): 248–267.

[3] Chang J. C. and Hanna S. R., 2004. Air quality model performance evaluation. Meteorology and Atmospheric Physics, 87(1): 167–196.

[4] Cole C. and Mickey D.2011, Medical Waste in NC: The need to reduce incineration by more effective waste segregation and use of non-incineration technologies, http://www.bredl.org/pdf3/ncmedwastereport-jan2011.pdf.

[5] Department of Statistics (DoS), 2015. Population and housing census, Amman, Jordan. http://census.dos.gov.jo/wp-content/uploads/sites/2/2016/02/Census_results_2016.pdf

[6] Derwen D., Fraser A., Abbott J., Jenkin M., Willis P. and Murrells T., 2010. Evaluation the Performance of Air Quality Models, Department for Environment Food and Rural Affairs (DEFRA)-UK, Issue 3. https://ukair.defra.gov.uk/assets/documents/reports/cat05/1006241607_100608_MIP_Final_Version.pdf.

[7] El-Hamouz, A. 2002. Medical Waste Incineration in Nablus City, West Bank: A Case Study. The Arabian Journal for Science and Engineering. 27, 1B:29-40.

[8] Hanna SR, Strimaitis DG, Change JC, 1991. Hazard response modeling uncertainty (A quantitative method), vol. I: User›s guide for software for evaluating hazardous gas dispersion models; prepared by Sigma Research Corporation, 234 Littleon Road, Suite 2E Wesford MA 01886.

[9] Hanna SR, Change JC, Strimaitis DG, 1993. Hazardous gas model evaluation with field observations. Atmos Environ, 27A: 2265 – 2285.

[10] Jang Y., Cargro L., Oh-Sub Y., Hwidong K. 2006. Medical waste management in Korea. Journal of Environmental Management, 80(2):107–115.

[11] Khare M., Nagendra S. and Gulia S., 2012. Performance evaluation of air quality dispersion models at urban intersection of an Indian city: a case study of Delhi city. WIT Transactions on Ecology and the Environment, (157): 249-259. http://www.witpress.com/Secure/elibrary/papers/AIR12/AIR12022FU1.pdf

[12] Kho WL., Sentian J., Radojevic M., Tan CL., Law PL., Halipah S., 2007. Computer simulated versus observed NO_2 and SO_2 emitted from elevated point source complex, Int. J. Environ. Sci. Tech., 4 (2): 215-222.

[13] Kumar J., 2009. Bio-medical waste management practices in a district government hospital of Haryana (India). Environment and Ecology 30 (3C):1099-1103

[14] Mediterranean Environmental Technical Assistance Program (METAP), 2005.Hazardous Waste Management in Jordan, Jordan.

[15] Ministry of Health (MoH), 2012. Annual Statistical Book, Amman, Jordan, http://www.moh.gov.jo/MOH/Files/Publication/report2010.pdf.

[16] Ministry of Health (MoH), 2014. Annual Statistical Book, Amman, Jordan, http://www.moh.gov.jo/MOH/Files/Publication/report2010.pdf

[17] Putter N. 2000. Comparison of monitored air quality data with the predictions of ADMS-3.Air Pollution VIII, C.A. Brebbia, H. Power & J.W.S Longhurst (Editors), http://www.witpress.com/Secure/elibrary/papers/AIR00/AIR00051FU.pdf .

[18] United States Environmental Protection Agency (USEPA), 1989. Model Evaluation Results for AERMOD, https://www3.epa.gov/scram001/7thconf/aermod/evalrep.pdf

[19] United States Environmental Protection Agency (USEPA), 1993. Emission Factor Documentation for Medical Waste Incineration, Solid Waste Disposal, AP-42 SECTION 2.6, July 1993.

[20] United States Environmental Protection Agency (USEPA), 2004. AERMOD: Description of Model Formulation, September 2004.

[21] United States Environmental Protection Agency (USEPA), 2012. AERMINUTE User's Instructions,https://www3.epa.gov/ttn/scram/models/aermod/aerminute_userguide_v11059_draft.pdf.

JJEES
Jordan Journal of Earth and Environmental Sciences

Volume 8, (Number 1), Sept, 2017
ISSN 1995-6681
Pages 11 - 16

Parametric Study and Empirical Modeling for the Equilibrium and Kinetic Adsorption of Milk Organics onto Stone Cutting Particles

Nareman Zahdeh, Maher Al-Jabari*, Nadia Iqefan, and Hiba Dweik

Palestine Polytechnic University, Hebron, Palestine

Received 11 July, 2016; Accepted 25 August, 2017

Abstract

The present paper investigates the treatment of dairy wastewater by adsorption on stone cutting solid waste. It implements the innovative concept of "treating waste by waste." Batch adsorption experiments were performed for obtaining kinetic curves of percentage reduction in COD. The treatment efficiency is investigated as functions of the operating parameters including: stirring rate, pH, particle dosage and contact time.

Both the rate of adsorption and the equilibrium removal efficiency increase with increasing particle dosage. Increasing the stirring rate increases the adsorption rate, while it has no effect on equilibrium efficiency. The effect of pH is found to be unique; the adsorption occurs mainly at a pH value of around 6. Pseudo second order model is found to fit experimental data.

Key words: Adsorption, COD, Equilibrium, Kinetics, Dairy, Stone, Wastewater.

© 2017 Jordan Journal of Earth and Environmental Sciences. All rights reserved

Keywords: Adsorption, COD, Equilibrium, Kinetics, Dairy, Stone, Wastewater.

1. Introduction

Dairy industry and stone cutting are two main industries in Palestine. Dairy industry is a major food processing industry which needs water in all manufacturing processes. Dairy industry generates wastewater effluents characterized by high Biological Oxygen Demand (BOD) and Chemical Oxygen Demand (COD). When released into valleys and open areas, major pollution problems are faced; it percolates through soil and thus polluting the ground water. Also, stone cutting industry generates large amounts of wastewater, which contains suspended particulate matter that affects soil and ground water.

In Palestine, dairy industry contributes by 6.8% in the food industry sector (Economy, 2004). On the other hand, Palestinian stone and marble industry constituted approximately 4% of world production. It contributes approximately 5.5% to gross domestic product and employs 15,000 workers with annual sales reaching 270 million dollars according to 2006 industrial survey (Economy, 2006).

Dairy wastewater contains massive amounts of organic matter (proteins, lactose and fat), sewage fungus, and inorganic compounds (Nitrogen, Phosphorus and Ammonia). The average values of BOD and COD in the dairy effluents were reported to be 1941 ± 864 ppm, 3383 ± 1345 ppm, respectively (Shete and Shinkar, 2013). The pH was reported to be 7.9 ± 1.2 and TSS was reported to be 831 ± 392. There have been no noticeable efforts for controlling dairy industry wastewater in Palestine. Currently, most of the industrial wastewater in Palestine is discharged directly into sewer system (62.8%). The rest (37.2 %) is discharged through cesspits

For stone industry, it has numerous major environmental impacts. Al-Jabari has previously emphasized its environmental impacts on agriculture, ground water and human beings(Al-Jabari, 2002). It is estimated that the stone cutting industry in Palestine annually uses about 0.5 million cubic meters of water. Thus, the resulting wastewater contains suspended solid particles (slurry). Then, these particles are separated from wastewater using various techniques (Al-Jabari, 2002; Al-Jabari and Sawalha, 2002) and the resultant separated particles are transported to open areas (Al-Jabari et al., 2012). It is estimated that this industry annually generates approximately 0.7-1.0 million tons of this slurry waste.

Various local trails tried to control or reduce the impact of stone industry. For example, sludge recycling projects. Where, the slurry powder can be used in PVC pipes, tiles and artificial stone production (Al-Joulani, 2006; Al-Joulani, 2007). In addition, Al-Jabari used stone cutting wastewater as a treatment option for local leather tanning industry (Al-Jabari, 2002).

Worldwide, there are various treatment methods for wastewater effluents from dairy industry. These include; activated sludge, trickling filters, sequence batch reactors, anaerobic sludge blanket, nanofiltration and others. These techniques are complicated, expensive, energy consuming and unable to reach effluent discharge standards of 50 ppm BOD and 250 ppm COD according to World Bank restrictions (Shete and Shinkar, 2013).

One of treatment methods is adsorption. Organic material in dairy wastewater can be adsorbed onto various solid adsorbents. Previous studies have confirmed the technical feasibility of adsorbing organics on various adsorbents. These

* Corresponding author. e-mail: mjabari@ppu.edu

adsorbents include; low molecular weight crab shell chitosan (Devi, 2012), Activated Carbon Commercial grade (ACC) (Kushwaha et al., 2010), Bagasse Fly Ash (BFA) (Kushwaha et al., 2010), acid mine drainage sludge (Wang et al., 2013), clay particles (Al-Jabari, 2016), marlstone (Al-Jabari, 2016) and Neem leaves powder (Sivakumar and Christyno, 2012). Investigated parameters in these studies included: pH, particle dosage, contact time, stirring rate and initial concentration of organics.

Various empirical models were used for adsorption kinetics. These included Elovich and Lagergren pseudo-first order and second-order models order, and second-order models. Such models were reviewed by Ho (Ho and McKay, 1998). Adsorption kinetics based on an nth-order kinetic model, and a double exponential model were used by Tosun (Tosun, 2012). Second-order adsorption models were reviewed by Ho [9 From marlstone]. First order model was used by Elagroudy to estimate the mass adsorbed in ith minutes (Mi) [10 From marlstone]. A full review of modeling papers is available in the literature [11 From marlstone]. Two new theoretical models for adsorption kinetics have been published recently. These include a mass transfer model [maher mass] and a model based on Langmuir kinetics [maher langmuir].

There are urgent needs to reduce environmental impacts associated with dairy wastewater. Since there are no noticeable efforts to control dairy wastewater, adsorption is believed to be the simplest solution for reducing COD in dairy industry wastewater. It is most preferred when a low cost abundant adsorbent is used. A recent paper by the present authors had demonstrated the technical feasibility of treating dairy wastewater with various local abundant adsorbents (Al-Jabari et al., 2015). These local natural adsorbents were used also to treat other types of industrial wastewaters, such as leather tanning wastewater (Al-Jabari et al., 2012, Al-Jabari et al., 2009a; Al-Jabari et al., 2009b).

The aim of the present experimental study is to investigate the effects of various operating parameters on adsorption process for treating wastewater from diary industry with solid waste from stone cutting industry. These parameters include solid content, pH, contact time, stirring rate and organics initial concentration.

2. Materials and Methods

2.1 Materials

Samples of stone cutting solid waste are obtained from a local factory in Hebron, that does not involve flocculation-sedimentation process for its wastewater treatment (i.e., no use of polymeric flocculating agents) see (Al-Jabari, 2002; Al-Jabari and Sawalha, 2002). Flocculated particles are not inefficient for adsorption (Al-Jabari et al., 2015). The obtained solid samples are dried in an oven at 120oC. The size of solid waste particles is determined to 34 μm,using settling test method. The obtained particle size agrees with results obtained by Al-Jabari (2002). The used solid particles contain 85% of calcium carbonate (obtained by reverse titration).

Real samples of dairy wastewater are obtained from a local dairy factory (AL-Jebreni Company, Hebron, Palestine). The measured COD of the wastewater sample was 5200 mg/L, with a percentage difference of 3%. No physical pretreatment of the wastewater was made. Wastewater samples are stored in a refrigerator at 4 oC. An amount of 2 mL of concentrated sulfuric acid (18M) is added to each one liter of wastewater to prevent natural biodegradation, according to the standard requirements(Clesceri et al., 1998). It is diluted at a ratio of (1:10) by adding distilled water. The initial COD and BOD of the wastewater used in the adsorption process are about 500 mg/L and 300 mg/L, respectively.

Chemical reagents used include Potassium Hydrogen Phthalate, Potassium Dichromate, Sulfuric Acid 99% purity, 1.1 Phanthroline and Ferrous Sulfate. All chemicals are from Sigma Aldrich, through Alfa Aesar Company in Palestine.

2.2. Methodology

A volume of 100 mL of wastewater is mixed with a required mass of stone cutting particles, for batch adsorption experiments. Batch adsorption experiments at ambient room temperature (22oC) are carried out in stirred vessels. At certain time intervals, small samples of wastewater are then taken from the adsorption vessel and analyzed using standard COD test procedure (Clesceri et al., 1998). Determination of measured COD and estimated BOD is illustrated in a previous paper (Al-Jabari et al., 2015).

2.3. Data Analysis

The efficiency of the adsorption process is obtained from the percentage COD reduction (or removal efficiency), as given by the following equation:

$$\text{Percentage removal efficiency} = \frac{COD_o - COD_t}{COD_o} \times 100\% \quad (1)$$

where CODo is the initial COD of wastewater (mg/L), CODt is the obtained COD after adsorption at certain time (mg/L).

The surface concentration of organics on stone particles (qtin mg/g) is obtained from batch massbalance for adsorption process as follows:

$$q_t = \frac{V(COD_o - COD_t)}{m} \quad \text{.....(2)}$$

where m is the mass of adsorbent (mg) and V is the volume of wastewater used in the adsorption experiment (100 mL).

3. Results and Discussion

The main results of the present paper are presented here as curves of COD, qt and percentage reduction in COD as functions of time. The validity of monitoring COD reduction in dairy wastewater for evaluating performance of wastewater treatment processes has been demonstrated experimental in previous works (Shete and Shinkar, 2013). The technical feasibility of organics removal from dairy wastewater by its treatment using stone cutting solid waste particles was confirmed previously by the authors of the present paper (Al-Jabari et al., 2015). The effects of various parameters on adsorption process are presented; these included contact time, bulk motion, solid content, pH and organics concentration.

3.1. Adsorption Kinetics

Typical adsorption kinetics is presented as a plot of qt versus time, as presented in Figure 1. It shows two groups of experimental data obtained from two identical adsorption experiments (circles and triangles), with a particle dosage of 5 g/100 mL, and at a temperature of 22^{o}C, pH= 6 and a stirring

rate of 250 rpm. It clearly confirms the reproducibility of data and the validity of the used experimental procedures.

Figure 1 indicates that the organic load on the surface of stone cutting particles increases with time, as a result of the adsorption of organics from the dairy wastewater. At equilibrium, the rate of adsorption equals the rate of desorption, and thus no further net change in qt occurs, resulting in constant equilibrium value. Figure 1 indicates that the adsorption process is relatively fast. Equilibrium is approached within 3 hours. A similar kinetic behavior was obtained on the same type of adsorbents, in a previous study on treating leather tanning wastewater with stone cutting solid waste (Al-Jabari et al., 2012). However, organic adsorption seems to be faster than chromium adsorption.

The obtained experimental kinetic adsorption curve is modeled using pseudo first order and second order rate equations, given in Eqn.4, Eqn.5 and Eqn.6, presented in linear forms:

$$\log(q_e - q_t) = \log q_e - \frac{K_1}{2.303} t \quad \text{.....(3)}$$

$$\frac{t}{q_t} = \frac{1}{V_o} + \frac{1}{q_e} t \quad \text{.....(4)}$$

$$V_o = K_2 q_e^{\,2} \quad \text{.....(5)}$$

where K1, K2 in (hour-1) are the pseudo first order and second order rate constant for the kinetic model, respectively, qe and qtin(mg/g) are the adsorption capacities at equilibrium and at a time tin(hours), respectively, and Vo is the initial adsorption rate.

The solid curve in Figure 1 is obtained from the pseudo second order model, while the dashed curve is from the pseudo first order model. Obviously, the second order model provides a better fit for the experimental results. This is in agreement with the findings in previous studies: pseudo second order model provided excellent fit for the adsorption kinetics of organic pollutants. These cases included the adsorption kinetics for the adsorption of methylene blue on high lime fly ash (Keleşoğlu et al., 2012), the adsorption kinetics of dairy proteins on silica (Sarvi et al., 2014), the adsorption kinetics of dairy organics on rice husk (Pathak et al., 2016), and the adsorption kinetics of organic pollutants in dairy wastewater on soil particles (Al-Jabari, 2016).

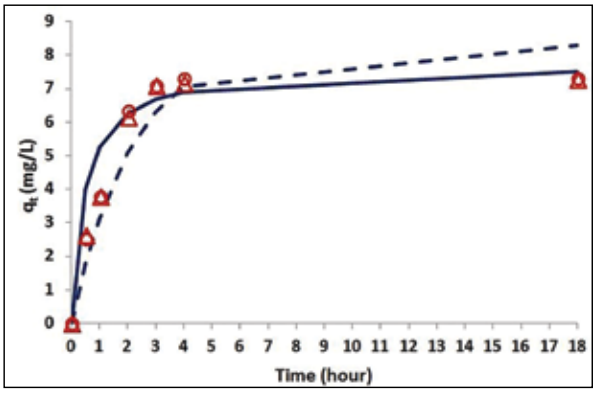

Figure 1. Experimental kinetic curve of qt (organics load on the adsorbent) and model curves using pseudo first order rate equation (dashed line) and second order (solid line), for adsorption experiments using stone cutting solid waste with a particle dosage of 5 g/100 mL at a temperature of 22°C, pH= 6 and stirring rate= 250 rpm.

3.2. Effect of Stone Particle Dosage

Increasing the particle dosage has a major effect on the final removal efficiency, since it increases the total available surface area for adsorption. Figure 2A shows the adsorption kinetic curves for different cases of stone particle dosages indicated in the figure caption. All experiments are performed at pH=6, a temperature of 22 oC and a stirring rate of 250 rpm. Table 1 summarizes the final-equilibrium removal efficiency for various particle dosages. With high particle dosage of 10 g/100 mL, the obtained percentage COD removal (83%) is relatively high, and the treated wastewater complies with the World Bank standards.

Figure 2A also shows that changing particle dosage affects the adsorption rate: Increasing the particle dosage increases adsorption rate; it decreases the time needed to approach equilibrium, and increases the slope of the kinetic curve at each time. This is attributed to the fact that with more particles in liquid, more collisions with particle surfaces occur and thus faster adsorption is obtained. Increasing solids to liquid ratio increases the mass transfer coefficient and decreases the characteristic time needed to approach equilibrium.

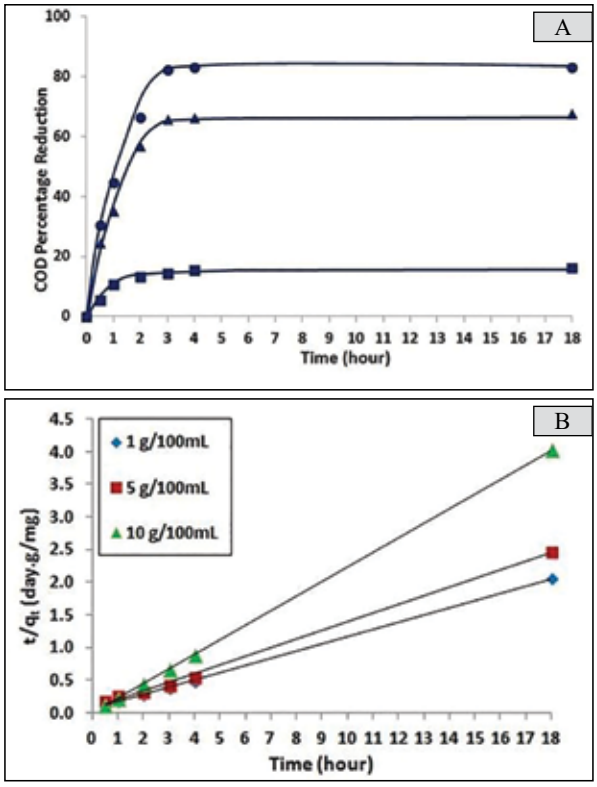

Figure 2. (A) Percentage COD removal as a function of time for different particle dosages (squares for 1 g/100 mL, triangles for 5 g/100 mL and circles for 10 g/100 mL), all at pH=6, 22 °C and a stirring rate= 250 rpm. **(B)** Second order kinetic model for the adsorption of organic molecules onto stone cutting particles for different particle dosages.

The obtained experimental kinetic adsorption curves are modeled using pseudo second order rate equation, given in Eqn.5 and Eqn.6, declared in linear forms and presented in Figure 2B.With the second order model, the plot of t/qt versus time is linear, with a positive slope of 1/qe. Obviously, the model provides good fit to the experimental data. Obtained model and fitting parameters are listed in Table 1.

Table 1. Obtained model and fitting parameters with pseudo second order model for the adsorption of organic molecules onto stone cutting particles and experimental equilibrium removal efficiency for various particle dosage, at pH=6, a temperature of 22°C and stirring rate of 250 rpm.

Dose (g/100mL)	Experimental	Pseudo Second Order Parameters				
	Percentage Reduction	qe (mg/g)	Vo	K2 (hour-1)	R2	SD
1	18%	9	19.53	0.241	0.9978	0.17
5	68%	7.51	16.23	0.288	0.9964	0.15
10	83%	4.48	3.3*1015	1.6*1014	1	0

3.3. Effect of Bulk Motion

The effect of increasing stirring rate is presented in Figure 3 (for similar conditions as in above cases in Figures 1 and 2. At low stirring speed of 70 rpm, equilibrium is approached within about 4 hours, which is larger than the time period for the case with 250 rpm (about 3 hours). It is believed that the liquid side mass transfer resistance controls the process. Increasing bulk motion increases the volumetric convective mass transfer coefficient and thus reduces the time needed to reach equilibrium. Thus, the adsorption rate increases with bulk motion. This is in agreement with previous work (Al-Jabari, 2016; Al-Jabari, 2016).

The final removal efficiency does not change with bulk motion, since it is characterized by the equilibrium adsorption capacity. Adsorption capacity is a surface property and does not depend on the surrounding hydrodynamic conditions. It is obtained from equilibrium isotherm.

These results are in agreement with various previous studies, where increasing stirring rate increased adsorption rate and had no effect on the final adsorption capacity (Asgari et al., 2013, Mehmet Doğan and Özmetin, 2006).

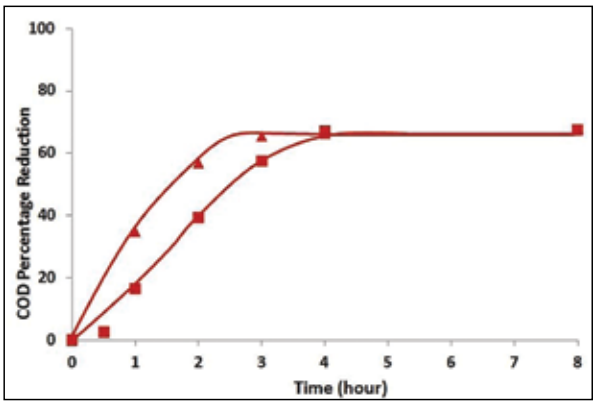

Figure 3. Percentage COD reduction as a function of time, at two stirring rates (squares for 70 rpm and triangles for 250 rpm) at pH=6, at a temperature of 22°C and a particle dosage of 5g/100 mL

The above fast adsorption rate was obtained when the system was kept under stirring (suspended particles in the vessel). When adsorption vessel is left unstirred (particles are settled at the bottom of the vessel), the adsorption process is extremely slow. Figure 4A shows results obtained for adsorption experiments at the same conditions as that in Figure 1 but with no stirring. Also, Figure 4A compares COD Kinetic curves for adsorption on soil and marlstone particles (Al-Jabari, 2016; Al-Jabari, 2016). With all types of adsorbents, nearly, 9 days are required to reach equilibrium. This emphasizes the hypothesis that the adsorption of organics on these mineral particles is mass transferred controlled. When the system is not stirred, the mass transfer occurs by diffusion which is a slow process compared with convection mass transfer (when the system is stirred).

With stone cutting particles, the COD value with stagnant particles has nearly the same value as that for the case of stirring. This is attributed to fact that the adsorption capacity is a surface property obtained from equilibrium isotherm, and does not depend on the hydrodynamic conditions.

Both soil and marlstone have similar adsorption behavior, but stone cutting particles have higher adsorption rate and removal efficiency. For the purpose of comparison, results from similar adsorption experiments, utilizing red clay soil (90.5 µm) and marlstone particles (53 µm), are summarized in Table 2. It lists the maximum adsorption rate and COD percentage reduction, for each adsorbent. Stone cutting particles are able to reduce COD twice more than marlstone. Soil particles exhibit one fifth of the maximum adsorption rate of stone cutting particles.

Table 2. Comparison between natural mineraladsorbents and their COD removal efficiencies, maximum adsorption rate and obtained model and fitting parameters with pseudo second order model for the adsorption of organic molecules onto natural adsorbents particlesperformed at stagnant conditions, pH=6, 22oC and using a dose of 5 g/100mL.

Adsorbent	Experimental	Pseudo Second Order Parameters				
	Maximum Specific Rate (mg/L. day)	Percentage Reduction	qe (mg/g)	Vo	K2 (day-1)	R
Soil	-20.72	27%	3.74	1.12	0.081	0.9874
Marlstone	-46.21	32%	4.12	1.31	0.077	0.9927
Stone cutting solid waste	-97.21	66%	8.69	2.87	0.038	0.9944

For the three kinetic curves (for soil, marlstone and stone cutting solid waste) in Figure 4A, the plots of t/qt versus time are linear, with positive slopes of 1/qe. The resulting lines for the second order model are plotted in Figure 4B. The obtained model and fitting parameters are listed in Table 2. Obviously, the pseudo second order model gives relatively good fitting to the experimental data. As listed in Table 2, both marl and soil adsorbents have higher pseudo second order rate compared to stone cutting solid waste. On the other hand, stone particles have a higher adsorption capacity (higher qe)

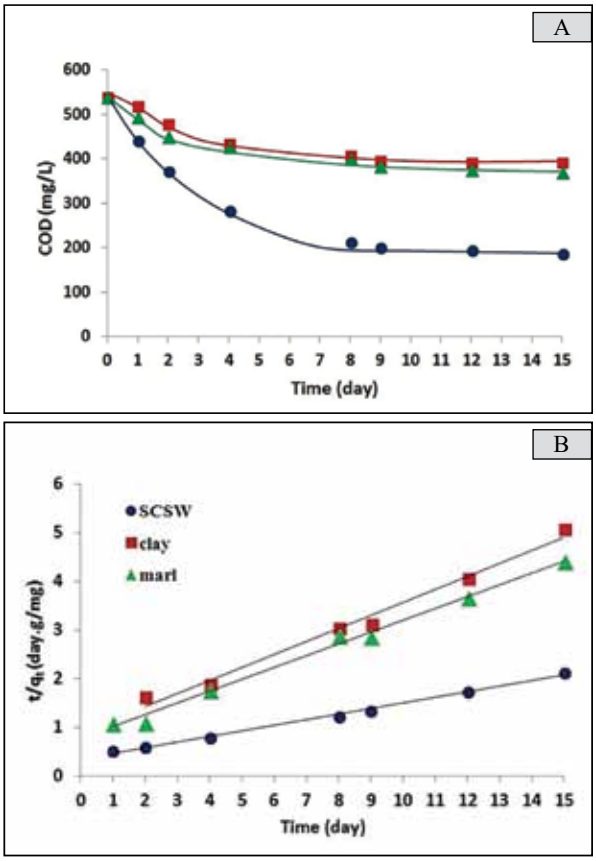

Figure 4. (A) Adsorption kinetics (COD versus time) for static conditions (no stirring) with a particle dosage of 5 g/100 mL of adsorbent, at a temperature of 22°C and pH= 6 (squares for soil, triangles for marlstone and circles for stone cutting). **(B)** Second order kinetic model for the adsorption of organic molecules onto various mineral adsorbents for stagnant particles

3.4. Effect of pH

It is well known that adsorption on surfaces is pH dependent. Figure 5 shows the obtained results of equilibrium removal efficiency (circles for stone particles) as a function of solution pH using a particle dosage of 5 g/100 mL, at a temperature of 22°C and a stirring rate of 70 rpm. A wastewater pH range between 2 to 12 is obtained by adjusting pH using concentrated hydrochloric acid and sodium hydroxide. Samples using the same mass (5 g/100 mL) with different pH values were stirred for 18 hours (sufficient time to reach equilibrium) and allowed to settle for 24 hours. Then the final equilibrium value of COD is measured. Obviously, for stone cutting particles, low COD percentage reduction is obtained at extremely acidic and alkaline conditions. There is a limited pH range for adsorption, which is nearly 5-7, with a maximum removal efficiency of 68% at pH=6 (for particle dosage of 5 g/100 mL).

This obtained type of pH dependence of organics uptake efficiency by stone cutting particles is unique .For adsorption on charged particles (like stone particles of the present work); usually the removal efficiency will be high at alkaline conditions and small at acidic conditions. In this case, the adsorption process is efficient mainly at pH value of around 6.

It is believed that this unique behavior of stone cutting particles is associated with physical adsorption, in which Van der Waals forces bond solute to the surface. This occurs when solution pH eliminates repulsion forces associated with high pH values. However, in the previous work of adsorption of positively charged trivalent chromium ions(Al-Jabari et al., 2009a), the surface charge of stone particles is essential in the adsorption mechanism, and thus high pH values resulted in attractive forces and yielded high adsorption efficiency. At low pH values, (obtained by the addition of sulfuric acid), a chemical conversion of stone particles occurs, i.e., reaction of H_2SO_4 with $CaCO^3$ producing calcium sulfate and releasing CO_2. The resulting product (yellow colored) does not have affinity for adsorption as stone particles, and thus zero removal efficiency is observed.

Also, Figure 5 compares the pH dependence for other mineral adsorbents: soil (squares) and marlstone (triangles) (Al-Jabari, 2016; Al-Jabari, 2016). Soil particles seem to favor acidic conditions to adsorb organic molecules. On the other hand, adsorption of organic matter on marlstone particles occurs in neutral to alkaline conditions. Soil in its nature is alkaline, and from Figure 5, soil pollution with organics is of small probability. However, if soil is acidic or contains a fraction of marlstone, it will be more suspected to pollution from dairy wastewater.

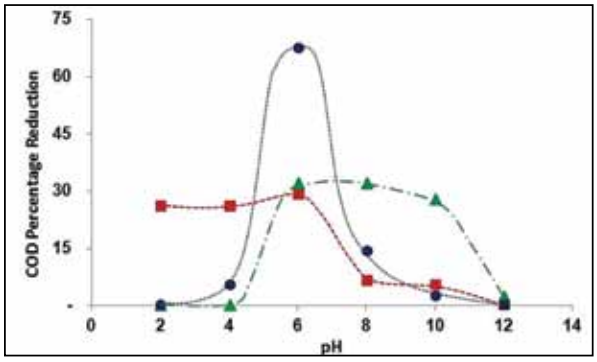

Figure 5. Equilibrium removal efficiency as a function of solution pH using a particle dosage of 5 g/100 mL, at a temperature of 22°C and a stirring rate of 70 rpm (squares for soil, triangles for marlstone, and circles for stone cutting).

3.5. Adsorption Isotherm

Figure 6 presents the adsorption isotherm as a plot of equilibrium concentration in the solution versus surface concentration on the stone particles, for equilibrium experiments with a particle dosage of 10 g/100 mL, pH= 6, and at a temperature of 22°C. Obviously, the isotherm is linear. This linearity supports the research hypothesis that physical adsorption occurs with a mass transfer process.

These results indicate that a kinetic adsorption model based on mass transfer rate equation can be developed in a similar fashion as the mass transfer desorption model developed by Al-Jabari and Weber for solute desorption from solid surface into fluid (Al-Jabari, 1999). In such a case, the

only difference is in the initial conditions, i.e., at zero time: the surface concentration (qt) is zero and the dimensionless bulk fluid concentration (COD/CODo) is 1.

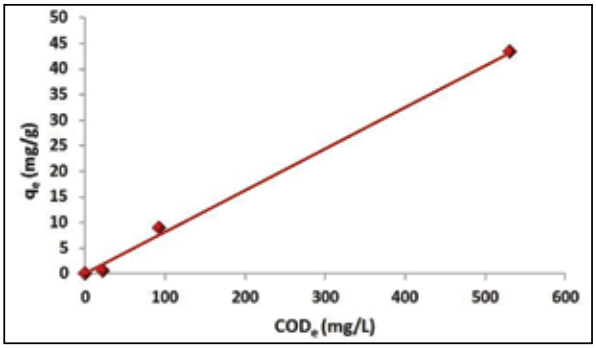

Figure 6. Adsorption equilibrium isotherm as a plot of equilibrium concentration in the solution versus surface concentration, for equilibrium experiments with a particle dosage of 10 g/100 mL, pH= 6, and at a temperature of 22°C.

Conclusion

The present paper demonstrates that the solid waste particles from stone cutting industry can reduce the organic load (COD) in the wastewater from dairy industry, in an efficient adsorption process. The process is mass transfer controlled with linear equilibrium isotherm. The rate of adsorption increases with increasing bulk motion. When the system is not stirred an extremely slow adsorption process occurs. Pseudo second order model is found to fit experimental data. Equilibrium removal efficiency is high at a pH of 6. It increases with increasing particle to wastewater ratio. Adsorption on stone cutting particles is more efficient than that on other similar mineral particles (marlstone and soil).

References

[1] AL-JABARI, M. 2002. Managing Wastewater Treatment in Stone Cutting Industry in Palestine, Basic Physicochemical and Engineering Aspects. RETEBE2. Egypt

[2] AL-JABARI, M. 2016. Kinetic models for adsorption on mineral particles comparison between Langmuir kinetics and mass transfer. Environmental Technology and Innovation, 6, 27–37

[3] AL-JABARI, M. 2017. Kinetic Mass Transfer Model for Treating Dairy Industry Wastewater with Stone Cutting Solid Waste. Environmental Technology & Innovation 7, 21-29.

[4] AL-JABARI, M., ABUALFAILAT, M. & SHAHEEN, S. 2012. Treating leather tanning wastewater with stone cutting solid waste. Clean – Soil, Air, Water, 40, 206-210.

[5] AL-JABARI, M., AQRA, F., SHAHEEN, S. & KHATIB, A. 2009a. Monitoring chromium content in tannery wastewater. The Journal of The Argentine Chemical Society, 97, 77-87.

[6] AL-JABARI, M., AQRAA, F., SHAHEEN, S. & KHATIB, A. 2009b. The treatment of chromium tanning wastewater using natural marl. Journal of The Chemical Speciation and Bioavailability, 21, 185-191.

[7] AL-JABARI, M., DWEIK, H., ZAHDEH, N. & IQEFAN, N. 2016a. Reducing Organic Pollution of Wastewater from Milk Processing Industry by Adsorption on Marlstone Particles. Int. J. of Thermal & Environmental Engineering, 13.

[8] AL-JABARI, M., IQEFAN, N., ZAHDEH, N. & DWEIK, H. 2016b. Adsorption of Organic Pollutants from Dairy Wastewater on Soil: Pollution Problem and Control. Int. J. Global Environmental Issues, 16.

[9] AL-JABARI, M. & SAWALHA, H. 2002. Experimental Investigation of Flocculation-Sedimentation Process Design Used in Stone Cutting Plants in Palestine. Jordan International Chemical Engineering Conference. Jordan.

[10] AL-JABARI, M. & WEBBER, M. 1999. Mass Transfer Model for Supercritical Fluid Extraction Tests. Separation Science and Technology, 34.

[11] AL-JABARI, M., ZAHDEH, N., IQEFAN, N. & DWIEK, H. 2015. Technical feasibility of treating dairy wastewater with natural low cost adsorbents. EWDR Conference. Turkey.

[12] AL-JOULANI, N. 2006. Stone slurry PVC pipes. Al-Waqa'e Journal

[13] AL-JOULANI, N. 2007. Engineering Properties, Industrial and Structural Applications of Stone Slurry Waste. Jordan Journal of Applied Science, 9.

[14] ASGARI, G., RAMAVANDI, B. & FARJADFARD, S. 2013. Abatement of Azo Dye from Wastewater Using Bimetal-Chitosan. The Scientific World Journal, 2013, 476271.

[15] CLESCERI, L., GREENBERG, A. & EATON, A. 1998. Standard methods for the examination of water and wastewater, Boston, APHA American Public Health Association.

[16] DEVI, M., DUMARAN, J. & FEROZ, S. 2012. Dairy Wastewater Treatment Using Low Molecular Weight Crab Shell Chitosan Journal of The Institution of Engineers 93, 9-14.

[17] ELAGROUDY, S. & EL-GOHARY, F. 2013. Microwave Pre-treatment of Mixed Sludge for Anaerobic Digestion Enhancement. Int. J. of Thermal & Environmental Engineering, 5.

[18] HO, Y. & MCKAY, G. 1998. A comparison of chemisorption kinetic models applied to pollutant removal on various sorbents. Process Safety and Environmental Protection, 76, 332-340.

[19] KELEŞOĞLU, S., KES, M., SUTCU, L. & POLAT, H. 2012. Adsorption of Methylene Blue from Aqueous Solution on High Lime Fly Ash: Kinetic, Equilibrium, and Thermodynamic Studies. Journal of Dispersion Science and Technology, 33, 15-23.

[20] KUSHWAHA, J. P., SRIVASTAVA, C. & MALL, I. 2010. Treatment of dairy wastewater by commercial activated carbon and bagasse fly ash: parametric, kinetic and equilibrium modeling, disposal studies. Bioresource Technology, 101, 3474-3483.

[21] MEHMET DOĞAN & ÖZMETIN, C. 2006. The Chemical Engineering Journal.

[22] PATHAK, U., DAS, P., BANERJEE, P. & DATTA, S. 2016. Treatment of Wastewater from a Dairy Industry Using Rice Husk as Adsorbent: Treatment Efficiency, Isotherm, Thermodynamics, and Kinetics Modelling. Journal of Thermodynamics.

[23] QIU, H., LV, L., PAN, B.-C., ZHANG, Q.-J., ZHANG, W.-M. & ZHANG, Q.-X. 2009. Critical review in adsorption kinetic models. Journal of Zhejiang University Science A, 10, 716-724.

[24] SARVI, M. N., BUDIANTO BEE, T., GOOI, C. K., WOONTON, B. W., GEE, M. L. & O'CONNOR, A. J. 2014. Development of functionalized mesoporous silica for adsorption and separation of dairy proteins. Chemical Engineering Journal, 235, 244-251.

[25] SHETE, B. & SHINKAR, N. 2013. Comparative study of various treatments for dairy industry. IOSRJEN, 3, 42-47.

[26] SIVAKUMAR, D. & CHRISTYNO, E. 2012. Isotherm studies on dairy industry wastewater using Neem leaves powder. Automation and Autonomous System, 4, 426-429.

[27] TOSUN, I. 2012. Ammonium removal from aqueous solutions by clinoptilolite: determination of isotherm and thermodynamic parameters and comparison of kinetics by the double exponential model and conventional kinetic models. Int J Environ Res Public Health, 9, 970-84.

[28] WANG, R., TSANG, C., OLDS, E. & WEBER, P. 2013. Utilizing acid mine drainage sludge and coal fly ash for phosphate removal from dairy wastewater. Environmental Technology, 34, 177-182.

JJEES
Jordan Journal of Earth and Environmental Sciences

Volume 8, (Number 1), Sept, 2017
ISSN 1995-6681
Pages 17 - 25

The Impact of Weather Parameters on Atmospheric PM2.5 at Al-Hasan Industrial Zone, East of Irbid- Jordan

Sana'a Odat[1*] and M. T. Alodat[2]

[1]Department of Earth and Environmental Science, Yarmouk University, Irbid, Jordan
[2]Department of Statistics, Yarmouk University, Irbid, Jordan

Received 24 May, 2017; Accepted 25 August, 2017

Abstract

Particulate Matters less than 2.5 micrometers (often referred to as $PM_{2.5}$) were measured in Al-Hassan Industrial Estate (HIE) in Irbid city, 72 Km north of Amman, the capital of Jordan. Data sets on the $PM_{2.5}$ emissions and meteorological conditions were collected over 6 years (from March 2010 to December 2016) by Jordan Ministry of Environment. The present paper studies the effects of the meteorological conditions on $PM_{2.5}$ levels. It is found that the largest average concentration of $PM_{2.5}$ is 39.77 $\mu g/m^3$ with standard deviation 49.42$\mu g/m^3$ which occurred in 2013, while the smallest average concentration of $PM_{2.5}$ is 22.2 $\mu g/m^3$ with standard deviation of 25.99 $\mu g/m^3$ which occurred in 2016; this is due to the positive relationship of $PM_{2.5}$ with temperature and its negative relationship with humidity. Furthermore, we conducted a nonparametric Kruskal-Wallis (KW) test to compare the average $PM_{2.5}$ level in working and nonworking hours. The KW test produced a p-value=0(<0.05), which indicates higher average $PM_{2.5}$ levels in working hours. The data indicate that the yearly average of $PM_{2.5}$ levels exceed the permissible limits of the Jordanian standards ambient air quality for the records of all years. Pronounced seasonal variation indicates that the $PM_{2.5}$ levels were generally higher in the summer months than its levels in the winter months, which means that the meteorological conditions have a significant impact on the $PM_{2.5}$ concentrations in the study site.

© 2017 Jordan Journal of Earth and Environmental Sciences. All rights reserved

Keywords: Air Pollution, Statistical Analysis, Al-Hassan Industrial Estate (HIE), Meteorological Parameter, Particulate Matter.

1. Introduction

Air pollution continues to receive considerable attention worldwide because of its negative effects on human health and welfare (Dockery and Pope, 1994; U.S. EPA 1999a; U.S. EPA 1999b; Jeff and Hans 2004). Particles less than 2.5 micrometers ($PM_{2.5}$) are classified as air pollutants with a diameter of less than 2.5 micrometers. $PM_{2.5}$ includes various directly emitted primary and secondary aerosols that are formed through chemistry of gaseous precursors in the atmosphere (Seinfeld and Pandis, 2006). Their small sizes enable them to reach deep parts of the respiratory system and lung airways in the human body. It is a mixture of microstructure solids and liquid droplets in the air (Y. Li, 2013). $PM_{2.5}$ particles consist of multiple compounds and are formed from primary and secondary participles (Zhao *et al*., 2013).

Aerosols are introduced into the atmosphere from a variety of anthropogenic sources, including transport, industrial activities, and biomass burning, as well as from natural sources, such as volcanic eruptions, sea salt, soil dust suspension, and forest fires. Most particulate emissions from combustion sources are $PM_{2.5}$ mass fractions. Fine particles can be directly emitted by sources or produced by condensation, coagulation, or gas-to-particle conversion, the last being common to combustion sources. Detailed descriptions of atmospheric aerosols can be found in the literature (Seinfeld and Pandis 1998; Finlayson-Pitts and Pitts, 2000).

Primary particles are emitted directly from the source, like combustion industrial processes and in natural processes (e.g., volcanic eruption). Secondary particles are formed indirectly through nucleation, condensation or processes where the gaseous pollutants (SOx, NOx, NH_3, VOCs) are involved in particle formation or growth. Secondary sulfate and nitrate particles formed from SOx or NOx precursors are usually the dominant component in $PM_{2.5}$ particles. As a result of the chemical components in secondary participles, the effect of high $PM_{2.5}$ concentrations on both environmental and human health (Wang and Hao, 2012).

Meteorological conditions play important roles in $PM_{2.5}$ concentrations due to their mixing, dispersion, transportation and formation of aerosol particles. Therefore, temporal variations in a pollutant concentration arises from the variations in local meteorological conditions, like wind speed, wind direction, temperature and relative humidity (Elminir, 2005; Satangi *et al*., 2004). To give a better understanding of the causes of air pollution, we must study the influences of meteorological parameters on the pollutants.

The development of industrial and services sectors in Jordan accompanied with the growth of Jordanian population result increase in the pollutants emitted to the ambient air, which in turn causes degradation of the air quality in many areas and adversely impact the public health (Cohen *et al*., 2005).

* Corresponding author. e-mail: sanaa.owdat@yu.edu.jo

A few studies were conducted to assess the air quality in Jordan. The Royal Scientific Association (RSS) have monitored PM_{10} and $PM_{2.5}$ in Al-Hashymeia, a town where most of Jordan industries are concentrated during the interval March, 2000 through February 2001 (Asi *et al*., 2001). Their results showed that PM_{10} and $PM_{2.5}$ have exceeded the Jordanian 24 hour standard of 120 µg/m^3 during 20 days out of 50 days constitute the whole sampling period. Hussein *et al*. (2011) measured the submicron particle number concentrations in the urban/suburban atmosphere of Amman–Jordan during the spring of 2009 and found that during the morning rush hours the number concentrations were as high as 120 × 103 and 75 ×103 1/cm^3 at the urban and suburban sites during weekly workdays. Abu-Allaban *et al*. (2011) measured air pollution (dust, SO_2, NO_x and CO) emitted from a modern cement plant that will be constructed in the Jordan Badia South-East of Amman. They found that the TSP concentration is expected to be high at the limestone quarry, which provides the factory with its main raw material, because it generates lots of dust as a result of rocks mining and crushing. Therefore, it is so important to study ambient air quality of the residential areas that are close to the air pollution sources.

The main aims of the present study are to identify $PM_{2.5}$ levels in (HIE) and to compare the recorded averages of $PM_{2.5}$ with the Jordanian standards JS 1140/2006. It aims also studying the impact of pollution controlling parameters, such as temperature, humidity and wind on the behavior of pollution (Ministry of Environment Reports unpublished between 2010 -2016).

2. Methodology

2.1. Study Site

With aim of assisting Jordanian economic development, in March 1998 the Trade Representative of the United States established the Al-Hassan Industrial Estate in Irbid city, north Jordan as the initial Jordanian Qualifying Industrial Zone QIZ, (Figure 1). The (HIE) is the largest QIZ in the Kingdome of Jordan which is located in Irbid Governorate, 72 Km north of Amman the capital. The HIE is established in 1991 and in 1998 was designated as the first QIZ in the world and Developed in three phases with a total area of 117.8 ha. Furthermore, it accommodates more than 101 industries with a total invested capital of more than JD 222.5 million creating 16440 Job opportunities (Amman Chamber of Industry, 2013).

2.2. Monitoring Procedures

Ministry of environment,based on its mandate, signed agreement NO. 75/2008 with air studied division energy, water and environmental consultations and projects of the royal scientific society to study the ambient air quality of industrial states including the HIE. Therefore, careful equipment selection, methods development and testing and thorough quality assurance and quality control (QA & QC) procedures are essential for producing reliable and comparable $PM_{2.5}$ data (Tu *et al*., 2007). Hence, Air monitoring station (2m X 2.5m X 3m) was placed on a concrete mat (3m X 4m) and provided with special instruments. The station is designed to provide continuous measurement of $PM_{2.5}$ using Beta – Attenuation analyzer. Additionally, meteorological parameters, such as temperature, wind direction, relative humidity and wind speed were also measured. Continuous automatic measurements of all identified parameters have been made every five minutes for the periods of 2010 through 2016 (Ministry of Environment Reports unpublished between 2010 -2016).

It is worth to mention that the monitored data have been received daily by the air studies division via telecommunication system, which were transferred to data analysis software accessible by Ministry of environment via internet (Ministry of Environment Reports unpublished between 2010 -2016).

2.3. Statistical Analysis

On hourly, daily, monthly and yearly scales obtained from unpublished sources conducted by both Ministry of Environment and RSS. The statistical Package for Social Sciences (SPSS) version 22 was used to analyze the data. Two types of statistical analysis will be used, namely the descriptive and inferential statistics. Descriptive statistics, such as average, standard deviation, Median, the interquartile range (IQR), Pie chart and lines charts. While inferential statistics, such as 95% confidence interval for the mean and kruskal-wallis test were used.

3. Results and Discussion

3.1. Statistical Characterization of Air Pollutants

Monitoring results shows that the yearly average concentration was 28.69 (µg)/m^3, Table 1. Whereas the Monthly average concentration was 28.56 (µg)/m^3, Table 2. The highest monthly rate is a record for the month of August 2013, it reaches 36.54(µg)/m^3, Table 3.

Figure 1. Location map of HIE

Table 1. Yearly average, standard deviation, median, IQR and 95% confidence interval for the $PM_{2.5}$ levels in HIE

Year	Average	St.Dev.	Median	IQR	95% Confidence Interval	
					Lower	Upper
2010	37.1035	80.8942	21.875	20.5057	22.6727	51.2753
2011	29.5972	23.8388	31.8201	14.6852	26.36261	32.54097
2012	23.9463	18.7919	23.820	17.1134	20.77615	26.82021
2013	39.7714	49.4184	29.140	24.5175	28.09758	50.20544
2014	26.5690	3.1596	27.0491	0.8992	25.24753	27.80115
2015	23.0492	46.7258	16.410	15.6265	16.25825	29.42693
2016	22.2041	25.9953	20.590	13.4780	17.57633	26.36342
Overall	28.6929	41.8811	26.23	16.750	22.40650	34.04152

Table 2. Monthly average, standard deviation, median, IQR and 95% confidence interval for the $PM_{2.5}$ levels in HIE

Month	Average	Std. Dev.	95% Confidence Interval	
			Lower	Upper
January	24.0381	19.0896	22.69030	25.38776
February	24.8819	23.6027	21.80771	28.07834
March	29.0672	37.5579	25.25550	31.58773
April	23.7215	31.6786	21.68449	25.75884
May	25.8802	29.9985	21.68449	25.75884
June	29.4490	31.3732	23.74753	28.01118
July	33.2296	44.4486	31.04164	35.41965
August	36.5494	86.7679	31.11956	41.97980
September	30.9106	57.2160	24.25743	37.56323
October	29.8027	37.3931	27.10813	32.49639
November	28.2640	18.8436	26.81223	29.71444
December	26.9519	25.3761	25.24194	28.66128
Overall	28.56212	36.9455	25.20121	30.86855

Table 3. Descriptive statistics and 95% Confidence interval (C.I) of $PM_{2.5}$ levels by month and year at HIE

Month		Year													
		2010	C. I	2011		2012		2013		2014		2015		2016	
Jan	Mean	-		36.20		20.181		23.412		27.862		22.945		13.626	
	St.Dev	-		34.03	(33.71, 38.69)	11.965	(19.32, 21.04)	13.262	(22.46, 24.37)	0.0442	(27.85, 27.86)	10.526	(22.19, 23.70	17.705	(12.35, 14.9)
	Min	-		12.87		0.050		0.030		27.790		0.000		0.000	
	Median	-	-	33.25		19.085		23.200		27.860		26.010		9.015	
	Max	-		804.5		67.19		74.92		27.940		77.180		138.19	
	IQR	-		0.08		21.605		18.513		0.0800		8.770		11.997	
	Feb.	-		33.120		23.699		20.876		27.717		28.90		15.359	
		-		0.0401	(33.12, 33.12)	21.539	(22.10, 25.30)	17.182	(19.57, 22.18)	0.0399	(27.71, 27.7)	45.06	(25.49, 32.31)	19.061	(13.94, 16.76)
		-	-	33.050		0.190		0.060		27.650		0.00		0.350	
		-		33.120		21.275		17.00		27.720		19.90		11.48	
		-		33.19		234.68		129.13		27.790		348.95		204.35	
		-		0.060		21.64		19.91		0.0700		19.88		12.365	
	March	52.30		30.402		30.85		24.112		27.571		21.374		16.862	
		83.28	(46.32, 58.28)	8.382	(29.80, 31.01)	38.89	(28.06,33.64)	11.181	(23.31, 24.92)	0.0442	(27.56, 27.57)	8.843	(20.74, 22.01)	19.582	(15.45, 18.27)
		0.00		0.100		0.09		0.160		27.490		0.070		0.090	
		24.20		32.97		24.16		29.350		27.570		25.780		11.655	
		1036.6		33.050		287.07		152.110		27.650		70.580		240.790	
		41.56		0.070		19.19		14.068		0.0800		11.445		16.185	
	April	32.27		18.524		22.765		25.34		27.421		17.673		22.06	
		54.15	(28.31,36.23)	17.350	(17.26,19.79)	10.346	(22.01,23.52)	45.87	(21.98,28.69)	0.0427	(27.42,27.42)	23.943	(15.92, 19.42)	29.30	(19.92, 24.20)
		0.01		0.000		0.150		0.66		27.350		0.070		0.01	
		16.91		14.350		22.760		16.38		27.420		13.795		13.27	
		588.80		138.00		61.650		589.15		27.490		439.880		309.76	
		19.23		016.50		16.587		19.03		0.0800		12.603		16.15	
	May	29.57		25.13		24.376		37.49		27.271		20.522		16.793	
		50.05	(25.97, 33.17)	41.62	(22.14, 28.12)	14.388	(23.3, 25.41)	34.45	(35.015, 39.1)	0.0442	(27.27, 27.28)	12.150	(19.65, 21.40)	16.190	(15.63, 17.96)
		0.25		1.00		1.090		1.47		27.190		0.070		0.040	
		15.72		18.70		25.075		29.13		27.270		19.800		13.420	
		501.20		552.80		181.03		505.80		27.350		82.170		250.710	
		15.74		19.48		16.535		16.14		0.0800		13.757		16.415	

Month	Year											
	2010	C. I	2011		2012		2013		2014		2015		2016	
June	22.57 29.46 0.01 14.89 379.60 13.21	(20.42, 24.72)	25.190 20.639 0.000 23.25 275.20 20.505	(23.68, 26.70)	30.719 0.0427 30.650 30.720 30.790 0.0800	(30.72, 30.72)	61.05 64.33 0.01 44.14 567.7 44.59	(56.35, 65.75)	27.120 0.0427 27.050 27.120 27.190 0.0800	(27.12, 27.12)	16.904 11.254 0.030 14.735 78.180 13.725	(16.08, 17.73)	22.589 7.907 0.000 23.530 81.750 0.070	(22.01, 23.17)
July	25.88 39.27 0.38 19.23 483.90 15.10	(23.06, 28.70)	30.698 24.775 0.000 32.30 244.30 18.175	(28.92, 32.48)	30.472 2.009 11.570 30.570 61.340 0.0800	(30.33, 30.62)	74.22 93.50 0.75 59.09 1664.3 61.36	(67.50, 80.94)	26.970 0.0442 26.890 26.970 27.050 0.0800	(26.97, 26.97)	15.419 12.637 0.130 12.615 186.050 16.387	(14.51, 16.33)	28.950 25.671 0.000 23.40 151.71 13.887	(27.11, 30.79)
August	88.93 208.38 1.04 33.95 1528.10 24.57	(73.96, 103.9)	30.31 29.53 0.00 32.17 351.10 17.75	(28.19, 32.43)	21.038 9.442 0.150 20.185 60.600 12.267	(20.36, 21.72)	46.32 59.95 0.80 34.96 989.10 29.38	(42.01, 50.63)	26.817 0.0443 26.740 26.820 26.890 0.0800	(26.81, 26.82)	16.935 24.866 0.060 12.950 459.890 12.063	(15.15, 18.72)	25.487 20.975 0.160 23.210 140.890 8.578	(23.98, 26.10)
September	25.985 17.101 2.950 26.130 179.900 18.660	(24.74, 27.23)	30.353 21.648 0.100 32.03 218.30 16.105	(28.77, 31.93)	17.514 8.310 0.120 15.950 63.730 9.567	(16.91, 18.12)	46.48 32.51 4.88 38.47 244.50 34.88	(44.11, 48.85)	26.667 0.0429 26.590 26.670 26.740 0.0700	(26.66,26.67)	52.40 140.95 0.19 16.60 1314.27 19.16	(42.1, 62.70)	16.971 8.190 0.320 16.20 54.230 11.780	(16.37, 17.57)
October	31.40 44.41 4.29 18.62 680.60 20.25	(28.21, 34.59)	32.417 23.440 0.200 31.86 154.45 16.275	(30.73, 34.10)	24.57 32.75 0.40 19.80 640.87 14.39	(22.22, 26.92)	48.83 64.94 7.21 34.96 1028.9 30.88	(44.16, 53.50)	26.516 0.0443 26.440 26.520 26.590 0.0700	(26.51, 26.52)	21.216 25.461 0.420 14.495 255.970 15.010	(19.37, 23.05)	23.67 28.59 0.59 22.03 517.5 9.44	(21.62, 25.72)
November	27.466 25.029 0.350 20.20 186.400 17.905	(25.64, 29.29)	32.246 17.395 1.500 31.74 166.30 0 0.110	(30.97, 33.52)	21.239 12.444 0.100 19.800 114.330 17.395	(20.33, 22.15)	39.815 20.943 7.840 34.665 173.200 21.407	(38.28, 41.34)	26.366 0.0429 26.290 26.370 26.440 0.0700	(26.36, 26.37)	22.720 19.610 0.000 23.440 181.360 13.680	(21.29, 24.15)	27.997 18.642 0.260 25.375 204.15 18.335	(26.64, 29.36)
December	33.367 11.882 4.740 33.41 140.20 00.078	(32.51, 34.22)	30.522 4.750 0.270 31.62 31.700 00.080	(30.18, 30.86)	19.799 12.972 0.730 16.900 86.770 20.560	(18.87, 20.73)	27.921 3.808 5.170 28.01 79.480 0.080	(27.65, 28.19)	20.683 8.794 0.660 26.23 71.390 13.078	(20.05, 21.31)	20.71 28.68 0.47 13.34 296.81 11.58	(18.65, 22.77)	35.67 54.83 0.02 22.60 525.79 0.09	(31.73, 39.61)

The Jordanian standard for annual average $PM_{2.5}$ is 15µg/m^3. Figure 2 shows that there is an exceeding for the Jordanian standards limits 1140/2006 for all the years' record.

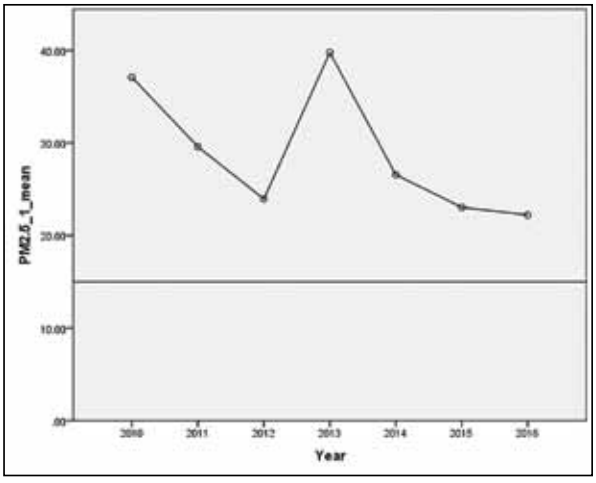

Figure 2. Yearly $PM_{2.5}$ levels at the monitoring site (March 2010 – December 2016)

Figure 3 and Table 4 illustrate the average hourly $PM_{2.5}$ concentration. It can be readily seen that the highest hourly $PM_{2.5}$ reading occurs during peak traffic movement around (9-10am) in the morning and (4-5 pm) in the evenning.

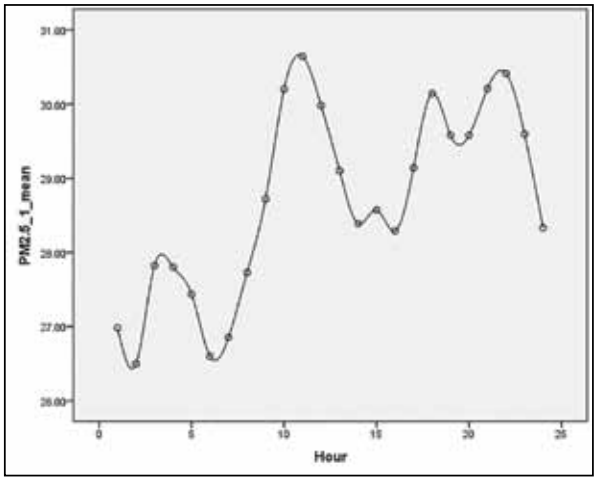

Figure 3. Yearly $PM_{2.5}$ levels at the monitoring site (March 2010 – December 2016)

Table 4. Descriptive statistics and 95% Confidence interval (C.I) of $PM_{2.5}$ levels by hours at HIE

Hour	Average	St.Dev	Min	median	Max	IQR	Confidence Interval 95%	
							Lower	Upper
1	26.9802	35.199	0	26.090	760.34	16.542	25.599	28.360
2	26.5016	40.197	0	24.945	885.30	17.412	24.925	28.078
3	27.8247	56.545	0	24.825	614.00	17.072	25.607	30.042
4	27.8004	58.450	0	23.685	499.30	17.525	25.508	30.092
5	27.4371	56.423	0	23.565	562.41	17.205	25.224	29.649
6	26.5999	41.331	0	23.550	563.28	17.242	24.979	28.220
7	26.8571	39.148	0	23.685	680.60	17.187	25.321	28.392
8	27.7316	37.283	0	25.610	1059.3	17.570	26.269	29.193
9	28.7197	34.829	0	26.390	1422.2	16.737	27.353	30.085
10	30.2009	46.114	0	26.620	951.60	16.277	28.392	32.009
11	30.6443	47.364	0	26.560	863.10	16.430	28.786	32.501
12	29.9824	43.755	0	26.520	760.34	17.042	28.266	31.695
13	29.1011	38.382	0	26.280	885.30	17.097	27.595	30.606
14	28.3909	36.200	0	26.260	614.00	17.382	26.971	29.810
15	28.5711	36.201	0	26.295	499.30	17.007	27.151	29.990
16	28.2904	28.814	0	26.315	562.41	16.790	27.160	29.420
17	29.1407	29.793	0	26.355	563.28	16.332	27.972	30.309
18	30.1429	33.646	0	26.545	680.60	15.902	28.823	31.462
19	29.5804	31.635	0	26.515	1059.3	15.540	28.339	30.820
20	29.5782	32.782	0	26.670	1422.2	15.167	28.292	30.863
21	30.2102	44.929	0	26.600	951.60	15.037	28.448	31.972
22	30.4159	56.269	0	26.550	863.10	15.557	28.209	32.622
23	29.5963	42.168	0	26.535	760.34	16.052	27.942	31.250
24	28.3319	36.210	0	26.320	885.30	15.897	26.911	29.752

Regional dust events and local soil erosion cause high $PM_{2.5}$ readings and the station record high dust measurements during regional dust storms. Figure 4 shows that the highest daily $PM_{2.5}$ concentration was around 36.75 µg/m^3 and 34.94 µg/m^3 occurred on 10 th and 20th day, respectivly. This is due to the widespread dust event as well as emissions emanated from local sources including motor vehicles, light industry and domestic heating that lead to high $PM_{2.5}$ readings.

The days in the Table 5 suggest a slightly difference between working and nonworking hours averages. In order to see whether difference is a real, we conducted a statistical hypothesis using the Kruskal-Wallis test. The test produced a statistic value 18.66 with one degree of freedom. The corresponding P-value is 0.00, which refers to highly significant test. So, at 5% level of significance, we conclude that the average $PM_{2.5}$ levels are higher in working hours than in nonworking hours.

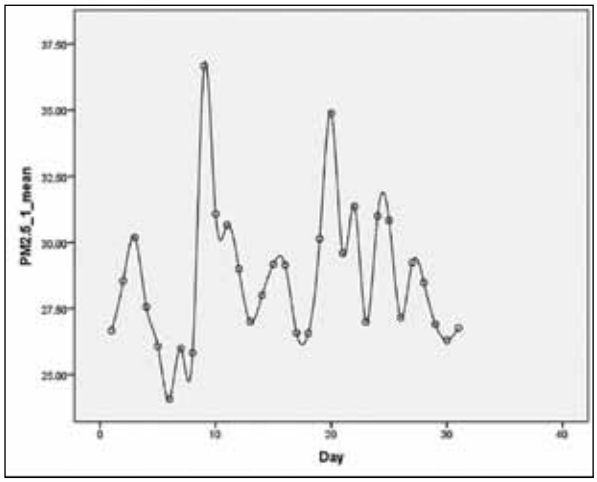

Figure 4. Daily average of $PM_{2.5}$ levels at the monitoring site (March 2010 – December 2016)

Table 5. Descriptive statistic and 95% confidence intervals for $PM_{2.5}$ levels by day status

Working Status	Average	.St. Dev	Min	Max	Median	IQR	Confidence 95% Interval	
							Lower	Upper
Working hours	29.07	39.18	0	1664.3	26.36	17.05	29.073	29.582
Non working hours	28.47	43.42	0	1528.1	26.02	16.52	28.026	28.906

Pronounced monthly variation of $PM_{2.5}$ concentrations showed that $PM_{2.5}$ concentrations were generally higher in the summer months compare with winter months. This might be attributed to the prevailing Khamasin winds, which become active in spring (first peak), where as the second peak it might be because of the low average of rainfall and the lack of humidity, thus helping the increase of the suspended air in the atmosphere (Figure 5).

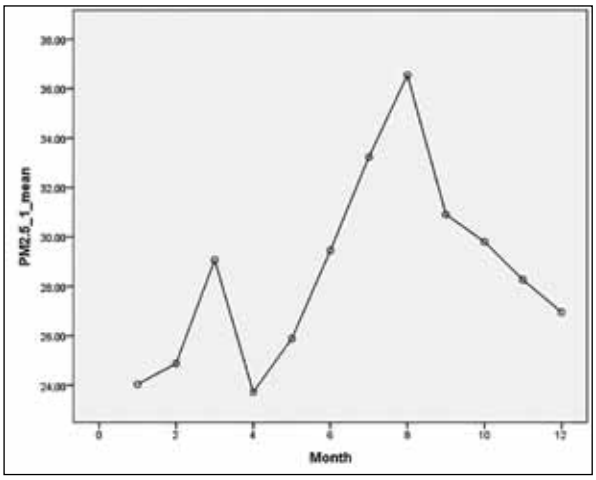

Figure 5. Monthly average of $PM_{2.5}$ levels at the monitoring site (March 2010 – December 2016)

3.2. Meteorology Effect

Meteorological factors, such as wind speed and precipitation, play an important role in determining the pollutant levels for a given rate of pollutant emission. The residence in the atmosphere and the formation of secondary pollutants is controlled not only by the rate of emission of the reactants into the air from the source, but also by meteorological factors wind speed, air temperature and precipitation, (Tayanc, 2000; Singal and Prasad, 2005).

3.2.1. Relative Humidity Effect

Humidity is considered among the meteorological factors that decrease the percent of pollutants concentration. The percent of humidity differs during the period of measurements. As we can see from Figure 6, the concentration of $PM_{2.5}$ in the atmosphere are greatly affected by relative humidity. A definite trend is observed between dust concentration and relative humidity. The $PM_{2.5}$ concentration increases as the relative humidity decreases. The lowest yearly average humidity 56.39% was recorded in 2016 and highest yearly average humidity 73.95% was recorded in 2013 see (Tables (6)–(7)). Whereas the lowest monthly average relative humidity of 47.57% which was recorded in May and highest monthly average relative humidity of 78.62% which was recorded in January (Figure 7). A negative relationship between $PM_{2.5}$ concentrations and humidity, the more relative humidity, the lower the concentration of $PM_{2.5}$. The main reason for this relation is attributed to the role of relative humidity in cleaning the atmosphere's pollutants and the fall of the acid rains.

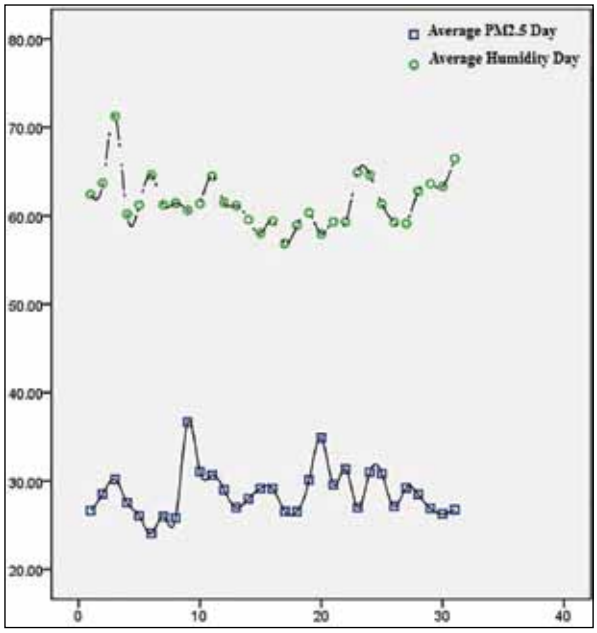

Figure 6. Daily average of humidity and average of $PM_{2.5}$ at the monitoring site (March 2010 – December 2016)

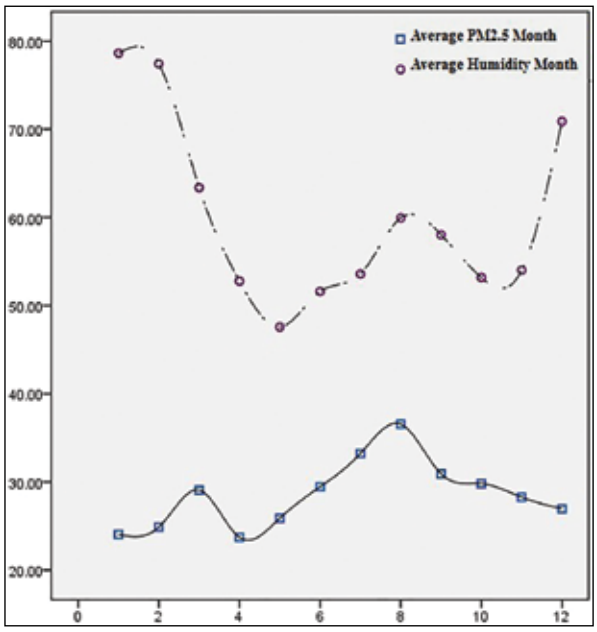

Figure 7. Monthly average of humidity and average of $PM_{2.5}$ at the monitoring site (March 2010 – December 2016)

Table 6. Descriptive Statistics for yearly Relative humidity levels HIE

Year	Maximum	Minimum	Average	Standard deviation
2010	486.53	12.93	56.99	31.63
2011	99.72	14.37	62.73	15.47
2012	98.01	21.07	65.76	18.06
2013	99.35	22.19	73.95	15.75
2014	95.44	21.22	72.87	14.89
2015	88.46	50.79	71.22	12.83
2016	89.42	7.63	56.39	17.75

Table 7. Descriptive statistics for monthly Relative humidity levels in HIE

Month	Maximum	Minimum	Average	Standard deviation
January	99.72	42.05	78.62	11.78
February	486.53	42.59	77.41	39.20
March	97.29	22.21	63.36	16.81
April	92.78	14.37	52.77	19.06
May	73.37	12.93	47.57	14.68
June	68.91	19.07	51.60	12.57
July	68.88	24.55	53.58	9.90
August	73.41	25.75	59.94	9.80
September	75.14	32.31	58.03	10.11
October	86.96	23.46	53.17	15.40
November	98.01	7.63	54.01	23.39
December	94.22	14.79	70.89	16.25

3.2.2. Temperature Effect

The lowest yearly average temperature is 9.42°C, which was recorded in 2015, and the highest yearly average temperature 20.02°C , which was recorded in 2010 (Table 8), whereas the lowest monthly average temperature, 9.08 °C, was recorded in January and highest monthly average temperature 27 °C, was recorded in August, (Table 9).

We found that temperature shows a positive relation between $PM_{2.5}$ concentration and temperature because of the role of the heat in warming up the surface of the earth which warms the air making the air that touch it warm and consequently reducing its density, so it expands and goes upward to be replaced by cold air and so on. This process increases the amounts of the up going air currents and leads to generating more air currents and shaping vertical winds. Thus causing dust and therefore $PM_{2.5}$ increases in the area (Figures 8 - 9).

Table 8. Descriptive statistics for yearly Temperature in HIE

Year	Maximum	Minimum	Average	Standard deviation
2010	92	5	20.02	7.91
2011	32	7	18.03	6.8
2012	30	1	16.09	7.54
2013	21	4	10.70	3.71
2014	19	5	10.01	1.52
2015	13	7	9.42	1.34
2016	32	3	19.14	7.10

Table 9. Descriptive statistics for monthly Temperature in HIE

Month	Maximum	Minimum	Average	Standard deviation
January	15	3	9.08	2.75
February	92	1	10.87	8.32
March	24	2	13.27	4.30
April	28	7	17.46	4.35
May	32	15	21.39	3.28
June	30	21	24.66	2.31
July	32	24	26.96	1.64
August	34	23	27.16	1.76
September	30	21	24.80	1.63
October	30	15	21.92	2.78
November	23	7	15.25	4.01
December	16	6	9.98	2.10

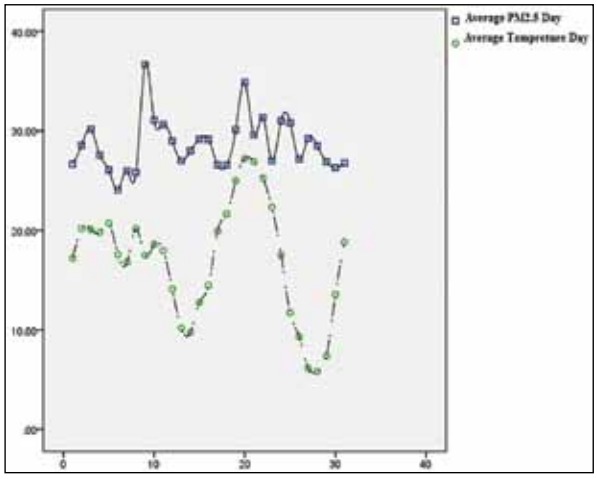

Figure 8. Daily average of Tempreture and average of $PM_{2.5}$ at the monitoring site (March 2010 – December 2016)

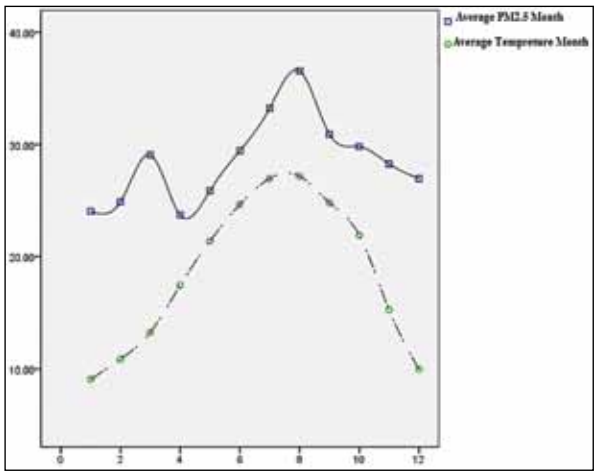

Figure 9. Monthly average of Temperature and average of $PM_{2.5}$ at the monitoring site (March 2010 – December 2016)

3.2.3 Wind Direction Effect

Figure 10 shows the distribution direction of wind during the period March 2010 – December 2016. This figure clearly shows that the calm and North West winds are relatively abundant and subsequently increased pollutants concentration there. Calm has winds increased to 72.23%, and North West winds reach to 10.87%. All together, those winds amounted to 83% a very high degree of wind accumulation that permanently exposes the monitoring site to pollution. This actually means that these winds do not disperse or reduce the emissions; rather they increase their concentration (Al-helou A., 2012).

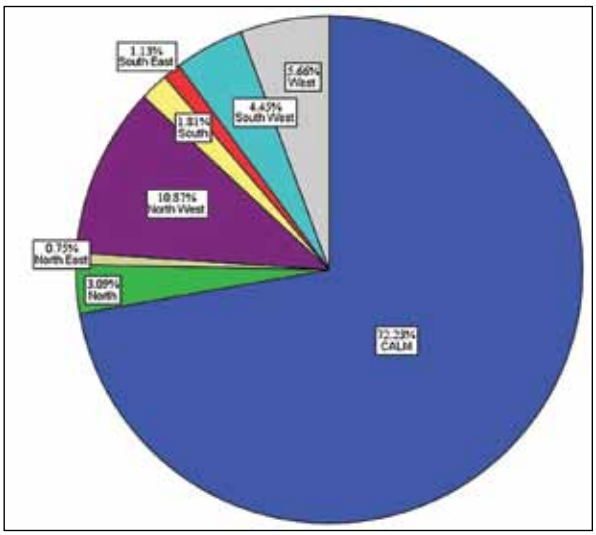

Figure 10. Wind direction at the monitoring site (March 2010 – December 2016)

3.2.4. Wind Speed Effect

Figure 11 shows the distribution of wind speed during the period March 2010 – December 2016. Air tranquility plays an important role in the distance, which the wind may reach, and in its concentration in the surrounding air as well (Al-helou A., 2012). Pollutants are expected to be carried away and diluted during day times with high wind speeds. More than 72.79% of wind blow at speed between 0 –2 m/s. This plays apart in having more concentration in dust in this place were low wind speed cannot carry pollutants for further distance.

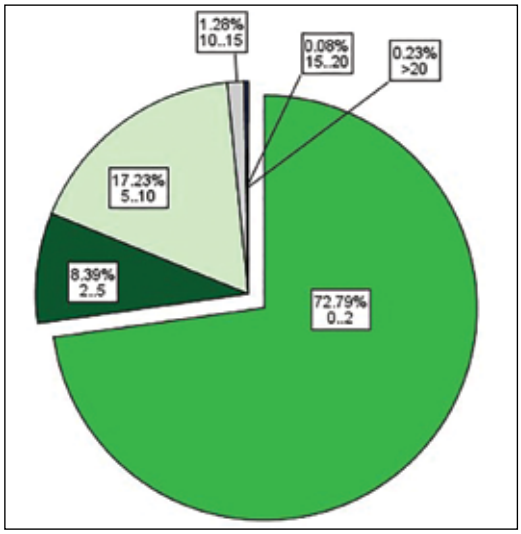

Figure 11. Wind speed distribution at the monitoring site (March 2010 – December 2016)

Conclusions

The results show that the monitoring site in HIE in Irbid has a fairly good air quality throughout most of the year in comparison with the Jordanian ambient air quality standard 1140-2006. The results prove that $PM_{2.5}$ levels are exceeded the permissible of the Jordanian standards ambient air quality limits. Regional dust storms and local soil abrasion contributed to the high $PM_{2.5}$ levels. The most prominent are natural dust from fuel burning, fine particles in stationary, mobile sources and dust emitted from various manufacturing processes in factories located in HIE. This study also shows that the concentration variations in $PM_{2.5}$ are closely related to those in local meteorological conditions (Jaber *et al*., 1997). A positive relationship was found between $PM_{2.5}$ concentrations and temperature, were it shows a negative relationship with humidity. Further, the results show also that calm winds and North West winds reach are the prominent. This actually means that these winds do not disperse or reduce the emissions; rather they increase their concentration (Al-helou, A., 2012). And more than 72.79% of wind blow at speed between 0 –2 m\s. This will play apart in having more concentration in dust in this place. It not possible by any means for low speed winds to carry pollutants for further distance.

Recommendations

Based on the findings, the following are specific recommendations to reduce the potential impacts of pollution in the site:

1. The monitoring process of pollutants in Al Hassan Industrial Estate has many disadvantages, such as changing the sites of the monitoring stations, loss of power, which hinders the data recording process and the discontinuity in recording data made temporal and spatial variability analysis almost impossible.
2. Restricting habitation east and southeast of Al Hassan Industrial Estate and permitting habitation west and northwest by reducing taxes and providing municipal services.
3. Making complete environmental health study including people, soil and water to discover the impact of air pollution on these environmental components.
4. Cooperation between government's research centers and industry will lead to the desired objectives. This is the time to make dialogue between those who make the rules and those who must comply with them.
5. Raising public –awareness and encouraging- public participation in decision making, public awareness has little effect without vigorous dissemination, which could be achieved through public campaigns, promotion of environmental education, and information exchange. This should be as a joint effort between NGOs and government departments. The government should make the flow of information to the public easier and more efficient by establishing service centers (Jaber *et al*., 1997).

Acknowledgment

The researchers are grateful for the staff of the monitoring and assessment directorate at the Ministry of Environment for providing the air quality data necessary for the present study.

References

[1] Al-helou, A., 2012. Mathematical analysis of how the electrical training center site is affected by air pollution, American Journal of Applied Sciences, 9, 1840-1848.

[2] Abu-Allaban, M. and Abu-Qudais. H., 2011. Impact Assessment of Ambient Air Quality by Cement Industry: A Case Study in Jordan. Aerosol and Air Quality Research, 11: 802–810.

[3] Amman Chamber of Industry, 2013 http :// www.aci.org. Jo/ development/en/, www.linkedin.com/company/amman.

[4] Asi, R., Anani, F. and Asswaeir, J., 2001. Studying Air Quality in Alhashemeiah Area/Zarqa, A Report Prepared by the Royal Scientific Association for the General Institution for the Protection of the Environment, Amman, Jordan.

[5] Cohen AJ, Anderson HR, Ostro B, Pandey KD, Krzyzanowski M, Ku¨nzli N, Gutschmidt K, Pope A, Romieu I, Samet JM, Smith K., 2005. The global burden of disease due to outdoor air pollution. J Toxicol Environ Health A 68(13):1301–1307.

[6] Dockery, D.W. and Pope, C.A., 1994. Acute Respiratory Effects of Particulate Air Pollution, Auun. Rev. Publ. Health, 15,107–132.

[7] Elminir, H.K., 2005. Dependence of urban air pollutants on meteorology, Science of the Total Environment, 350, 225–237.

[8] Finlayson-Pitts BJ, Pitts J., 2000. Chemistry of the upper and lower atmosphere: theory, experiments and applications. San Diego: Academic Press.

[9] Jaber, J.O.Probert,S.D. and Bader,O.,1997 .Energy and environmental issues for Jordan. Applied Energy, 57, 45-101.

[10] Jeff, G. and Hans, P., 2004. Assessment of Environmental Impact of the Holcim Cement—Dundee Plant, Ecology Centre, Retrieved October 13, 2007, from http://www. wbsed.org/web/ project/cement/tf5/ holcmm.htm.

[11] Hussein, T., Abu Al-Ruz, R., Petäjä, T., Junninen, H, Arafah, D., Hämeri, K. and Kulmala, M., 2011. Local Air Pollution versus Short–range Transported Dust Episodes: A Comparative Study for Submicron Particle Number Concentration. Aerosol Air Qual. Res. 11: 109– 119.

[12] Ministry of Environment. (2010 -2016). Amman, unpublished annual report

[13] Satsangi, G.S. Satsangi, A., Lakhani, P. R., Kulshrestha and Taneja. A., 2004. Seasonal and diurnal variation of surface ozone and a preliminary analysis of exceedance of its critical levels at a semi-arid site in India, Journal of Atmospheric Chemistry, 47, 271–286.

[14] Seinfeld JH, Pandis SN., 1998. Atmospheric chemistry and physics: from air pollution to climate change.New York: Wiley.

[15] Seinfeld, J. H., and Pandis, S. N., 2006. Atmospheric Chemistry and Physics: from Air Pollution to Climate Change 2nd Edition, John Wiley & Sons, Inc., Hoboken, New Jersey.

[16] Singal, S.P. and Prasad, R., 2005. Analytical Study of some Observed Micro Meteorological Data, J. Air Pollut. Contr., 1, 44–49.

[17] Tayanc, M., 2000. An Assessment of Spatial and Temporal Variation of Sulfur Dioxide Levels over Istanbul, Turkey, Environ. Pollut., 107, 61–69.

[18] Tu, J.,Xia,Z., wang, H and Lia,W., 2007 .Temporal variations in surface ozone and its precursors and meteorological effects at an urban site in China, AtmosphericResearch, 85, 310-337.

[19] U.S. EPA, 1999a. Environment Fact Sheet: Management Standards Proposed for Cement Kiln Dust Waste. Retrieved October 10, 2003, from http://www.epa.gov/ fed.gstr/EPA-AIR/199/Some/Day-14/a12893.htm.

[20] U.S. EPA, 1999b. National Emission Standards for Hazardous Air Pollutants for Source Categories, Cement Manufacturing Industries Federal Register: 64, 113. Retrieved October 10, 2002, from http://www. epa.gov/ fed.gstr/EPA-AIR/199/Some/ Day-14/a12893.htm.

[21] Wang. S., and Hao. J., 2012. Air Quality Management in China: Issues, Challenges, and Options, Journal of Environmental Sciences, 24, 2-13.

[22] Y. Li, 2013. Construction Dust Accounted for 15.8% of PM2.5 Particles, Beijing Authority Reinforce Construction Waste Management.

[23] Zhao,Ji. H., Kong,H.S. Bai ,Z and Han, B., 2013. Seasonal Variation of Inorganic Composition in Ambient Particulate Matter in Tianjin Offshore Area and Its Source Analysis.China Environmental Science, 31, 177-185.

JJEES

Volume 8, (Number 1), Sept, 2017
ISSN 1995-6681
Pages 27 - 34

Jordan Journal of Earth and Environmental Sciences

Electrical Resistivity Tomography Modeling of Vertical Lithological Contact using Different Electrode Configurations

Hani Al-Amoush[1*], Jafar Abu Rajab[2], Eid Al-Tarazi[2],
Abdel Rahman Al-Shabeeb[3], Rida Al-Adamat[3] and A'kif Al-Fugara[4]

[1]Department of Applied Erath and Environmental Sciences, Institute of Earth and Environmental Sciences, Al al-Bayt University, Mafraq, Jordan.
[2]Department of Earth Sciences and Environment, Faculty of Natural Resources and Environmnet, Hashemite University, Zarqa, Jordan
[3]Department of Geographic Information System and Remote Sensing, Institute of Earth and Environmental Sciences, Al al-Bayt University, Mafraq, Jordan
[4]Department of Engineering Survey, Faculty of Engineering, Al al-Bayt University, Mafraq, Jordan

Received 27 May, 2017; Accepted 25 August, 2017

Abstract

In the present study, three different electrical resistivity electrode configurations (Dipole-Dipole, Wenner-Schlumberger, and Wenner configurations) were applied to a geological outcrop that demonstrates a lateral lithological variation at sub-vertical contact. The main target was to examine the intrinsic characteristics of resistivity configurations and consequently to determine the optimum one that has to be selected in such a geological environment. The results of resistivity models provided comparable tomograms at different number of accepted quadripoles and varied RMS%. Based on statistical fitting criteria between four simulated tomograms and three measured inverted tomograms, the inversed twelve data sets produced for three resistivity configurations are capable of defining vertical and horizontal structures with varied sensitivity and fitting values. In particular and according also with known geological outcrop's dimension and lithological layers, Dipole-Dipole resistivity tomogram can be considered as the most sensitive configuration to localized and extended conductive structure at the highest correlation coefficient. On the other hand, Wenner-Schlumberger and Wenner tomograms based configurations can resolve localized horizontal conductive layer beneath resistive layer. In particular, the high resistivity contrast for geoelectrical layers allowed producing similar resistivity tomograms down to 20 m depth.

© 2017 Jordan Journal of Earth and Environmental Sciences. All rights reserved

Keywords: Electrical Resistivity Tomography (ERT), Geological outcrop, Modeling and Inversion.

1. Introduction

Electrical Resistivity Tomography (ERT) has become a powerful method to investigate subsurface shallow structures and geology for various environmental and engineering applications. ERT has been largely used to investigate faulting in shallow subsurface to depths of few tens of meters (e.g., Seminsky et al., 2016; Olenchenko and Kamnev, 2014; Carbonel et al., 2013; Improta et al., 2010; Reiser et al., 2009). In ERT method, the apparent resistivity can be measured by using different electrical configurations. Several electrical configurations have been widely used for various geological applications, e.g., the Schlumberger configuration has been used for Landfill investigation (Monier-Williams et al., 1990) and for hydro-geological purposes (Al-Amoush, 2006). For deep exploration using pole-dipole configuration (Alfano, 1974). The Dipole-Dipole configuration was used for measuring earth conductivity (Alpine et al., 1966). The Gradient configuration was used for veins investigation (Furness, 1993). The Square Array techniques was used for resistivity measurements and fractures distribution (Habberjam, 1979). The Null and Collinear configuration were used to investigate near surface karstic fractures (Szalai et al., 2002; Szalai et al., 2004). The surface and cross-hole resistivity tomography were used to detect foundations of archaeological structures (Tsokas et al., 2011). The Equatorial and Schlumberger configuration were used jointly for groundwater investigation (Zohdy, 1969). Brass et al. (1981) conducted resistivity profiling survey over a graphite deposits utilizing three different electrode arrays (Single pole, Half-Wenner and Half-Schlumberger), the study showed that half-Schlumberger configuration prove to be the most reliable array among others since it shows fine details which were not shown by the other configurations.

A valuable review geophysical study provided a classification of the surface geo-electrical configurations through collecting more than one hundred different independent geoelectric configurations from published geophysical literature (Szalai and Szarka, 2007a; Szalai and Szarka, 2007b). This classification was based on three parameters: superposition of measurements, focusing of currents and co-linearity of configuration producing eight classes of electrical configurations (Szalai and Szarka, 2007a). Wenner and Dipole – Dipole configurations are the most widely used and the others are of less frequently used among possible electrical resistivity configurations (Szalai and Szarka, 2007a). Each of electrical configurations has its advantages and disadvantages in terms of signal strength, vertical / horizontal resolution and data coverage (Table 1)

* Corresponding author. e-mail: hani.alamoush1@gmail.com

(Loke, 2014). Wenner and Wenner-Schlumberger arrays have a moderate depth of investigation and strong signal strength, which permits to be relatively sensitive to vertical variations in the subsurface, but it has less sensitivity to horizontal variations in the substratum. Dipole-Dipole array has better horizontal data coverage but weak signal strength at a greater depth, which makes it the most sensitive to horizontal variations and relatively insensitive to vertical variations of the substratum. A discussion on the properties of different arrays can be found in (Dahlin and Zhou, 2004; Zhou and Dahlin, 2003).

The objective of the present study is to carry out three different electrical resistivity tomography configurations (ERC) over a geological section exhibiting lateral and sharp lithological sub-vertical boundary. The electrical resistivity configurations used in this study are Dipole-Dipole (DD), Wenner-Schlumberger (WS) and Wenner (W) configurations (Figure 1). The choice of ERC configurations was basically built on their wide-varied sensitivity and intrinsic characteristic to geological materials (Table 1). Consequently, to determine the optimum electrical configuration that would be applied in such geological environment. The ERC profiles' azimuth are mainly constrained only to consider the effect of two-dimensional (2D) geological structure, where the lithology is changing abruptly along survey line, and in medium assumed of high- resistivity contrast. Furthermore, statistical investigations are demonstrated at the level of experimental modeled data and for synthetic modeled data. These models data were tested and analyzed for the three ERC models at different geological scenarios. The present study is incorporate a real data measurements and synthetic data modeling collected from Jordan.

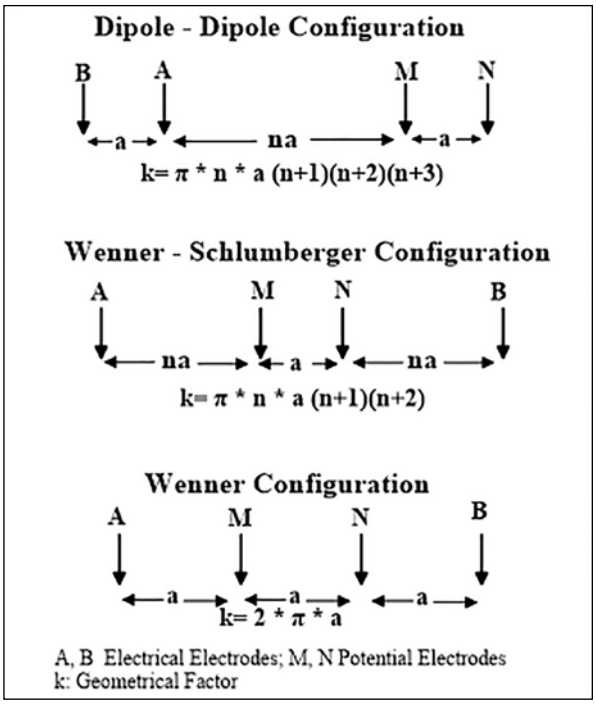

Figure 1. Electrical electrodes configurations used in this study

Table 1. 2D resistivity configurations and survey characteristics, four stars implies the most effective and one star is the least effective (Loke, 2014)

Configuration / Characteristics	Dipole - Dipole (DD)	Wenner - Schlumberger (WS)	Wenner (W)
Sensitivity of the array horizontal structures	*	**	****
Sensitivity of the array vertical structures	****	**	*
Depth of investigation	***	**	*
Horizontal data coverage	***	**	*
Signal Strength	*	***	****

1.1. Description of Study Area

The investigated site is located along Amman - Irbid Highway with coordinates [35.84916º] E, [32.15815º] N according to WGS 1984 coordinate system (Figure 2). The height of the exposure reaches about 14-17m. The site is located at an altitude of 500 masl, and at a distance of 1 km to the south of Philadelphia Private University. The site shows a sharp contact and a pronounced lateral variation in lithology. A nearly sub-vertical contact is cutting the outcrop into two parts. The outcrop consist of two main geological rock types; the northern part consists of a sequence of hard limestone, marly limestone and a weathered top zone, but the southern part of the exposure consists of transported soft sediments and soil material overlying a basal zone of weathered conglomerate and gravel to the lower south (Figure 2).

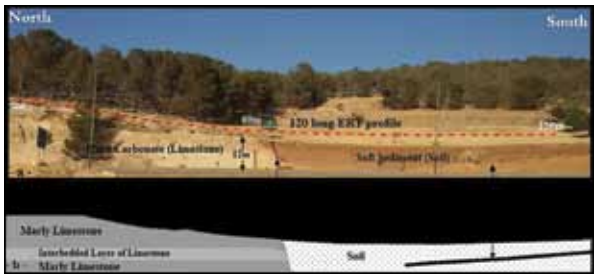

Figure 2. a- Field photo shows an exposure of study site and the extension of ERT survey line, **b-** An illustration of lithological description and the sub-vertical lithological contact. The thick dark black line illustrates the contact between the basal conglomerate, the transported soft sediments and soil material.

2. Materials and Methods

2.1. Survey Design and Instrumentation

In the present study, 2D Electrical resistivity tomography surveys (2D-ERT) were conducted long 120 m, using a multichannel system of 24-electrode with an inter-electrode spacing of 5m, along profile in North- South direction. The designed profile was extended normal to the strike of the fault structure, as shown in Figure (2).

The SYSCAL R-1 resistivity meter (IRIS Instruments, France) was used to survey the area using several electrical resistivity configurations. The multichannel system operates automatically once the type of electrical configuration and geometrical parameters are defined. The system has an internal microprocessor controlled together with electronic automatic switching unit used to recording independently a

hundred of resistivity data (Loke, 2014). Electrical resistivity tomography is usually performed using 24-electrode or more, connected together with a multi-core cable (Griffiths and Barker, 1993; Reynolds, 2011). After instrumentation and field setup, resistivity measurements are automatically recorded and saved in resistivity meter system.

The sequence of measurements, such as type of configuration, survey parameter and electric current duration, can be set manually at the field or prepared preliminary and transferred to microprocessor of the system using laptop. The 2D electrical resistivity tomography survey was carried out using Wenner, Dipole-Dipole and Wenner-Schlumberger configurations. ELECTRE PRO software was used to create the measurements sequence, and PROSYS II was used to download, edit and filter the stored data after field survey completion.

2.2 Data Quality and Error Sources

Resistivity measurements are routinely subjected to systematic errors resulting from insufficient current injection due to the high electrode-ground contact resistance. Further minor effects are commonly resulted from different sources, e.g., electrode polarization and position, inductive and capacitive coupling of wired system of instrument, and external low frequency currents effects (Zhou and Dahlin, 2003; Dahlin and Leroux, 2012).

The presentation of resistivity pseudo-sections of three different configurations enables to investigate the noise of each data level (quadripoles datum). SYSCAL R-1 resistivity-meter introduces a quality factor that based on the estimated Standard Deviation (SD) (i.e., known also as the repeatability error). The instrument calculates the resistance (R=V/I) for each datum up to six stacking. In the present study, the standard deviation of the (V/I) ratio was set to be less than 5% at two seconds current pulse length. The presented pseudo-sections for three configurations showed unsystematic character for resistivity data level at poorly performing electrodes. Many of noisy data were associated with the threshold value of received voltage Vp (< 5 mV) (Table 2). Generally, we rejected data and determined the cut off margin of at which SD is more than 5%. Nevertheless, the vast majority of stacking errors have reached 1% of their SD value (see average SD in Table 2).

Table 2 lists the statistical summary of the processed measured parameters for three ERC profiles, including the accepted and rejected quadripoles and their statistical annotations; maximum, minimum, mean, and standard deviation values for different acquiring parameters.

Table 2. Statistical summary of the processed measured parameters for three resistivity configurations

Noise %	Quadripole (accepted/ acquired)	Average Standard deviation (quality factor, in %)	Vp (mV) (Min/Max)	Average measured primary voltage Vp (mV):	Average Injected current intensity (mA)	Average Injected voltage (V)	Average grounding resistance value of the injection dipole (in kOhm)	Resistivity Configuration
5.8	195/207	0.6	92/575	98	148.2	371.9	16.4	Dipole-Dipole (DD)
28.3	367/512	0.8	17/23.6	11	20.6	202.1	28.1	Wenner-Schlumberger (WS)
5	76/84	0.6	6/18	12.1	17.9	202.0	31.8	Wenner Array (W)

2.3. Forward Modeling and Inversion

In designing Electrical Resistivity Tomography survey line, forward modeling is commonly used to investigate the possibility of creating ground resistivity models such that the measured ERT data can be better interpreted and explained prior inversion procedure. According to Dey and Morrison (1979), the measured or simulated electrical potential divided by applying electrical current provided between pairs of electrodes allow to calculate resistivity values at different datum based on equation (1):

$$\nabla \cdot \sigma \nabla \phi = I\,\delta(x - xs, y - ys, z - zs \quad \text{.....(1)}$$

where

σ is the electrical conductivity, an intrinsic property of the material;

φ is the electrical potential;

I is the electrical current source;

δ is the Dirac delta function;

x ,y, z are the spatial position vectors; and

xs, ys, zs are the spatial coordinates of the current source.

The modeling procedure of 2D resistivity measurements is commonly solved based on Finite-Difference (FD) or Finite-Element (FE) solution of the electrical resistivity. In the present study, a forward modeling calculation implemented by RES2DMOD software (Loke, 2014) using the Finite-Element (FE) mesh method in order to calculate the two-dimensional resistivity distribution. The measured data for the three conducted ERT profiles anticipated to create four synthetic models using three different configurations (Figure 1) and provide insight into the possibility of resolving power of different survey geometries at different geological structures.

The resistivity data are inverted to create a model section of the area under the investigated ERT line. Owing to resistivity distribution of three conducted data sets, the resis¬tivity inversion procedure entails the Robust Data Constraint (L1-norm), which is commonly applied to emphasize the boundary between soil and the bedrock or vertical fault contacts. In addition, it is used to minimize the effect of outliers in the data (Loke, 2014). The inversion problem is solved to determine the resistivity of the discretised cells that will minimize the difference between calculated and measured apparent resistivity values (Loke et al., 2003). Applying the inversion setting to observed data requires the use of regularization to solve the non-linear inversion problem and to produce a stable solution for the ill-posed problem. Therefore, the measured ERT sections are processed and inverted to produce a unique smooth model with proper resolution according to

the optimization equation proposed by Loke (2014):

$$(\mathbf{J^T J} + \lambda \mathbf{F_R})\mathbf{\Delta q_K} = \mathbf{J^T R_d g} - \lambda \mathbf{F_R}\, \mathbf{q_K} \quad \text{.....(2)}$$

with $\mathbf{F_R} = \alpha_x \mathbf{C_x^T R_m C_x} + \alpha_z \mathbf{C_z^T R_m C_z}$,

$\mathbf{\Delta q_K}$ represents the change in the i-th model response due to changes in the j-th model parameter, is the Jacobian matrix (of size m×n) of partial derivatives, and is the transpose of .The factor represents the damping factor, g is the discrepancy vector between the observed data and the model response (i.e., the data misfit error), and Rd and Rm are the weighting matrices introduced so that different elements of the data misfit and model roughness vectors are given equal weight in the inversion process (Loke, 2014). Cx and Cz are the smoothing matrices in the x- and z-directions, respectively, and αx and αz are the relative weights given to the smoothness filters in the x- and z-directions, respectively (Loke, 2014).

The resistivity pseudo-sections for measured and synthetic data were inverted using the RES2DINV software package (Loke, 2014). The inversion parameters were unified and implemented for the three ERT's configurations.

For quantitative comparison criteria, a statistically-based procedure was performed between inverted resistivity data and inverted synthetic resistivity data for the four proposed models of each ERT configuration. The statistical procedure implemented in the present study is a direct link between real resistivity model parameters (inverted resistivity, cell coordinates: Xi and Zi) with synthetic model parameters (synthetic resistivity, cell coordinates: Xi and Zi). So that both models parameters are fixed in model space. The regression line defines the degree of closeness between model parameters. In order to make cross plot fitting and for the reason that the RES2DINV and RES2MOD codes are two independent programs: a quantitative comparisons can be implemented by adjusting the thicknesses of known electrical layers for the measured and synthetic data cells such that they exist in the same location and their corresponding boundaries; this procedure implies that the discretised cells from both models must coincide with the positions of the electrodes.

2.4 Sensitivity Analysis and Inversion Resolution

To gain insight into the reliability and resolving quality of the ERT tomograms in terms of their investigative depth and inversion criteria, the Res2dinv package (Loke, 2010) is used to calculate a models' resolution and sensitivity matrices (Friedel, 2003). During the inversion process of each ERT line, both resolution and sensitivity matrices are computed; the resolution scale can be used to directly indicate the presence of possible artifacts in electrical structures and used to define the depth below which electrical structures do not depend on the measured data but rather result from a poorly resolved inversion process. Moreover, the sensitivity scale achieve semi- quantitative insight into how resolution varies spatially over a tomogram; a cell of high sensitivity values are relatively well constrained by the measured data, whereas low values indicate poorly performing measured data (Oldenburg and Li, 1999).

In the study area, the sensitivity values located in the range between 0.05 to about 2.5 for the domain of three sensitivity tomograms. According to our study area, the outcrop's depth is about 12-15 m, where the resolution value of 0.24 apparently coincides with the depth ranges from 10 to 13 m for W and WS models (Figures 4 and 5). Hence, the value of 0.24 is the line apparently separates poorly performing quadripoles from well-performing quadripoles (i.e., many of rejected quadripoles located below this line). However, the 0.24 resolution line in the DD model denotes a higher depth to about 19 m and it was limited to the north direction of the tomogram (Figure 3). Thus, we consider this resolution line as a reliable depth limit to interpret resistivity structures.

3. Results and Interpretation

The inverted ERT models of three ERT lines converged after seven iterations and yielded root mean square error (RMSE in %) or misfit values for resistivity that are varied with respect to the survey data error (i.e., 5%). Dipole-Dipole resistivity tomogram presented the highest error (13.4%) (Figure 3), whereas the RMSE for Wenner-Schlumberger and Wenner configurations was found to be below 5% (Figures 4 and 5, respectively). In order to make visual comparison among different resistivity tomograms, the resistivity distribution of measured, calculated and inverted data were displayed using a fixed and unified resistivity scale and applied to all resistivity tomograms. Hence, we present the term "resistivity tomogram" to describe the final inversion resistivity model for measured or synthetic data sets.

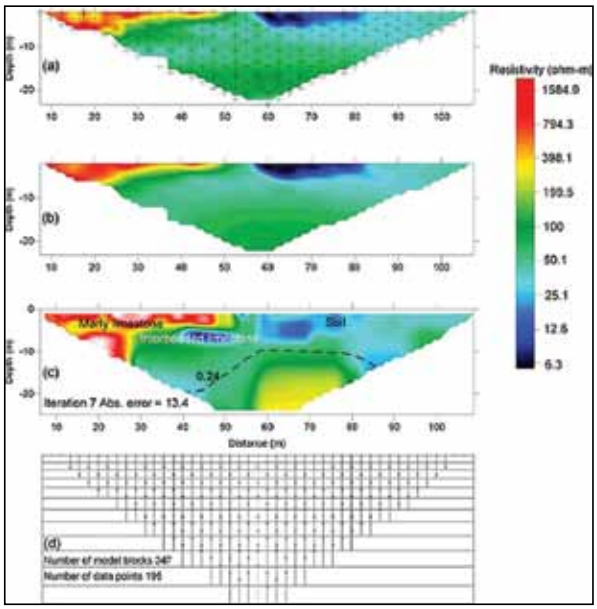

Figure 3. Electrical resistivity model of the Robust inversion using Dipole - Dipole configuration; **(a)** Measured apparent resistivity (pseudo-section) tomogram, **(b)** Calculated resistivity tomogram, and **(c)** The inversion model converged at RMS% = 13.4. Dashed line indicates model sensitivity value, and **(d)** Arrangements of model blocks and resistivity data points.

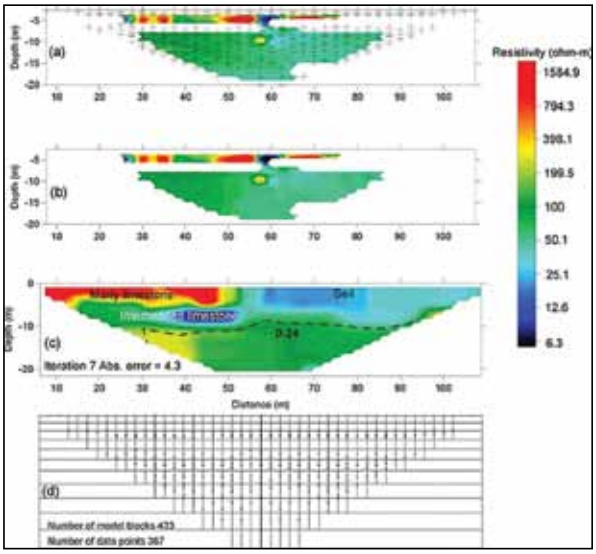

Figure 4. Electrical resistivity model of the robust inversion using Wenner-Schlumberger (WS) configuration; **(a)** measured apparent resistivity (pseudo-section) tomogram, **(b)** calculated resistivity tomogram, **(c)** The inversion model converged at RMS% = 4.3. Dashed line indicates model sensitivity value, and **(d)** Arrangements of model blocks and resistivity data points.

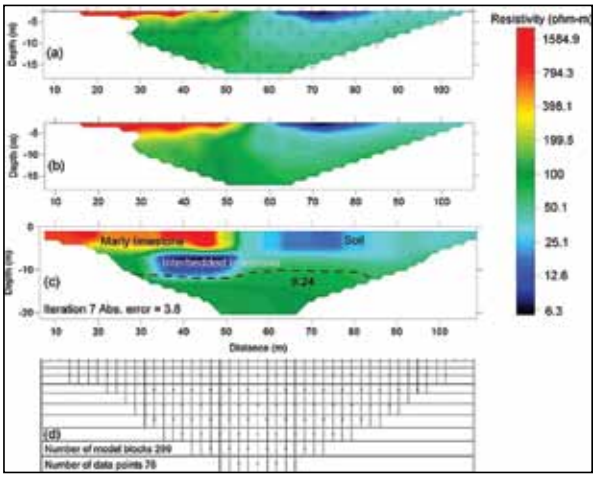

Figure 5. Electrical resistivity model of the robust inversion using Wenner (W) configuration; **(a)** Measured apparent resistivity (pseudo-section) tomogram, **(b)** Calculated resistivity tomogram, **(c)** The inversion model converged at RMS% = 3.6. Dashed line indicates model sensitivity value, and **(d)** Arrangements of model blocks and resistivity data points.

All resistivity tomograms resolved earth's structure down to a depth of 20 m, which exceed outcrop's depth dimension. The number of data points below 0.24 resolution line are varied, and mainly dependent on resistivity configurations (Figures 3, 4, 5; Table 1), however, a 20 m depth seems to be consistent, as all recovered models have approached this range.

The field investigation of the site (Figure 2) shows lateral variation between hard carbonate rock and soft sediments where the sub-vertical sharp contact outlines the boundary between two types of lithology down to 10m depth. The pseudo-sections obtained by (DD) (Figure 3a) and (W) (Figure 5a) demonstrated certain resistivity variation at horizontal distance located between 40 to 60 m, but the (WS) pseudo-section (Figure 4a) did not recognize this anomaly due to many rejected quadripoles at shallow datum (Table 2). As a result, the three resistivity tomograms revealed three resistivity blocks as; hard carbonate layer (~2000 ohm-m), soft sediment (soil) layer (~20 ohm-m) and an unknown (unexposed) layer of 200 ohm-m (Figures 3c, 4c, and 5c).

Additionally, the three resistivity tomograms confirmed the development of a conductive layer of ~10 ohm-m at a depth less than 10 m located below the resistive hard carbonate (limestone) rock. Furthermore, the resistivity contrast across sharp contact has changed and became unclear at the depth located between 6 to 20 m in all resistivity tomogram.

The presented inversion outcomes provide three anomalies that need to be inspected using forward modeling, first, the existence of such conductive layer of ~20 ohm-m at two-setting (i.e., localized or extended horizontal feature), second, the presence of moderate resistivity layer of 200 ohm-m (i.e., extended horizontal feature), third, the continuation of sharp contact down to the tomograms' depth at two-setting (i.e., localized or extended vertical feature).

Therefore, it was possible to develop four synthetic models encompass the possibility to answer the aforementioned cases. Figures 6, 7, 8, and 9 use the measured ERT lines' design in term of electrode spacing, separation, and length. In addition, all synthetic models were included by the domain of two to three resistivity values, such as 20, 200, and 2000 ohm-m, which are related to soft sediment, unexposed layer, and exposed hard rock, respectively. Each synthetic model produces resistivity data for the three applied configurations (i.e., DD, WS, and W), and inverted by applying inversion parameters similar to those used for inversion of measured data. Moreover, each synthetic data set was incorporated by adding 5% Gaussian error. This error value coincides roughly with the error obtained from the associated errors propagated into measured resistivity values (Table 2).

The results of twelve resistivity tomograms rendered resistivity distribution in the domain of measured resistivity scale (see resistivity scale for Figures 3, 4, and 5). This implies that the presentation of resistivity variations by two to three resistivity layers as 20 ohm-m, 200 ohm-m, and 2000 ohm-m is adequate to describe the possible and varied geological setting of the area under investigation.

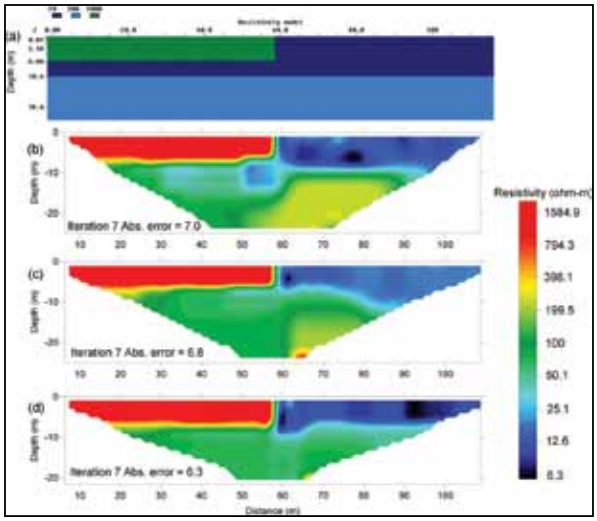

Figure 6. (a) Synthetic model simulating MODEL1 structure based on reference of three –resistivity blocks; conductive layer of ~20 ohm-m at extended horizontal feature. **(b)** Inverted forward model of Dipole-Dipole data. **(c)** Inverted forward model of Wenner-Schlumberger data **(d)** Inverted forward model of Wenner data.

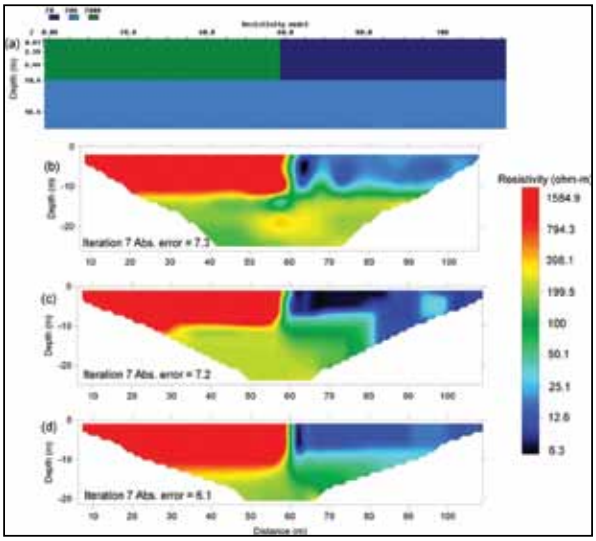

Figure 7. (a) Synthetic model simulating MODEL2 structure based on reference of three –resistivity blocks; moderate resistivity layer of 200 ohm-m of extended horizontal feature and localized sharp contact. **(b)** Inverted forward model of Dipole-Dipole data. **(c)** Inverted forward model of Wenner-Schlumberger data **(d)** Inverted forward model of Wenner data.

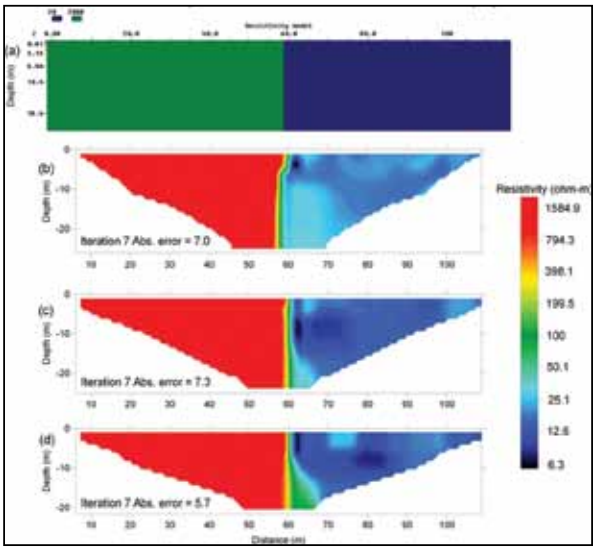

Figure 8. (a) Synthetic model simulating MODEL3 structure based on reference of two–resistivity blocks; sharp contact of extended vertical feature. **(b)** Inverted forward model of Dipole-Dipole data. **(c)** Inverted forward model of Wenner-Schlumberger data **(d)** Inverted forward model of Wenner data.

4. Discussion

The present case study performed shallow resistivity imaging using three different resistivity configurations (DD, WS, and W) applied across an outcrop of 10-15 m thickness at road cut exposure. The geological outcrop consists of sharp sub-vertical contact located between the left-hand exposure composed of hard rocks of limestone and marly limestone and the right-hand exposure composed of soil intercalating with a thin zone of conglomerate and gravel.

The three ERC data sets were classified on the basis of the number of data measurements or quadripoles. The classes revealed three categories as low (W), intermediate (DD), and high (WS) (Tables 1 and 2).

The resistivity models have converged at survey data error (i.e., <5%) particularly for (WS) and (W), and reached

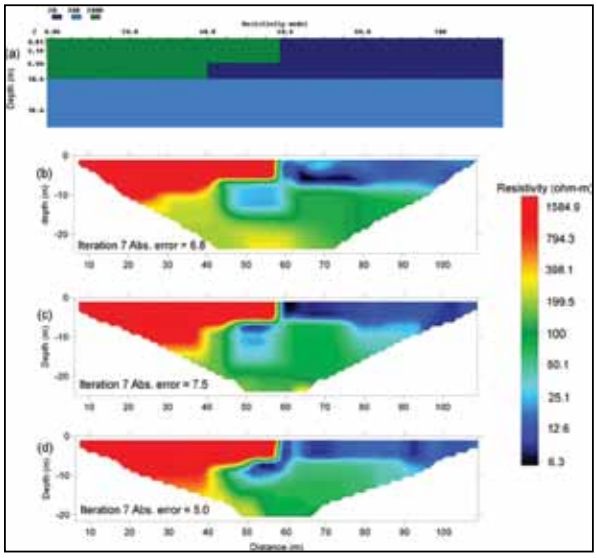

Figure 9. (a) Synthetic model simulating MODEL4 structure based on three reference resistivity; conductive layer of ~20 ohm-m at localized horizontal feature. **(b)** Inverted forward model of Dipole-Dipole data. **(c)** Inverted forward model of Wenner-Schlumberger data **(d)** Inverted forward model of Wenner data.

to about 13.4% for (DD). It should be mentioned here that the high-density data related to near surface quadripoles obtained by (WS) configuration (Figure 3 and Table 2) are mainly attributed to poor performing electrodes due to high resistance of ground surface. Despite the high noisy data involved in (WS) configuration, but the final resistivity model can be comparable to other models. Consequently, the results of inversion show correlated resistivity models although they have different numbers of accepted/rejected quadripoles and varied RMS % (Figures 3, 4, and 5).

In order to test the results at different scenarios recommended for this case study, the pseudo-resistivity section of each ERC allowed to build four electrical models based on resistivity distributions with respect to known geological materials (i.e., up to three resistivity zones), resistivity variations (i.e., 5-2000 ohm-m), and model resolution (i.e., down to 20 m depth). Thus, the modeling procedure permitted to create and synthesize four possible geoelectrical signatures. For example, in Model (1) and Model (4) where the forward modeling tests incorporated a conductive layer (20 ohm-m) (see Figure 6 for interbedded layer of limestone) embedded between the resistive sequences. The conductive layers was treated as an extended and as a localized layer model, respectively (see Figures 6 and 9, respectively). Moreover, Model (2) shows extended horizontal layer of moderate resistivity (200 ohm-m) overlain by two layers demonstrate lateral variation (Figure 7), and Model (3) shows sharp contact of extended vertical feature between two layers of high resistivity (2000 ohm-m) and low resistivity (20 ohm-m) (Figure 8).

The resistivity models obtained from measured and synthetic data sets show that all arrays are capable of defining vertical and horizontal structures with varied sensitivity in vertical and horizontal dimensions. For instance, Model 1 and Model 4 reveal that (DD) configuration is almost more sensitive to localized and extended conductive

structure (Figures 6b, 9b). On the other hand, (WS) and (W) configurations can resolve horizontal conductive layer beneath resistive layer at localized area (Figures 6c, 6d; 9c, 9d). Figures 7 and 8, Model 2 and Model 3, respectively, show similar horizontal and vertical sensitivity presented for the three configurations assuming simple near surface lateral variation and involving limited vertical structure and lateral variation, built at extended vertical structure. Accordingly, based on forward and inverse models, the variation in configurations' sensitivity demonstrated in Table (1) can be slightly ignored. The slight variation in configurations' sensitivity can be distinguished in this study where the geoelectrical layers show a strong resistivity contrast, the procedure of filtering noisy quadripoles, and the choice of inversion method and its parameters. For instance, 100 times resistivity difference from the low resistivity layer (10-20 ohm-m) to the highest resistivity layer (2000 ohm-m) is adequate to sharply image near surface geoelectrical structures in proper details. This can be concluded from the localized conductive structure presented in Figure 9. However, we propose that the variations of configurations' characteristics (Table 1) could be triggered at least in such environment characterized by low resistivity contrast. This could tested numerically using variable electrodes' spacing and configurations applied for similar case studies, where the target is placed at greater depth, and this was beyond the objective and field design of this study.

In order to give quantitative comparisons between real earth tomograms and the synthetic tomograms, each measured tomogram was quantitatively connected and correlated to the four synthetic tomograms. The fitting criteria results entail statistically significant variation using R-squared values (i.e., correlation coefficient). Figures 10, 11, and 12 compare resistivity values at datums of equal depths and spacing among the four synthetic tomograms presented in Figures 6, 7, 8, and 9.

In order to improve data display, we used logarithmic scale axis and applied the logarithmic value "Log10" of resistivity for measured and synthetic models. At this point, the fitting line established the degree of misfit (closeness) between the measured and modeled data for the whole data set. The three resistivity configurations are considered to be moderately resolved (i.e., R2 > 50 %), such as the measured tomogram and synthetic tomogram are probably fit Model 1 and Model 4 (Figures 6 and 9). In addition, the fitting plot parameters for Model 4 revealed the highest correlation (i.e., R2 ~ 70%) and has fairly resolved the existence of localized conductive layer (i.e., interbedded limestone) at the contact between hard rock and soft sediment at depth of 6 m (Figure 2). Furthermore, it confirms the limited extent of near surface sharp contact, and also provided the existence of resistive marly limestone layer at depth of 10 m down to resistivity tomogram's depth (see Figure 9, and model 4 data in Figures 10, 11, and 12).

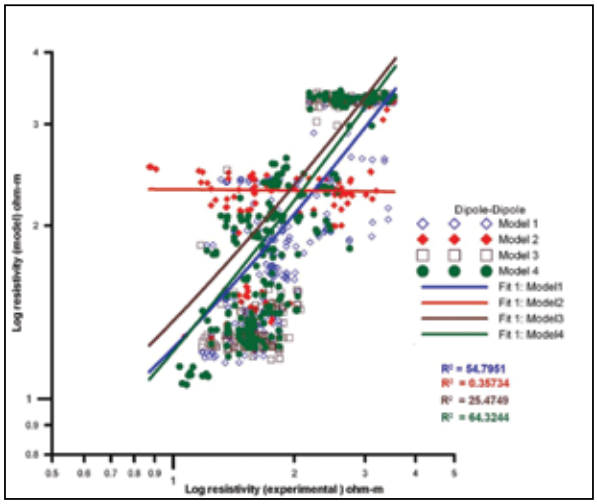

Figure 10. Statistical analysis and fitting parameter between measured (Dipole-Dipole) and four resistivity models

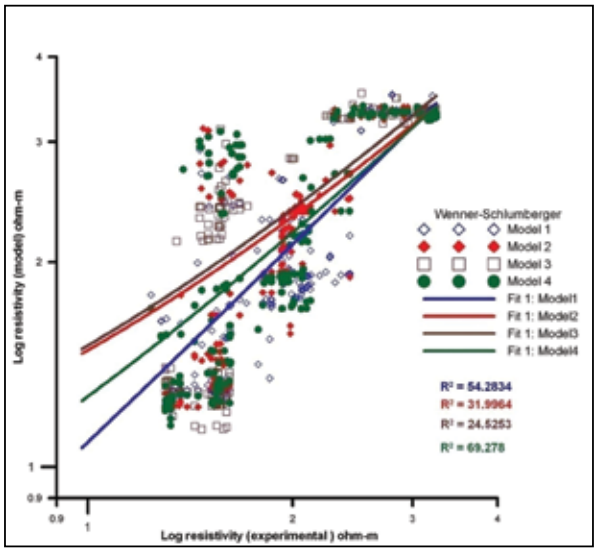

Figure 11. Statistical analysis and fitting parameter between measured (Wenner-Schlumberger) and four resistivity models

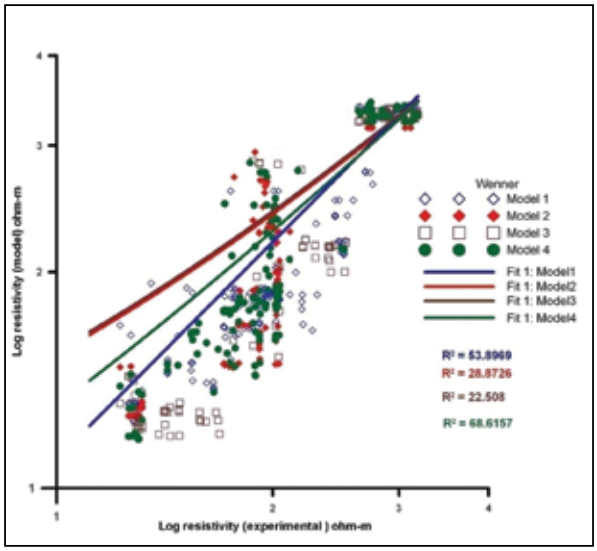

Figure 12. Statistical analysis and fitting parameter between measured (Wenner) and four resistivity models.

Conclusions

Experimental and synthetic electrical resistivity tomography were used to study lithological variation at geological outcrop area. The sequence of hard rocks of limestone, marly limestone, and soil have posed several geoelectrical signatures on resistivity tomograms. Three resistivity configurations (ERC) including Wenner-Sclumberger (WS), Dipole-Dipole (DD), and Wenner (D) have yielded a varied number of data measurements and classified as low, intermediate, and high, respectively.

The results of three resistivity tomograms provided similar geoelectrical structures and can be correlated to real earth model. All models show similar sensitivity to high and low resistivity layers and can be effectively resolve resistivity variations at different degree of data noises. The DD and W configurations seem to be less contaminated by noise levels comparable to Wenner–Schlumberger (WS) configuration. Besides, many of rejected near surface noisy data observed in WS pseudo-section do not have fundamental influence to resolve resistivity structures at greater depth. Moreover, the present study, where the depth of investigation is 20 m and the medium resistivity contrast, is relatively high for the different embedded structures; the applied ERCs have recovered real earth resistivity models at fine details where it was not compulsory to acquire large number of measurements.

The synthetic resistivity models allowed producing four geoelectrical scenarios to imitate possible geological structures. The resolution of DD configuration appears to be more effective at larger depth than WS and W configurations, and exhibited a model of quite more sensitive to small and localized conductive layer at shallow depth.

References

[1] Al-Amoush, H. R. 2006. Hydro-Geophysical Investigations for the Purposes of Groundwater Artificial Recharge in the Jordan Valley Area, Ph.D. Dissertation, University of Jordan, Amman.

[2] Alfano, L., 1974. A modified geoelectrical procedure using polar-dipole array – An example of application to deep exploration, Geophysical prospecting, 22: 510-525.

[3] Alpine L.M, Berdichevsky, M.N., Vedriintsev, G.V and Zagramister, A.M., 1966. Dipole methods for measuring earth conductivity (selected and translated from russion by G.V Keller). Colorado School of Mines, Golden co.

[4] Brass, G., Flathe, H., and Schulz, R., 1981. Resistivity Profiling with Different Electrode Arrays over a graphite deposits, Geophysical Prospecting, 29: 289-600.

[5] Carbonel, D., Gutiérrez, F., Linares, R., Roqué, C., Zarroca, M., McCalpin, J., Guerrero, J., and Rodríguez, V., 2013. Differentiating between gravitational and tectonic faults by means of geomorphological mapping, trenching and geophysical surveys. The case of the Zenzano Fault (Iberian Chain, N Spain), Geomorphology 189: 93–108.

[6] Dahlin, T., and Leroux, V., 2012. Improvement in time-domain induced polarization data quality with multi-electrode systems by separating current and potential cables, Near Surface Geophysics 10: 545-656.

[7] Dahlin, T., and Zhou, B., 2004. A numerical comparison of 2D resistivity imaging with 10 electrode arrays, Geophysical Prospecting, 52: 379-398.

[8] Dey, A., and Morrison, H.F., 1979. Resistivity modeling of arbitrary shaped two-dimensional structures, Geophysical Prospecting, 27: 106-136.

[9] Friedel, S., 2003. Resolution, stability and effciency of resistivity tomography estimated from a generalized inverse approach, Geophys. J. Int, 153: 305–316.

[10] Furness, P., 1993. Gradient Array profiles over thin sensitive veins, Geophysical prospecting, 41: 113-130.

[11] Habberjam, G.M., 1979. Apparent resistivity observations and the use of square Array Techniques. In Saxov, S and H. Flathe (eds), Geoexploration Monographs, series 1, (9), pp.1-152. Geopublication Associates, Gebruder Borntraeger.

[12] Improta, L., Ferranti, L., De Martini, P.M., Piscitelli, S., Bruno, P.P., Burrato, P., Civico, R., Giocoli, A., Iorio, M., D'Addezio, G.,and Maschio, L., 2010. Detecting young, slow-slipping active faults by geologic and multidisciplinary high-resolution geophysical investigations: A case study from the Apennine seismic belt, Italy. J. Geophys. Res. 115, B11307. doi:10.1029/2010JB000871.

[13] Griffith, D. H., and Barker R.D., 1993. Two-dimensional resistivity imaging and modeling in areas of complex geology, Journal of Applied Geophysics, 29: 211-226.
Loke, M. H., 2010. Tutorial: RES2DINV version 3.59, Rapid 2-D Resistivity & IP Inversion Using the Least-Squares Method Malaysia. Geotomo Software.

[14] Loke, M.H., 2014. Tutorial: 2-D and 3-D electrical Imaging Surveys, Malaysia. Geotomo Software.

[15] Loke, M. H, Acworth, I., and Dahlin, T., 2003. A comparison of smooth and blocky inversion methods in 2D electrical imaging surveys, Exploration Geophysics, 34: 182-187.

[16] Monier-Williams, M.E., Greenhouse, J.P., Mendes, J.M. and Ellert, N., 1990. Terrain conductivity mapping with topographic corrections at three waste disposal sites in Brazil, in Geotechnical and Environmental Geophysics, Vol. 2: Environmental and Groundwater (ed. S.H. Ward), Society of Exploration Geophysicists, Tulsa, Oklahoma, USA, pp. 41–55.

[17] Olenchenko, V.V., and Kamnev, Ya .K., 2014. A resistivity model of permafrost in the Zhosaly Kezen Pass (Ilei Alatau), from ERT data, in: Proc. Geo-Siberia Int. Conf. & Expo, Vol. 2 (2): 1–5.

[18] Oldenburg, D.W. and Li. Y., 1999. Estimating the depth of investigation in dc resistivity and IP surveys, Geophysics 64: 403–416.

[19] Reiser, F., Dalsegg, E., Dahlin, T., Ganerod, G.V., and Ronning, J.S., 2009. Resistivity modeling of fracture zones and horizontal layers in bedrock, Geol. Survey Norway, Report No. 2009.070, pp.1-120.

[20] Reynold, M. J., 2011. An Introduction to Applied and Environmental Geophysics, 2nd edn., Wiely Blackwell, UK. 696p.

[21] Seminsky, K., Zaripov, R. and Olenchenko, V., 2016. Interpretation of shallow electrical resistivity images of faults: tectonophysical approach, Russian Geology and Geophysics 57: 1349–1358.

[22] Szalai, S., Szarka, L., 2007b. Auxiliary Results of Collection and Classification of Surface Geoelectric Arrays, 13th European

[23] Meeting of Environmental and Engineering Geophysics, Istanbul A09.

[24] Szalai, S., and Szarka, L. 2007a. On the classification of surface geoelectrical arrays, Geophysical Prospecting, 56: 159-175.

[25] Szalai, S., Szarka, L., Praceser, E., Bosch, F., Muller, I. and Turberg, P., 2002. Geoelectrical mapping of near-surface karstic fractures by using null arrays, Geophysics 67: 1769-1778.

[26] Szalai, S., Szarka, L., Marquis, G., Sailhac, P., Kakkonen, P. and Lahti, I., 2004. Colinear null arrays in geoelectrics. Proceeding of the 17th workshop on electromagnetic induction in the earth, S.3-P3 IAGA WG 1.2 , Hyderabad, India.

[27] Tsokas, G.N., Tsourlos, P.I., Vargemezis, G.N., and Pazaras, N.T., 2011. Using surface and cross-hole resistivity tomography in an urban environment: an example of imaging the foundations of the ancient wall in Thessaloniki, North Greece, Physics and Chemistry of the Earth, 36 (16): 1310–1317.

[28] Zhou, B, and Dahlin, T., 2003. Properties of effects of measurements errors on 2D resistivity imaging, Near Surface Geophysics, 1: 105-117.

[29] Zohdy, A., 1969. The use of Schlumberger and equatorial soundings in groundwater investigations near El Paso, Texas, Geophysics 34: 713-728.

JJEES

Volume 8, (Number 1), Sept, 2017
ISSN 1995-6681
Pages 35 - 44

Jordan Journal of Earth and Environmental Sciences

Soil Metal Distribution under Different Land Uses of Emerging Mega Cities in Southwest Nigeria and the Associated Ecological Risk

Azeez Jamiu Oladipupo

Department of Soil Science and Land Management, Federal University of Agriculture Abeokuta, Nigeria

Received 12 May, 2017; Accepted 24 August, 2017

Abstract

Data on Inventory, distribution and risk assessment of heavy metals in soils of emerging megacities in sub-Saharan African countries is necessary to assess pollution sources and environmental safety. The present study evaluated Ni, Cr, Cu, Cd, Zn, Mn, and Pb concentrations in soils from different land uses in Ibadan and Abeokuta, Nigeria. Samples were collected at 0-20 and 20-40cm depths from crop-farm, industrial site, animal-farm, natural forest, roadside, educational institution, residential estate and markets. Results showed that the depth distribution of the metals were similar, Cu and Pb were concentrated in the top 20cm soil depth at both locations. There were higher concentrations of Ni, Cu and Zn in Ibadan soils while Abeokuta had higher levels of Mn. Copper and Zn contamination were higher in animal farm and industrial land, respectively. Roadside soil had a significantly higher Pb ($p < 0.05$), comparable to forest, educational and residential lands; however, market land use was more acidic. The soil metals accumulated and appeared bound to organic matter, while nickel was positive and significantly correlated with soil Cr, Cu, Zn and Mn while soil Zn and Mn correlated positively with Cr. Contamination/pollution factor across soil depth, locations and land use was in the order Cd > Zn > Mn > Cr > Pb > Cu > Ni. The soils' contamination indices are high with Cd, moderate with Zn and low for other metals. Cadmium has a high potential ecological risk, while the potential ecological risk indices of the locations were moderate. Generally, the metal concentrations were lower than those of other developed megacities.

© 2017 Jordan Journal of Earth and Environmental Sciences. All rights reserved

Keywords: Alfisols, Ecological risk, Heavy metals, Land use, Soil contamination, Urban soils.

1. Introduction

The soil is a repository of contaminants and of importance in ecosystems research (Luo *et al*., 2007) and pollution studies (Madrid *et al*., 2002). Among the components of the environment (soil, water, air), soil receives most of its pollutants from other components of the environment. Urban soils however, have high concentrations of heavy metals (Xia *et al*., 2011; Adedeji *et al*., 2013). Soils from urban areas are not usually used for farming. This is because of other high valued alternative uses to which the land are used for. However, alternative anthropogenic activities on urban soils have impacted high metals input in the soil, usually above permissible limits. Some of the pathways of exposure to soil contaminants are the inhalation and swallowing of pollutants, and at times, there is dermal contact with the pollutants (Nicholson *et al*., 2003). This has resulted in toxicological health disorders in adults and children, affecting the central nervous systems and fatty tissues (Xia *et al*., 2011).

Sources of pollution in urban soils are many and at times metal specific. Soil pollutants could have their sources from vehicle emission, chemical industry, coal combustion, municipal solid waste, drug contamination and dust sedimentation (Adedeji *et al*., 2013; Azeez *et al*., 2014; Jalili and Azizkhan, 2009; Xia *et al*., 2011). For example, the concentrations of Cu, Pb and Zn are reported to be via traffic sources while most Cd sources are industrial (Imperato *et al*., 2003; Xia *et al*., 2011). Other identified sources of soil heavy metals include agricultural inputs (Huang and Jin, 2008), urbanization, industrialization, and mining (Zhong *et al*., 2012). Agricultural and industrial wastes are reported to be the most damaging anthropogenic activities in the world (Krami *et al*., 2013). Several studies have also credited heavy metals pollution to anthropogenic sources (Zhang *et al*., 2009; Acosta *et al*., 2011; Bini *et al*., 2011; Gu *et al*., 2012; Li and Feng, 2012; Chabukdhara and Nema, 2012; Cai *et al*., 2012; Guo *et al*., 2012). Despite the negative effects (toxic effects) of these metals in human, their build-up in the soil is not properly monitored in emerging megacities of sub-Saharan Africa. Aside been present in the soils, these metals can also persist for a long time because they are not biodegradable and are immobile. The metals have been reported to be responsible for chronic and acute health disorders in adults and children (Madrid *et al*., 2002; Lee *et al*., 2006).

Human activities have been reported to affect the natural, geological and biological redistribution of heavy metals in soils (Peter and Adeniyi, 2011). Such activities in urban areas have contributed to the high metal profiles. Recently, research attention has focused on contamination of soils in urban cities in developed countries of Europe, America and Asia. Many of these studies have focused on urban soils as a part of the environment but not on specific land use types. This indicates a research gap, this aspect of research is, however,

* Corresponding author. e-mail: azeez2001ng@yahoo.com

important because different land-use exert different pollution pressures on the land, and the changes in the environmental chemistry, particularly of heavy metals is also dependent on anthropogenic impact on the environment. The toxicological health risks associated with the land use also differs. Thus, information on soil distribution of heavy metals is necessary to assess soil specific pollution sources and soil quality (Gu *et al*., 2012). This approach will allow for the evaluation of the potential risk of pollutants to other organisms and the potential impact on human.

Abeokuta and Ibadan (capitals of Ogun and Oyo states, respectively) are representative towns of southwestern Nigeria by human population, activities and geographical location. They are emerging megacities that border Lagos State, the most populous and commercial capital of Nigeria. The two cities in recent times have become foreign investor's destination of choice and emerging commercial hub in southwestern Nigeria. The two cities are old with a constantly growing population. Ibadan (with 11 local governments) has a population estimate of 3.6 million while Abeokuta (comprising of Abeokuta north and south, Odeda, Ifo and Ewekoro local governments) has a population of about 1.2 million inhabitants in 2006 national population census. Their nearness to Lagos has attracted several residents to the cities. These high populations have resulted into increase in human activities and the attendant problems of soil pollution. In the developed world, several studies have been reported on the heavy metal concentrations in urban and suburban soils (Xia *et al*., 2011; Zheng *et al*., 2008; DEFRA, 2009) of China, Netherlands, United Kingdom and Spain (Adriano, 2001) but only few in Nigeria have been reported in literature (Peter and Adeniyi, 2011; Bolaji *et al*., 2009; Atayese *et al*., 2008; Iwegbue, 2014; Iwegbue *et al*., 2012; Iwegbue *et al*., 2015). Specifically, there are scanty published researches on the concentrations of heavy metals in different land use in sub-Saharan Africa and particularly southwestern Nigeria except those related researches on Lagos State, Nigeria (Peter and Adeniyi, 2011; Bolaji *et al*., 2009). The present study is aimed at evaluating the effect of land use on the environmental chemistry of the metals, the toxicological effects and the potential ecological risk on the populace, hence it was hypothesized that there is a relationship between land use and soil concentrations of heavy metals. Therefore, the objectives of the present study are to determine the effect of land use on the depth distribution of Ni, Cr, Cu, Cd, Zn, Mn and Pb in soils of Abeokuta and Ibadan; to evaluate the contamination/ pollution factor and ecological risk associated with the metals and to determine the relationship between some soil chemical characteristics and metal concentrations.

2. Materials and Methods

2.1. Site Description

Abeokuta

Abeokuta is described by Wikipedia (2017) as a city in southwestern Nigeria and capital of Ogun State, with an average temperature of 28 ^{0}C and annual rainfall of 1270 mm. The city lies on 7.15^0 N latitude and 3.35^{0}E longitude, bounded by the eastern bank of Ogun River, 74 km north of Lagos by railway and 130 km by water. Abeokuta is connected to Lagos by rail and serves as the commercial centre for an area in which cacao, palm kernels, and palm oil are produced. The city is known for its traditional style of hand-woven cotton fabric known as *Adire*, which is dyed with locally produced indigo. A granite outcropping known as Olumo rock is at the city center, and it is the site of traditional local celebrations. The city is home to the Federal University of Agriculture Abeokuta and Ogun State Polytechnic among other institutions.

Ibadan

Ibadan is the capital of Oyo State, with its center at 7.39^{0}N and 3.9^{0}E (Wikipedia, 2017). It is also located in the southwestern part of Nigeria, 128 km northeast of Lagos and 530 km southwest of Abuja. It has an average temperature of 27.5^0 C and rainfall range of 24.0 to 708.0 (mm/month). Ibadan is a major transit point between the coast and areas to the north. The city is on the railroad line linking Lagos with Kano and is well connected by road to other cities in the region. It is the center of trade for farming areas producing cacao, palm oil, yams, cassava, corn, and fruit. Industries include agricultural processing, brewing, vehicle assembly, and the manufacture of cigarettes. The University of Ibadan and Ibadan Polytechnic are located here. Also Ibadan is the site of several major research institutes, notably the International Institute of Tropical Agriculture, Cocoa Research Institute, Forestry Research Institute, National Horticultural Research Institute, and Nigerian Institute of Social and Economic Research. Most of Nigeria's leading publishing companies are based in the city.

2.2. Sampling and Sample Analyses

The whole sampled areas in Abeokuta and Ibadan have similar geologic formation. The soils are derived from coarse grained granites and gneisses while some parts are of fine grained biotite gneisses and schicsts. A total number of 96 soil samples were collected from the selected areas. The sampling area at each location is approximately 400 m^2. The soil samples were collected at two depths (20 cm and 40 cm), in three replications, from 8 different land uses in Abeokuta and Ibadan. The samples were collected using soil auger. The coordinates of each sampling point from a contagious area (400 m^2) were taken with Global Positioning System (GPS). Details of the sampling areas and their characteristics are shown in Table 1. The detailed soil World Reference Based Classes of the soils are also given in the Table.

The collected soil samples were air-dried; stones and tree leaves were removed and then passed through 2 mm sieve. The digestion of the samples were done with ternary mixtures of nitric, sulphuric and perchloric (3:1:1) and concentration of the metals (Ni, Cr, Cu, Cd, Zn, Mn, and Pb) were determined using Atomic Absorption Spectrophotometry, AAS (Donisa *et al.*, 2000). A portion of the sieved soil was also used to determine the following soil properties: soil organic carbon using chromic acid oxidation procedure (Walkley and Black 1939), soil pH using glass electrode pH meter (McLean *et al*., 1982). The available phosphorus content of the soils was determined by Bray 1 method (Nelson and Sommers, 1996), while total nitrogen was determined using macro-Kjeldahl method (Bremner and Mulvaney, 1982). Electrical conductivity was determined using a conductivity meter while the particle size analysis was done using Bouyoucos

(1962) method. The estimation of the contamination/pollution factor (CPF) of the metals was calculated as CPF= C/C_0 [eq. 1] where C is mean concentration of metal in soil and C_0 is background or preindustrial concentrations. The appropriate background value was obtained from values reported for European soils with similar parent materials as indicated above and with pH value between 5 and 6. No such up to date and reliable data/information exists for southwestern Nigerian soils. The values in mg kg^{-1} dry soil are 0.5 Cd, 50 Cr, 40 Cu, 30 Ni, 50 Pb, 100 Zn (Gawlik and Bidoglio, 2006); the value used for Mn (476) was the target value reported by the department of petroleum resources, Nigeria (DPR, 2002). The degree of contamination (DC) of the metals was calculated as the sum of all CPFs: DC = ∑ CPF (Fiori *et al*., 2013) [eq. 2]. Potential risks (*PER*) posed by the presence of the metals was calculated as *PER:* PER = TRF× CPF [eq. 3], this is calculated separately for each metal, where TRF was the toxic response factor of the element (Hakanson, 1980) as reported by Iwuegbu *et al*. (2015). The TRF values used are: 5, 2, 30, 1, 5, 5, for Pb, Cr, Cd, Zn, Ni and Cu, respectively (Fiori *et al*., 2013). Potential risks index (*PERI*) was calculated as the sum of all PER calculated for each metal: PERI = ∑ PER. [eq. 4] (Fiori *et al*. (2013); USDOE (2011); USEPA (2001; 2011)).

Table 1. Description of the selected areas used for sampling

Land Use	Latitude (^{0})	Longitude (^{0})	Altitude (m)	WRB# Soil Class	Description
Abeokuta[a]					
Crop farm	7.20913	3.46024	197	Typic Acrisol	Presence of vegetation including arable crops (yam and cassava). Cropped continuously for 5 years with history of fertilizer application.
Animal farm	7.22683	3.44903	154	Arenic Lixisol	Heap of animal dung, with little or no vegetation
Education	7.09665	3.33038	84	Eutric Leptosol	Presence of vegetation such as weeds. Presence of little stone in the soil
Residential	7.12383	3.34723	110	Typic Acrisol	Presence of vegetation including shade trees and ornamental plant garden
Roadside	6.87846	3.1925	56	Typic Acrisol	Bare land
Industrial	6.89005	3.19866	38	Arenic Lixisol	Bare land, near cement factory
Market	6.84112	3.19208	114	Typic Acrisol	Bare land
Forest	7.21123	3.45953	204	Eutric Nitisol	Secondary forest with little vegetation
Ibadan[b]					
Crop farm	7.40309	3.85048	223	Eutric Leptosols	Presence of plantation crops and ornamental plant. Crops grown for more than seven years with fertilizer application and incorporation of crop residues
Animal farm	7.38663	3.83676	192	Eutric Luvisol	Heap of animal dung, with little or no vegetation
Education	7.36710	3.90379	211	Eutric Leptosol	Bare soil with the presence of little stone in the soil
Residential	7.39317	3.79553	218	Typic Acrisol	Presence of little rock and vegetation including weed.
Roadside	7.39985	3.77526	200	Haplic Leptosol	Bare land
Industrial	7.36574	3.85489	184	Haplic Leptosol	Bare land
Market	7.36851	3.66648	241	Typic Acrisol	Bare land
Forest	7.40309	3.85045	218	Typic Acrisol	Secondary forest with little vegetation

#: WRB, 2006 ; [a b]: Soil classification according to Senjobi 2007, Aiboni 2001, respectively.

2.3. Statistical Analysis

Data collected were analysed for their variance using the Statistical Analysis System (SAS) statistical package. The Significant treatment means were separated using Duncan's multiple range test at 5 % probability level. The correlation between the metals and other soil chemical properties were done using same software.

3. Results

3.1. Soil Chemical Properties and Heavy Metal Concentration

Effect of Soil Depth

The effect of soil depth on soil chemical properties and heavy metal content (mean across land use) is shown in Table 2. It was observed that soil depth had no effect on pH, electrical conductivity (EC) and clay content at Abeokuta while the pH and clay at 20-40 cm were significantly ($p < 0.05$) higher than those of 0-20 cm at Ibadan. At both locations, 0-20 cm soil depth had significantly higher soil total nitrogen and organic carbon. Analytical values of soil P, Ni, Cr, Cd, Zn and Mn at both soil depths were similar in Abeokuta and Ibadan but the concentrations of Cu and Pb were significantly higher in 0-20 cm at both locations (Table 2).

Table 2. Effect of soil depth on soil properties and the heavy metals concentration

Depth (cm)	Soil pH	EC	Clay	N	Org C	P	Ni	Cr	Cu	Cd	Zn	Mn	Pb
		µS cm^{-1}	---------- (%) ---------			----------mg kg^{-1} ----------							
Abeokuta													
0-20	5.69a	0.12a	7.91a	0.08a	^{a}0.98	16.33a	2.88a	15.25a	16.03a	5.28a	48.43a	288.00a	16.03a
20-40	5.72a	0.08a	8.38a	0.04b	^{b}0.46	10.57a	2.79a	15.77a	8.95^{b}	2.08a	33.66a	279.00a	8.95b
Ibadan													
0-20	5.56^{b}	0.28a	5.17^{b}	0.08a	^{a}1.03	24.19a	6.99a	16.49a	21.72a	6.35a	223.60a	557.00a	21.72a
20-40	5.74^{a}	0.57a	6.28^{a}	0.02b	^{b}0.37	22.75a	6.35a	16.48a	14.83b	6.99a	238.70a	596.60a	14.83b

Alphabets a,b, are Duncan alphabets. Means with the same alphabet(s) in a column under same location are not significantly different from each other at $p < 0.05$

Effect of Land Use

Table 3 shows the effect of land use types on the soil heavy metals and other soil properties. At Ibadan, the soil EC, clay, N, organic C were not statistically different ($p > 0.05$) across land use types. However, at Abeokuta, crop farm had statistically similar soil pH with those of the industrial, animal farm, and forest land uses but significantly higher than those of other land uses. The lowest soil pH was recorded at the market land use. Similarly, at Ibadan, industrial land use had significantly higher soil pH compared with those of animal farm, educational and market land uses. Crop farm and market land use had significantly higher soil clay than other land use. At both locations, the soil P was significantly higher at the animal farm while the least soil P was observed at Ibadan residential area and crop farm at Abeokuta. The concentrations of Ni, Cr, and Cu at both locations; Zn at Abeokuta, Cd and Pb at Ibadan were similar among the different land uses. Educational site at Abeokuta, however, had significantly ($p < 0.05$) higher soil Cd with the least value in animal farm while industrial land use had the highest amount of soil Zn at Ibadan. The value is significantly ($p < 0.05$) higher than educational and residential land uses that recorded the least values. Manganese is more concentrated in the industrial area at Ibadan with the lowest concentration at the market sites. Conversely, market, animal farm and forestland uses had the highest Mn at Abeokuta. The concentration of Pb at the education land use was significantly higher than the values in the other land uses.

Table 3. Some soil chemical properties and heavy metals concentration (values across soil depths)

Depth (cm)	Soil pH	EC	Clay	N	Org C.	P	Ni	Cr	Cu	Cd	Zn	Mn	Pb
		µS cm^{-1}	---------- (%) ----------			---------- mg kg^{-1}----------							
Abeokuta													
Crop farm	6.06^{a}	0.05c	6.57a	0.07^{ab}	0.67a	5.23^{b}	3.04a	15.08a	3.28a	3.02^{ab}	13.91a	318.40ab	5.72b
Industrial	5.81^{ab}	0.07bc	9.58b	0.06^{ab}	0.70a	11.48^{b}	2.33a	15.59a	3.81a	3.80^{ab}	20.13a	349.20b	7.58ab
Animal farm	5.75^{abc}	0.25a	5.80b	0.092^{a}	0.99a	43.62^{a}	3.12a	14.64a	4.20a	1.69^{b}	84.75a	373.10a	9.73ab
Forest	5.74^{abc}	0.08bc	6.33b	0.08^{ab}	0.73a	9.05^{b}	3.16a	17.79a	3.81a	2.72^{b}	18.43a	452.00a	11.41ab
Road side	5.68^{bc}	0.04c	6.67b	0.05^{ab}	0.64a	9.18^{b}	3.22a	13.98a	4.40a	1.78^{b}	66.65a	283.30ab	12.01ab
Education	5.66^{bc}	0.07bc	6.00b	0.07^{ab}	0.76a	8.47^{b}	2.40a	13.82a	3.91a	11.50^{a}	55.38a	359.50a	14.17a
Residential	5.56^{bc}	0.09bc	9.33b	0.05^{ab}	0.53a	10.55^{b}	2.89a	14.58a	2.80a	3.06^{ab}	24.13a	240.40ab	9.65ab
Market	5.41^{c}	0.15ab	14.90a	0.04^{b}	0.72a	9.99^{b}	2.53a	18.60a	5.16a	1.86^{b}	44.99a	467.00a	9.68ab
Ibadan													
Crop farm	5.79^{ab}	0.11a	4.93a	0.05a	0.63a	12.49^{c}	4.74a	16.33a	7.65a	3.59a	55.9^{b}	587.70ab	15.65a
Industrial	5.98^{a}	0.29a	5.83a	0.06a	0.65a	14.56^{c}	13.81a	17.52a	12.71a	3.68a	664.0^{a}	834.00a	15.93a
Animal farm	5.42^{cd}	0.62a	5.47a	0.08a	1.00a	66.31^{a}	5.49a	16.81a	18.45a	1.13a	117.5^{b}	494.40b	14.60a
Forest	5.73^{abc}	1.70a	6.53a	0.04a	0.40a	24.19^{bc}	4.43a	19.38a	11.63a	3.90a	385.6^{ab}	649.30ab	15.28a
Road side	5.76^{ab}	0.15a	5.60a	0.05a	0.74a	9.31^{c}	4.90a	14.89a	16.80a	5.23a	119.9^{b}	508.80b	18.34a
Education	5.63^{bc}	0.22a	6.03a	0.04a	0.68a	15.20^{c}	4.41a	14.87a	9.28a	0.80a	86.9^{b}	472.80b	14.48a
Residential	5.69^{abc}	0.14a	5.13a	0.05a	0.57a	8.65^{c}	5.10a	16.29a	9.43a	1.17a	89.2^{b}	654.50ab	17.34a
Market	5.22^{d}	0.18a	6.23a	0.07a	0.92a	37.05^{b}	10.49a	15.80a	9.13a	3.49a	330.1^{ab}	421.70b	15.68a

Alphabets a,b,c, are Duncan alphabets. Means with the same alphabet(s) in a column under same location are not significantly different from each other at $p < 0.05$

Effect of Soil Depth, Location and Land Use

The effect of soil depth, location and land use on the soil properties and heavy metal content for the combined data is shown in Table 4. It was observed that soil depth has no significant effect on the soil properties and heavy metals studied except soil organic carbon. The soil organic C was concentrated at the 0-20 cm depth; the value is twice that of 20-40 cm depth. On comparing both locations, the results shows that soil pH, EC, total nitrogen, organic carbon, soil Cd and Pb were similar between the locations. Soil clay and Mn concentration was however, significantly higher at Abeokuta. On the other hand, the amount of soil P, Ni, Cu and Zn were significantly higher at Ibadan. Soil pH was significantly higher in crop farm, industrial, forest and roadside. The values noted in the crop farm and industrial land use was significantly higher than the pH values observed in educational and residential land use. The land use types have no effect on the soil EC, N, organic C, Ni, Cr, Cd and Mn, but clay at the market is significantly higher than the values from other land uses. There was significantly higher concentration of phosphorus in the animal farm. The value observed was more than double that observed in market land use. The lowest P concentrations were observed at residential, educational, crop farm and roadside. The likely reasons for the high P in animal farm have been given earlier in the text. The concentration of Cu was significantly higher in animal farm, though not statistically different from the values from other land uses. The lowest value was observed at the crop farm. Soil Zn concentration was highest in the industrial land; the value was however, similar to the Zn concentration at animal farm, forest and roadside and market land. The lowest soil Zn was recorded in crop farm, educational and residential land uses, the values were significantly lower than that of the industrial land use.

Table 4. Effect of soil depth, location and land use (means of the locations) on some soil chemical properties and heavy metal concentration

	Soil pH	EC	Clay	N	Org. C	P	Ni	Cr	Cu	Cd	Zn	Mn	Pb
		µScm-1	---------- (%) ----------			---------- mg kg^{-1}----------							
Soil Depth(cm)													
0-20	5.63a	0.19a	7.33a	0.08a	0.98a	20.26a	4.62a	15.25a	8.99a	3.64a	135.99a	457.80a	16.37a
20-40	5.73a	0.33a	6.54a	0.06a	0.46b	16.66a	4.89a	15.77a	6.81a	2.92a	136.18a	436.80a	11.89a
Locations													
Abeokuta	5.71a	0.09a	8.15a	0.06a	0.74a	13.45b	2.84b	14.53a	3.92b	3.68a	41.04b	567.80a	10.00a
Ibadan	5.65a	0.46a	5.72b	0.05a	0.70a	23.47a	6.67a	16.48a	11.88a	2.88a	231.13a	317.9b	13.27a
Land Use													
Crop farm	5.93a	0.08a	5.75b	0.05a	0.67a	8.88c	3.89a	15.08a	5.46b	3.30a	34.90b	433.80a	10.68b
Industrial	5.89a	0.18a	7.71b	0.06a	0.70a	13.02bc	8.07a	15.59a	8.26ab	3.74a	342.10a	441.60a	11.75ab
Animal farm	5.58b	0.43a	5.63b	0.08a	0.99a	54.97a	4.30a	14.64a	11.33a	1.41a	101.1ab	433.80a	12.16ab
Forest	5.73ab	0.89a	6.43b	0.06a	0.73a	16.67bc	3.79a	17.79a	7.72ab	3.31a	202.00ab	550.70a	13.34ab
Road side	5.72ab	0.09a	6.13b	0.05a	0.64a	9.25c	4.06a	13.98a	10.60ab	3.51a	93.30ab	396.10a	21.61a
Education	5.65b	0.14a	6.02b	0.05a	0.76a	11.84c	3.41a	13.82a	6.59ab	6.15a	71.10b	416.10a	14.32ab
Residential	5.63b	0.11a	7.23b	0.05a	0.53a	9.59c	3.99a	14.58a	6.11ab	2.15a	56.60b	443.00a	17.99ab
Market	5.31c	0.17a	10.57a	0.05a	0.72a	23.52b	6.51a	18.60a	7.14ab	2.68a	187.50ab	444.40a	11.18b

Alphabets a,b,c,are Duncan alphabets. Means with the same alphabet(s) in a column under same depth, location and land use are not significantly different from each other at $p < 0.05$

Relationship between Soil Chemical Properties and Metal Concentrations

The correlation between the soil chemical properties and heavy metal content is shown in Table 5. The soil pH was negatively correlated with the soil phosphorus while the soil EC was positively correlated with Cr, Cu and Zn ($p<0.05$). Soil nitrogen was also shown to be positively correlated with organic C, P, Cu, Zn and Pb. Similar significant and positive correlation were observed between organic C and P, Ni, Cu, Zn and Pb. Soil P and Cu was also positive and significant ($p<0.01$). Nickel was positive and significantly correlated with soil Cr, Cu, Zn and Mn while soil Zn and Mn correlated with Cr. There was also a positive and significant correlation between soil Cu and soil Zn, Mn and Pb. The correlation between soil Zn and Mn was significant and positive. The correlation coefficient between soil Mn and Pb

Table 5. Correlation between soil chemical properties and metal concentrations (mean of the locations) n=96

Depth (cm)	pH	EC	Clay	N	Org C	P	Ni	Cr	Cu	Cd	Zn	Mn
EC	0.01											
Clay	-0.04	-0.07										
N	-0.12	0.04	-0.14									
Org C	-0.13	-0.01	-0.14	0.93**								
P	-0.33**	0.05	-0.11	0.20*	0.21*							
Ni	-0.03	0.01	-0.12	0.21*	0.33**	0.14						
Cr	-0.17	0.24*	-0.01	-0.02	0.03	0.04	0.41**					
Cu	-0.20	0.07*	0.25*	0.33**	0.44**	0.30**	0.33**	0.20				
Cd	-0.10	0.08	-0.04	0.10	0.12	-0.08	0.10	0.03	-0.06			
Zn	0.02	0.42**	-0.11	0.22*	0.28**	0.06	0.81**	0.43**	0.36**	0.16		
Mn	-0.10	0.20	-0.30**	0.11	0.18	0.05	0.45**	0.47**	0.33**	0.19	0.46**	
Pb	-0.18	0.01	-0.02*	0.26*	0.32**	0.02	0.20	0.11	0.68**	0.13	0.18	0.39**

*, ** significant at P≤0.05 and ≤0.01, respectively; EC = Electrical conductivity; Org C = organic carbon

Soil Contamination and Ecological Risk Indices

The estimation of the contamination/pollution factor (CPF) and the degree of contamination of the metals are shown in Table 6. It was observed that Cd and Zn had the highest CPF across soil depth, locations and land use. The least CPF values were observed in Ni. The general sequence of CPF values are as follows: Cd > Zn > Mn > Cr > Pb > Cu > Ni. However, the degree of contamination values indicated that the top soil was more contaminated with metals while Ibadan soils were also marginally more polluted compared with Abeokuta soils. Among the land uses, educational, industrial and forestland uses have higher degree of contamination than other land use while the least value was observed in the animal farm.

Table 6. Contamination/pollution factor and degree of contamination of the soil heavy metals as affected by soil depth, location and land use types

	Contamination/pollution factor							Degree of Contamination
	Ni	Cr	Cu	Cd	Zn	Mn	Pb	
***Soil Depth*(cm)**								
0-20	0.15	0.31	0.22	7.28	1.36	0.96	0.33	10.61
20-40	0.16	0.32	0.17	5.84	1.36	0.92	0.24	9.01
Mean	0.16	0.31	0.20	6.56	1.36	0.94	0.28	9.81
Locations								
Abeokuta	0.09	0.29	0.10	7.36	0.41	1.19	0.20	9.65
Ibadan	0.22	0.33	0.30	5.76	2.31	0.67	0.27	9.85
Mean	0.16	0.31	0.20	6.56	1.36	0.93	0.23	9.75
Land Use								
Crop farm	0.13	0.30	0.14	6.60	0.35	0.91	0.21	8.64
Industrial	0.27	0.31	0.21	7.48	3.42	0.93	0.24	12.85
Animal farm	0.14	0.29	0.28	2.82	1.01	0.91	0.24	5.70
Forest	0.13	0.36	0.19	6.62	2.02	1.16	0.27	10.74
Road side	0.14	0.28	0.27	7.02	0.93	0.83	0.43	9.90
Education	0.11	0.28	0.16	12.30	0.71	0.87	0.29	14.73
Residential	0.13	0.29	0.15	4.30	0.57	0.93	0.36	6.73
Market	0.22	0.37	0.18	5.36	1.88	0.93	0.22	9.16
Mean	0.16	0.31	0.20	6.56	1.36	0.93	0.28	9.81

The potential risks and the risk index posed by the presence of the metals are shown in Table 7. It was evident that Cd is a serious ecological risk in the study area irrespective of soil depth and location. The risk however, is higher at 0-20 cm depth and also at Abeokuta. The Zn and Pb in the soil also has higher ecological risk that Cu, Cr and Ni but lower than Cd. Similar pattern of risk was observed across land use, however educational, industrial and road side land uses had higher risk index than other land use types. The least risk index is obtained in the animal farm.

Table 7. Potential ecological risk and ecological risk index of the soil heavy metals as affected by soil depth, location and land use types

	Potential Ecological risk						Potential Ecological Risk Index
	Ni	Cr	Cu	Cd	Zn	Pb	
***Soil Depth*(cm)**							
0-20	0.77	0.61	1.12	218.40	1.36	1.64	223.90
20-40	0.82	0.63	0.85	175.20	1.36	1.19	180.05
Mean	0.79	0.62	0.99	196.80	1.36	1.41	201.97
Locations							
Abeokuta	0.47	0.58	0.49	220.80	0.41	1.00	223.75
Ibadan	1.11	0.66	1.49	172.80	2.31	1.33	179.69
Mean	0.79	0.62	0.99	196.80	1.36	1.16	201.72
Land Use							
Crop farm	0.65	0.60	0.68	198.00	0.35	1.07	201.35
Industrial	1.35	0.62	1.03	224.40	3.42	1.18	232.00
Animal farm	0.72	0.59	1.42	84.60	1.01	1.22	89.55
Forest	0.63	0.71	0.97	198.60	2.02	1.33	204.26
Road side	0.68	0.56	1.33	210.60	0.93	2.16	216.25
Education	0.57	0.55	0.82	369.00	0.71	1.43	373.09
Residential	0.67	0.58	0.76	129.00	0.57	1.80	133.38
Market	1.09	0.74	0.89	160.80	1.88	1.12	166.51
Mean	0.79	0.62	0.99	196.88	1.36	1.41	202.05

4. Discussion

4.1. Effect of Land Use

High soil organic matter is known to correlate with high biological activities. The top 20 cm (plough layer) is known to be concentrated with microorganisms that are involved in the mineralization of applied organic materials, therefore the high soil N and organic C. Data on soil depth indicated that there is a movement of the metals in the soil; hence the similarities in values across depth except Cu and Pb that were concentrated in the top soil relative to the subsoil. Similar results have been reported by Azeez *et al*. (2011). It, thus, implies that the inhalation of these metal polluted dusts from these sites could prove dangerous since metals, like Pb is concentrated at the uppermost soil layer.

The higher pH of the crop farm at Abeokuta and other land use implies that the heavy metals and other micronutrients may be comparatively deficient or unavailable in the soil of the land uses compared with others; however the low pH of the market land use suggests the likelihood of having higher metal content. Low soil pH has been reported to cause low soil adsorption and high concentration of heavy metals in soil solution (Salt *et al*., 1995). The soil pH was acidic and expected to promote the build-up of the metals in soil solution (Salt *et al*., 1995). At Abeokuta, significantly higher EC and soil N was observed in animal farm while the corresponding lowest values were observed at the roadside and market land use. The deposition of animal manures on the farm could have increased the soil dissolved salt and enriched the soil with N. Typical of animal farm on free-range, the farm animals are known to scavenge for food and in the process excrete urine and faeces indiscriminately on the soil. Similar, high EC values have been reported by Azeez *et al*. (2011) in market dumpsite where animals have been known to graze. The reason for high soil P at animal farm is most probably because of free-range adopted on the animal farms in the study areas. Here animal scavenge for food, and in the process litter the soil with their litter and urine. The implication of the high Cd and Pb at educational sites and Zn and Mn at the industrial land uses is that soils of these land uses are potential risk. The industries might have polluted the soil through their waste discharge by the air and wastewaters while the soils of the educational areas are potential contaminants if ingested or inhaled (Moller *et al*., 2005). The high soil P (above the critical soil P of 15 mg kg $^{-1}$ for southwest Nigerian agricultural soils), Ni, Cu and Zn at Ibadan implies that Ibadan is more polluted with metals compared with Abeokuta. This is because of its higher population and the residents of Ibadan are known to engage in several commercial and industrial activities more than Abeokuta. Ibadan (with 11 local governments) has a population estimate of 3.6 million while Abeokuta (comprising of Abeokuta north and south, Odeda, Ifo and Ewekoro local government) has a population of about 1.2 million inhabitants in 2006 national population census. The concentration of industries is more in Ibadan and the city is the largest city in West Africa. On the other hand, Abeokuta is

popularly referred to as a 'civil service' city because majority of the inhabitant are government workers or workers of the private sectors. The number of industries in Abeokuta town is low. Due to the positive relationship between low soil pH and metals build-up (Salt *et al*., 1995), it then means soil of the market land use probably will be more contaminated. This is evident in the present study, most of the significantly higher metal concentration levels are observed in the market dumpsite.

Figure 1. Map of Abeokuta. Source https://www.google.com.ng

4.2. Effect of Soil Depth, Location and Land Use

The high zinc content of the industrial soils could be related to the continuous input of the metal from the industries through vehicle and heavy machines exhaust emissions (Ward, 1989). Concentration of soil Pb was significantly higher at the roadside and lowest in the crop farm. The high Pb on the roadside could be due to the atmospheric deposition of Pb from the exhaust of vehicles using the roads. There are evidences of Pb from gasoline and Cu, Zn, and Cd from car parts (Wilcke *et al*., 1998). The values of soil Pb in industrial, animal farm, forest, educational and residential were statistically similar. Atmospheric deposition (due to industrialization and human activities) of the metal pools has also been given as the reason for the accumulation of the metals in the soil close to industries (Niu *et al*., 2013; Luo *et al*., 2009). A similar result was reported in Sweden, where increasing industrial activity was reported to increase soil Pb and Cd concentration by 50 % (EEA, 1998) and in Nigeria by Iwegbue *et al*. (2012). The rather high amount of Cd in the crop farms could have been due to the application of phosphatic fertilizers on the farm. The two farms studied have histories of phosphorus fertilizer application. Most phosphate fertilizers have been reported to contain Zn, As, Cd and Cr from the phosphate rock used as the raw material for the P fertilizer manufacture (Iwegbue *et al*., 2012; Yang *et al*., 2004; Luo *et al*., 2007). Generally, the mean concentration of the metals in both locations shows the values were lower than those reported for some cities in developed countries. The values were lower than those of Naples, Italy (Imperato *et al*., 2003); Palermo, Italy (Manta *et al*., 2002); Bangkok, Thailand (Wilcke *et al*., 1998); Seville, Spain (Madrid *et al*., 2002); Madrid, Spain (Miguel *et al*., 1998);Seoul, Korea (Chon *et al*., 1995);Turku, Finland (Salonen and Korkka-Niemi, 2007); Damascus, Syria (Moller *et al*., 2005); Hong Kong, China (Li *et al*., 2004); Shenyang, China (Sun *et al*.,2010); Shanghai, China (Shi *et al*., 2008); Beijing, China (Xia *et al*., 2011). The values are however higher than that previously reported for some southwestern Nigerian soils (Azeez *et al*., 2011, 2014), including some of the sites sampled for the present study, but lower than that reported for Ijebu-North in Ogun state, Nigeria (Adedeji *et al*., 2013). Similar results have also been reported for some dumpsite soils by Iwegbue *et al*. (2010). This implies the gradual build-up of the metals in the cities with time. Soil Zn in Ibadan at industrial sites is higher than the averages of the other cities. This connotes Zn pollution of the soil.

4.3. Relationship between Soil Chemical Properties and Metal Concentrations

Positive and significant correlation observed between organic matter (measured as organic carbon) implies the soil heavy metals are mostly organic bound. Studies have also reported correlation between Pb and organic matter (Kabała and Szerszen, 2002), due to the complexation of Pb by humic substances (Donisa *et al*., 2000; Azeez *et al*., 2011). Gonzalez *et al*. (2006) and Du Laing *et al*. (2009) opined that organic carbon is a major sink for heavy metals. Correlation of soil nitrogen and the metals is also expected because, soil N is closely related to organic matter in most tropical soils.

Figure 2. Map of Ibadan. Source https://www.google.com.ng

4.4. Soil Contamination and Ecological Risk Indices

Data obtained from the estimation of the contamination/ pollution factor, degree of contamination, potential ecological risk and the ecological risk indices revealed that the soils were highly contaminated with Cd. The contamination of the soil by Zn was moderate while the levels of contamination of the other studied metals were low in the soil. However, the degree of contamination of the soils were generally very high irrespective of the soil depths, location and the land use types except the considerable degree of contamination observed in the animal farm. The metals generally have low potential ecological risk except Cd, which poses a high ecological risk. The ecological risk index revealed that the soil has moderate index (Fiori *et al*., 2013); similar results was reported by Iwegbue (2014) and Iwegbue *et al*. (2012) for the Niger Delta region of Nigeria.

Conclusions

Depth distribution of metals in Abeokuta and Ibadan soils were similar but soils from Ibadan were more contaminated. Nickel, Cu and Zn accumulated in Ibadan soils while soils from Abeokuta had higher concentration of Mn. Animal farm had higher amount of Cu but concentration of Zn was higher in industrial, animal farm, forest, roadside, and market. The values were higher than those of crop farm, educational and residential land use. Soil from roadside had the highest amount of lead. The soil metals appeared bound to organic matter. Source identification indicated that the contamination of the soil was mainly from industrial and anthropogenic sources. There is a gradual build-up of metals in the selected

land uses. The soil is highly contaminated with Cd moderately contaminated with Zn while the levels of contamination of the other studied metals are low. The metals generally have low potential ecological risk except Cd which poses a high ecological risk. The ecological risk index revealed that the soil has moderate index. The soil metal concentrations are lower than the amount in other developed cities around the world.

References

[1] Acosta, J., Faz, A., Martinez-Martinez, S., Zornoza, R., Carmona, D., Kabas, S., 2011. Multivariate statistical and GIS-based approach to evaluate heavy metals behaviour in mine sites for future reclamation. Journal of Geochemical Exploration 109(1–3): 8 -17.

[2] Adedeji, O.H., Olayinka, O.O., Oyebanji, F.F., 2013. Assessment of traffic related heavy metalspollution of roadside soils in emerging urban centres in Ijebu-North area of Ogunstate, Nigeria. Journal of Applied Science Environmental Management 17 (4): 509-514.

[3] Adriano, D.C., 2001. Biogeochemistry of trace metals. In SJ Buckland, H K. Ellis & R T Salter (Eds), Ambient concentrations of selected organochlorines programme. Wellington, New Zealand: Ministry for the Environment.

[4] Aiboni, V.U., 2001. Characterization of Some Soils under Different Land Uses along a Toposequence in Ibadan, Nigeria. ASSET Series A. 1 (1): 51-61.

[5] Atayese, M.O., Eigbadon, A.I., Oluwa, K.A., Adesodun, J.K., 2008. Heavy metal contamination of amaranthus grown along major highways in Lagos, Nigeria. African Journal of Crop Science 16 (4): 225-235.

[6] Azeez, J.O., Mesele, S.A., Sarumi, B.O., Ogundele, J.A., Uponi, A.O., Hassan, A.O., 2014. Soil metal pollution as a function of traffic density and distance from road in emerging cities: a case study of Abeokuta, southwestern Nigeria. Archives of Agronomy and Soil Science, 60 (2): 275–295.

[7] Azeez, J.O., Hassan, O.A., Egunjobi, P.O., 2011. Soil contamination at dumpsites: Implication of soil heavy metals distribution in municipal solid waste disposal system- a case study of Abeokuta, south-western Nigeria. Soil and Sediment Contamination: An International Journal. 20, 370–386.

[8] Bini, C., Sartori. G., Wahsha, M., Fontana, S., 2011. Background levels of trace elements and soil geochemistry at regional level in NE Italy. Journal of Geochemical Exploration 109 (1–3):125 - 133.

[9] Bolaji, O.M., Okekearu, I.R., Sridhar, M.K.C., 2009. Survey of lead levels in sampled food itemsand indoor environment of three selected areas of Lagos metropolis. Nigerian Journal of Science 43: 1- 6.

[10] Bouyoucos, G.H., 1962. Hydrometer method for making particle size analysis of soils. Agronomy Journal. 54: 464–465.

[11] Bremner, J.M., Mulvaney, C.S., 1982. Pages 600-01 in A. L. Page et al., Eds. Methods of soil analysis. Part 2. 2nd ed. American Society of Agronomy, Madison, WI.

[12] Cai, L., Xu, Z., Ren, M., Guo, Q., Hu, X., Hu, G., Wan, H., Peng, P., 2012. Source identification of eight hazardous heavy metals in agricultural soils of Huizhou, Guangdong Province, China. Ecotoxicological and Environmental Safety 78, 2–8.

[13] Chabukdhara, M., Nema, A.K., 2012. Assessment of heavy metal contamination in Hindon river sediments: a chemometric and geochemical approach. Chemosphere 87(8): 945–953.

[14] Chen, Z., He, M., Sakurai, K., Kang, Y., Iwasaki, K., 2007. Concentrations and chemical forms of heavy metals in urban soils of Shanghai, China. Journal of Soil Science and Plant Nutrition 53: 517–529.

[15] Chon, H., Kim, K., Kim, J., 1995. Metal contamination of soils and dusts in Seoul metropolitan city, Korea. Environmental and Geochemical Health 17: 139–146.

[16] DPR (Department of petroleum resources), 2002. Environmental guidelines and standards for the petroleum industry in Nigeria (revised edition).Department of Petroleum Resources, Nigeria: Ministry of Petroleum and Natural Resources.

[17] DEFRA (Department for Environment, Food and Rural Affairs) and Environment Agency, 2009. Soil Guideline Values for Cadmium in Soil, Department for Environment, Food and Rural Affairs and Environment Agency, Bristol.1998.96 pp. Boca Raton, Florida: Lewis

[18] Donisa, C., Mocanu, R., Steinnes, E., Vasu, A., 2000. Heavy metal pollution by atmospheric transport in natural soils from the northern part of eastern Carpathians. Water Air and Soil Pollution 120: 347–358.

[19] Du Laing, G., Rinklebe, J., Vandecasteele, B., Meers, E., Tack, F.M.G., 2009. Trace metal behaviour in estuarine and riverine floodplain soils and sediments: a review. Science of Total Environment 407:3972–3985.

[20] EEA (European Environment Agency), 1998. Europe's environment: The second assessment. Amsterdam: Elsevier Science, pp 293.

[21] Fiori, C.S., Rodrigues, A.P., Santelli, R.E., Cordeiro, R.C., Carvalheira, R.G., Araujo, P.C., Castilhos, Z.C., Bidone, E.D., 2013. Ecological risk index for aquatic pollution control: a case study of coastal water bodies from the Rio de Janeiro State, southeastern Brazil. Geochimica Brasiliensis 27(1): 24-36.

[22] Gawlik, B.M., Bidoglio, G., 2006. Background values in European soils and sewage sludges. Results of a JRC-coordinated study on background values. PART III, conclusions, comments and recommendations. European Commission Directorate-General Joint Research Centre Institute for Environment and Sustainability. Via Enrico Fermi, 21020 Ispra (Va), Italy. http://ies.jrc.cec.eu.int, http://www.jrc.ec.europa.eu/

[23] Gu, Y.G., Wang, Z.H., Lu, S.H., Jiang, S.J., Mu, D.H., Shu, Y.H., 2012. Multivariate statistical and GIS-based approach to identify source of anthropogenic impacts on metallic elements in sediments from the mid Guangdong coasts, China. Environmental Pollution 163: 248–255.

[24] Guo, G., Wu, F., Xie, F., Zhang, R., 2012. Spatial distribution and pollution assessment of heavymetals in urban soils from southwest China. Journal of Environmental Science 24(3): 410–418.

[25] Gonzalez, Z.I., Krachler, M., Cheburkin, A.K., Shotyk, W., 2006. Spatial distribution of natural enrich ments of arsenic, selenium, and uranium in a minerotrophic peat land, Gola diLago, Canton Ticino, Switzerland. Environmental Science Technology 40: 6568–6574.

[26] Hakanson, L., 1980. An ecological risk index for aquatic pollution control. A sedimentological approach. Water Resources 14: 975–1001.

[27] He, M., Chen, Z., Iwasaki, K., 2004. Physico-chemical characteristics of the soils from the Coastal Plain in Shanghai, China. Soil Science and Plant Nutrition 50: 1237–1244.

[28] Huang, S.W., Jin, J.Y., 2008. Status of heavy metals in agricultural soils as affected by different patterns of land use. Environmental Monitoring and Assessment 139 (1–3): 317–327.

[29] Imperato, M., Adamo, P., Naimo, D., Arienzo, M., Stanzione, D., Violante, P., 2003. Spatial distribution of heavy metals in urban soils of Naples city (Italy). Environmental Pollution 124: 247–256.

[30] Iwegbue, C.M.A., Stephen, A.O., Cyril, I.E., Godwin, E.N., 2015. Concentrations, Human and Ecological Risks of Metals in Soils in the Vicinity of Asphalt Plants in Delta States, Nigeria. Jordan Journal Earth Environmental Sciences 7(1): 49 – 63.

[31] Iwegbue, C.M.A., 2014. Impact of land use types on the concentrations of metals in soils of urban environment in Nigeria. Environmental and Earth Science 72 (11): 4567-4585.

[32] Iwegbue, C.M.A., Nwajei, I.G., Eguavoen, O.I., 2012. Impact of land use patterns on chemical properties of trace elements in soils of rural, semi-urban and urban zones of the Niger Delta, Nigeria. Soil and Sediment Contamination: An International Journal. 21 (1): 19-30.

[33] Iwegbue, C.M.A., Nwajei, G.E., Ogala, J.E., 2010. Determination of trace metal concentrations in soil profiles of municipal waste dumps in Nigeria. Environmental Geochemical Health 32 (5): 415-430.

[34] Jalili, M., Azizkhan, R., 2009. Lead toxicity resulting from chronic ingestion of opium. West Journal of Emerging Medicine 10 (4): 244-246.

[35] Kabała, C., Szerszen, L., 2002. Profile distributions of lead, zinc, and copper in dystric cambisols developed from granite and gneiss of the Sudetes Mountains, Poland. Water Air and Soil Pollution 138: 307–317.

[36] Krami, L.K., Amiri, F., Sefiyanian, A., Mohamed-Shariff, A.R.B., Tabatabaie, T., Pradhan, B., 2013. Spatial patterns of heavy metals in soil under different geological structures and land uses for assessing metal enrichments. Environmental Monitoring and Assessment 185: 9871–9888.

[37] Lee, C.S., Li, X.D., Shi, W.Z., Cheung, S.C., Thornton, I., 2006. Metal contamination in urban, suburban and country park soils of Hong Kong: a study based on GIS and multivariate statistics. Science of the Total Environment 356: 45–61.

[38] Li, X., Feng, L., 2012. Multivariate and geostatistical analyzes of metals in urban soil of Weinan industrial areas, Northwest of China. Atmospheric Environment 47: 58–65.

[39] Li, X.D., Lee, S.L., Wong, S.C.L., 2004. The study of metal contamination in urban soils of Hong Kong using a GIS-based approach. Environmental Pollution 129: 113–124.

[40] Luo, L., Ma, Y., Zhang, S., Wei, D., Zhu, Y.G., 2009. An inventory of trace element inputs to agricultural soils in China. Journal of Environmental Management 90: 2524–2530.

[41] Luo, W., Lu, Y., Giesy, J.P., Wang, T., Shi, Y., Wang, G., Xing, Y., 2007. Effect of land use on concentrations of metals in surface soils and ecological risk around Guanting Reservoir, China. Environmental and Geochemical Health 29: 459-471.

[42] Madrid, L., Diaz-Barrientos, E., Madrid, F., 2002. Distribution of heavy metal contents of urban soils in parks of Seville. Chemosphere 49:1301-1308.

[43] Manta, D.S., Angelone, M., Bellanca, A., Neri, R., Sprovieri, M., 2002. Heavy metals in urbansoils: a case study from the city of Palermo (Sicily), Italy. Science of the Total Environment 300: 229–243.

[44] McLean, E.O., Dumford, S.W.F., Coronel, S.W., 1982. A comparison of several methods of determining lime requirements of soil. Soil Science Society of America Proceedings 30: 26-30.

[45] Miguel, E., JimInez-De Grado, M., Llamas, J.F., MartCn-Dorado, A., Mazadiego, L.F., 1998. The overlooked contribution of compost application to the trace element load in the urbansoil of Madrid (Spain). Science of the Total Environmental 215: 113–122.

[46] Moller, A., Muller, H.W., Abdullah, A., Abdelgawad, G., Utermann, J., 2005. Urban soil pollution in Damascus, Syria: concentrations and patterns of heavy metals in the soils of the Damascus Ghouta. Geoderma 124: 63–71.

[47] Nelson, D.W., Sommers, L.E., 1996. Total carbon, organic carbon, and organic matter. pp. 961-1010, In D. L. Sparke (ed) Methods of soil analysis. Part 3. Chemical Methods SSSA Book Series no. 5. ASA and SSSA. Madison, WI.

[48] Nicholson, F.A., Smith, S.R., Alloway, B.J., Carlton-Smith, C., Chambers, B.J., 2003. An Inventory of heavy metals inputs to agricultural soils in England and Wales. Science of the Total Environmental 311: 205-219.

[49] Niu, L., Yang, F., Xu, C., Yang, H., Liu, W., 2013. Status of metal accumulation in farmland soils across China: from distribution to risk assessment. Environmental Pollution 176: 55–62.

[50] Peter, E., Adeniyi, G., 2011. Spatial relationships of urban land use, soils and heavy metal concentration in Lagos Mainland area. Journal of Applied Science and Environmental Management 15 (2): 391-399.

[51] Salonen, V., Korkka-Niemi, K., 2007. Influence of parent sediments on the concentration of heavy metals in urban and suburban soils in Turku, Finland. Applied Geochemistry 22: 906–918.

[52] Salt, D.E., Blaylock, V., Kumar, P.B.A.N., Dushenkov, U., Ensley, B.D., Chet, L., Raskin, I., 1995. Phytoremediation: A novel strategy. Biotechnology 13: 468–474.

[53] Senjobi, B.A., 2007. Comparative Assessment of the Effect of Land Use and Land Type on Soil Degradation and Productivity in Ogun State, Nigeria. 161pp. Unpublished Ph.D. Thesis submitted to the Department of Agronomy, University of Ibadan, Nigeria.

[54] Shi, G.T., Chen, Z.L., Xu, S.Y., Zhang, J., Wang, L., Bi, C.J., Teng, J.Y., 2008. Potentially toxic metal contamination of urban soils and roadside dust in Shanghai, China. Environmental Pollution 156: 251–260.

[55] Sun, Y., Zhou, Q., Xie, X., Liu, R., 2010. Spatial, sources and risk assessment of heavy metal contamination of urban soils in typical regions of Shenyang, China. Journal Hazard Material 174: 455–462.

[56] US DOE (United States Department of Energy), 2011. The Risk Assessment Information System (RAIS); U.S. Department of Energy's Oak Ridge Operations Office (ORO): Oak Ridge, TN, USA.

[57] US EPA (United States Environmental Protection Agency), 2001. Risk assessment guidance for superfund. Volume 1: Human evaluation Manual (Part E, Supplemental guidance for defined risk assessment). EPA/540/R/99/005.7. Washington, DC, USA: Office of Emergency and Remedial response, United states Environmental Protection Agency.

[58] US EPA (United States Environmental Protection Agency), 2011. Regional Screening Level Table (RSL) for Chemical Contaminants at Superfund Sites. U.S. Environmental Protection Agency: Washington, DC, USA.

[59] Walkey, A., Black, I.A., 1939. An examination of Degtjareff method for determining soil organic matter and a proposed modification of the chronic acid titration method. Soil Science 37: 29-37.

[60] Ward, N.I., 1989. Multielement contamination of British motorway environments. In: Vernet, J.P. (Ed.), Heavy metals in the environment. International Conference. Vol. II. Geneva. September 1989, (Ed.), CEP Consultants Edinburgh.

[61] Wikipedia 2017. (https://en.wikipedia.org/wiki/States_of_Nigeria). Accessed in March 2017.

[62] Wilcke, W., Muller, S., Kanchanakool, N., Zech, W., 1998. Urban soil contamination in Bangkok: heavy metal and aluminium partitioning in topsoils. Geoderma 86: 211–228.

[63] WRB. World Reference Base for Soil Resources, 2006. World Soil Resources Reports, 103, FAO, Rome.

[64] Xia, X., Chen, X., Liu, R., Liu, H., 2011. Heavy metals in urban soils with various types of land use in Beijing, China. Journal of Hazardous Material 186: 2043–2050.

[65] Yang, L.L., Mao, R.Z., Li, H.J., 2004. Discussion on the patterns and techniques of optimum utilization of water and land in Huailai County (in Chinese). Research on Soil and Water Conservation 11: 27-30.

[66] Zhang, X., Lin, F., Wong, M.T., Feng, X., Wang, K., 2009. Identification of soil heavy metal sources from anthropo-genic activities and pollution assessment of Fuyang County, China. Environmental Monitoring and Assessment 154(1): 439–449.

[67] Zheng, Y.M., Chen, T.B., He, J.Z., 2008. Multivariate geostatistical analysis of heavy metals in topsoils from Beijing, China. Journal of Soil and Sediment 8: 51–58.

[68] Zhong, L., Liu, L., Yang, J., 2012. Characterization of heavy metal pollution in the paddy soils of Xiangyin County, Dongting lake drainage basin, central south China. Environmental and Earth Science, 1–8. doi:10.1007/s12665-012-1671-6.

JJEES
Jordan Journal of Earth and Environmental Sciences

Volume 8, (Number 1), Sept, 2017
ISSN 1995-6681
Pages 45 - 53

Uptake of Arsenic (As), Cadmium (Cd), Chromium (Cr), Selenium (Se), Strontium (Sr), Vanadium (V) And Uranium (U) by Wild Plants in Khan Al- Zabib Area /Central Jordan

Asma Fayyad Bzour[1*], Hani Nicola Khoury[1] and Sawsan Attalah Oran[2]

[1]Department of Geology, University of Jordan, Jordan
[2]Department of Biological Sciences, University of Jordan, Jordan

Received 19 May, 2017; Accepted 24 August, 2017

Abstract

The wide distribution of Redox-Sensitive Elements (RSE) as Arsenic (As), Cadmium (Cd), Chromium (Cr), Selenium (Se), Strontium (Sr), Vanadium (V) and Uranium (U) in the top soil of Khan Al-Zabib area are related to the weathering action of alkaline surface and groundwater on the parent rocks. The bioavailability, distribution, sorption, and ecotoxicity of As, Cd, Cr, Se, Sr, V, and U of the wild plants and top soils, in the present study area, were evaluated. A total number of 10 surface soil samples and 10 plant samples were collected and analyzed for the most toxic elements. The uptake of elements by plants was dependent on the plant species and the concentration of elements in the soil. The results of the present work provide valuable knowledge for understanding the bioavailability of some toxic elements in the soil and plants of Central Jordan. The results are expected to be of great interest for the Jordanian Uranium Mining Company during their environmental risk assessments.

© 2017 Jordan Journal of Earth and Environmental Sciences. All rights reserved

Keywords: Bioavailability, Central Jordan, Trace elements Uptake, Transfer Factor.

1. Introduction

Heavy metals and trace elements, such as Arsenic (As), Cadmium (Cd), Chromium (Cr), Selenium (Se), Strontium (Sr), Vanadium (V) and Uranium (U), are naturally occurring in rocks and soil environment resulted from pedogenetic processes of weathering (Pierzynsiki et al., 2000). These elements are important in contaminating surface and ground water and decreasing crop production as a result of bioaccumulation and biomagnification in the food chain. Knowledge of basic chemistry, environmental and associated health effects of these heavy metals is important to understand their speciation, bioavailability, and remedial options. Heavy metals are adsorbed onto the soil, by initial fast reactions (minutes, hours), followed by slow absorption reactions (days, years) by plants, redistributed into different chemical forms with varying bioavailability, mobility, and toxicity (Shiowatana et al., 2001). Heavy metals distribution in soils take place as a result of mineral precipitation and dissolution, ion exchange, adsorption, aqueous complexation, biological immobilization and mobilization, and plant uptake (Levy et al., 1992). Potentially toxic elements in soils and plants may come from the bedrock itself and anthropogenic sources, like solid or liquid waste deposits (Wilson and Pyatt, 2007). Plants are important components of ecosystems as they transfer elements from abiotic into biotic environments. All plants have the ability to accumulate essential elements from soil in different concentrations for growth and development. This ability also allows plants to accumulate other non-essential elements, which have not known biological function (Djingova and Kuleff, 2000). Several studies have been carried out and investigated by many authors in different regions to evaluate and describe the accumulation of toxic trace elements and its impacts on the plant diversity (Tomé et al., 2002; Chen et al., 2005). The soils and plants contain all naturally occuring radioactive elements with half-lives comparable to the age of the earth, although their concentrations in plants may be rather low (Buck et al., 1996). The uptake of heavy metals by plant parts is real and not due to contamination by aerosols and was best illustrated by higest Ni uptake index in Atriplex leuceclada (Abed and Al- Eisawi, 1994). Bzour et al. (2016) investigated the potential mobilization and accumulation of Cr, V and U in wild plants in Siwaqa area/ Central Jordan and the results indicated that the highest TF for U is (0.25) and was recorded in Onopordum transjordanicum. Top soils of central Jordan are enriched in redox sensitive trace elements, such as U, Cr, Zn, Cr, Ni, Cu, Co, As, and Cd in the form of sulphides and selenides (Nassir and Khoury, 1982; Khoury and Nassir, 1982; Khoury, 2012; Fourcade et al., 2007; Techer et al., 2006; Khoury et al., 2014, 2015). The highest concentrations of trace elements from Central Jordan are present in the altered marble, chalk marl/travertine, and top soil (Elie et al., 2007; Khoury, 2015). Limited research was carried out on the the impact of trace elements on the wild plants in central Jordan. The impact of dust and heavy metals emitted from petroleum refinery on plant diversity in Tafila / Jordan was investigated (Oran and Abu Zahra, 2014; Oran; Al- Zo'ubi, 2016). Recent work on central Jordan has indicated that redox sensitive elements are present in the structure of high and low

* Corresponding author. e-mail: asma.bzour.geo@gmail.com

temperature minerals and are adsorbed by the organic matter of the parent bituminous rocks (Fourcade et al., 2007; Techer et al., 2006; Khoury et al., 2014, 2015; Khoury et al., 2016). Heavy metals, such as U, Cd, As, Cr, Pb, Ni, Zn and V, are also enriched in the phosphate rocks of Central Jordan. (Abed et al., 2008). The lack of knowledge about the behavior of some toxic trace elements in soils and plants in Central Jordan, in addition to the planned mining activities by Jordan Uranium Minning Company (JUMCO) in the area have encouraged the authors to carry out the present work. The transfer of As, Cd, Cr, Se, Sr, V and U to the wild plants in terms of sorption, toxicity and speciation will be studied.

1.1. Geology of Central Jordan

The northern boundaries of the first and second areas of Central Jordan (Daba- Khan Al-Zabib- Siwaqa) are located 25 km and 60 km south of Amman with the first area situated between E 36o 00' to 36o 15' and N31o 15' to 31o 30' and the second area between E 35o 00' to 36o 15' and N 31o 15' to 31o 30'. Figure 1a shows the location map of the studied area. The studied area was mapped in detail by the Natural Resources Authority (NRA) (Barjous, 1986; Jaser, 1986) and the geology, stratigraphy and sedimentology were described in details by Powell (1989) and Powell and Moh'd (2011).

Figure 1c is a generalized geological map of the study area (Barjous, 1986; Jaser, 1986; Khoury et al., 2014). Most of the outcropping rocks are of Upper Cretaceous age. The outcropping rocks of Central Jordan are sedimentary in origin and the exposed bed rock ranges in age from Turonian (Upper Cretaceous) to Eocene (Lower Tertiary) REF. Outcrops in central Jordan illustrate the presence of three main rock types: Bituminous marl; varicolored marble (pyrometamorphic rocks); travertine and top soil. The Bituminous Marl Unit overlies the Phosphorite Unit and underlies the varicolored marble and all are of Maestrichtian – Lower Paleocene age (Blake & Ionides, 1939; Quennel, 1956; Burdon, 1959; Barjous, 1986; Jaser, 1986; Khoury et al., 2014). In central Jordan, unusual redox-sensitive elements (RSE) cover large areas and are mainly associated with the varicolored marble, Pleistocene-Recent travertine and top soil. Yellow uranium encrustations and green Cr-rich smectites are also associated with the varicolored marble (pyrometamorphic rocks) and the underlying bituminous marl (oil shale) and phosphorites (Khoury, 2006; Khoury and Abu-Jayabb, 1995; Khoury et al., 1984; Khoury et al., 2014). The mineralogy of surficial top soil in central Jordan and RSE source rocks, transport conditions, and deposition processes were explained in detail by Khoury et al. (2014). The geochemistry of uranium and vanadium of the mineral phases was not investigated in detail. The general chronological sequence of the different lithological units is illustrated in Figure 1d. The Upper Cretaceous to Tertiary rocks in Central Jordan were deposited at the margin of the Tethys shelf-sea in environments ranging from super-tidal to deep sub-tidal (Bender, 1986). Transgression took place during Cenomanian times and marine sedimentation continued until the Late Eocene, despite fluctuations in sea level. Gentle folding, block faulting and possible strike- slip faulting were related to continued tectonic movement on the Jordan Rift structure which is located 60 Km to the west of the study area (Bender, 1986; Powell, 1989; Powell & Moh'd, 2011).

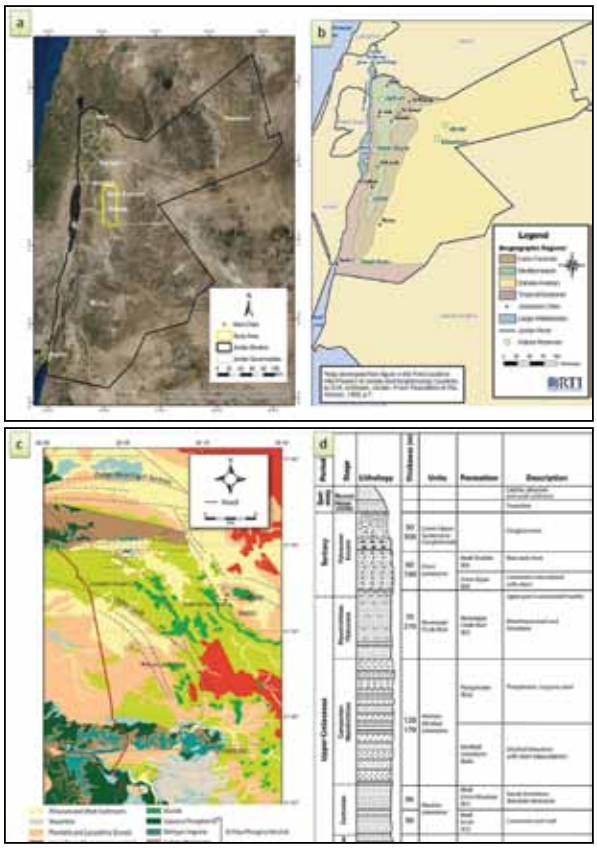

Figure 1. (a) Location map of Jordan showing the study area. **(b)** Location map of the study area showing the vegetation regions (after Al- Eisawi, 1996). **(c)** Geological map of central Jordan (modified after Barjous 1986; Jaser 1986; Khoury et al. 2014). **(d)** Simplified geologic section of central Jordan.

1.2. Bioclimatic and Vegetation Regions of Central Jordan

Central Jordan is classified as arid Mediterranean bioclimate; cool, warm and very warm varieties (Al- Eisawi, 1996). The largest area of Central Jordan is located in arid Mediterranean warm variety bioclimatic zone and located in Irano-Turanian vegetation region, while the north west of Central Jordan is in Mediterranean vegetation region and a very small part of south east of central Jordan located in Saharo-Arabian vegetation regions Figure 1b. The vegetation is mostly herbs, shrubs and bushes with no trees (Al-Eisawi, 1996).

2. Field and Laboratory Work

Field trips were conducted extensively to Khan Al-Zabib area, Central desert of Jordan. Fresh plant samples and soil samples were collected for every plant species available at the time of investigation and were placed in plastic bags according to standards. Global positioning system (GPS) records were made from the sampling sites during the period of the study. Sample locations were chosen randomly referring to the availability of plant species and sampling was based on ease of access, adequate vegetation growth to

provide vegetation samples. Plant specimens were identified based on: Flora Palaestina (parts 1, 2, 3 and 4) (Zohary, 1966; Feinbrun, 1986). Field Guide to Wild Flowers of Jordan and Neighboring Countries (Al-Eisawi, 1998). Khan Al-Zabib area is dry with scare vegetation; wild plants and green grass cover the landscape during springtime that is used by locals for grazing and as folk medicine (Figure 2a). A number of 10 soil samples and 10 plant samples were collected. Figure 2b shows a general view of the landscape in Khan Al-Zabib area indicating the scarcity of vegetation cover. The top soil is porous and is mainly composed of calcite and gypsum. Secondary green Cr-rich smectite and yellow uranium minerals are common features filling voids and planes of weakness. Yellow secondary uranium minerals (source of U and V) together with green Cr- rich smectites are almost always associated together in the top soil and the underlying travertine and altered marble (Figs 2c and 2d). Figure 3 (a - h) are selected photographs of some typical wild plants from Khan Al-Zabib area.

Plant samples were carefully brush- washed with tab water and again washed and rinsed with distilled water to remove externally adhered metals and dust from the surface of the plants. The plants were oven dried at 100 ºC overnight. The samples were ground in a small coffee grinder. Finally, the samples were ground into fine powder by using Mill mix.

Soil samples were oven dried at 100 ºC overnight, then sieved through 63 microns mesh screen into fine powder. The samples were characterized using chemical methods. All the analytical work was carried out in the laboratories of the Department of Geology, University of Jordan and the Jordan Atomic Energy Commission (JAEC).

Inductively coupled plasma mass spectrometry (ICP- MS) analyses were carried out in the Chemical Analysis Section, chemical and physical analysis laboratories, Nuclear Fuel Cycle Commission (NCC- CPAL), Jordan Atomic Energy Commission (JAEC). The ICP- MS (ELAN® DRC-e, PerkinElmer SCIEX) was used to measure the amount of toxic trace elements in plants and soil particles. All samples were sent via Jordanian Uranium Mining Company (JUMCO) to ALS Arabia Co. Ltd. Jeddah, Saudi Arabia to be analyzed.

The transfer factor (TF) is defined as a factor used to describe the amount of element, which is expected to be transferred to plant from soil. It is also defined as the ratio of specific activities in plant parts and soil (in Bq kg-1 dry weight plant part divided by Bq kg1 dry weight soil). The TF was used as an index for the accumulation of trace elements by plants or the transfer of elements from soil to plants in mg. Kg-1 (Whicker et al., 1999; Yanagisawa et al., 1992).

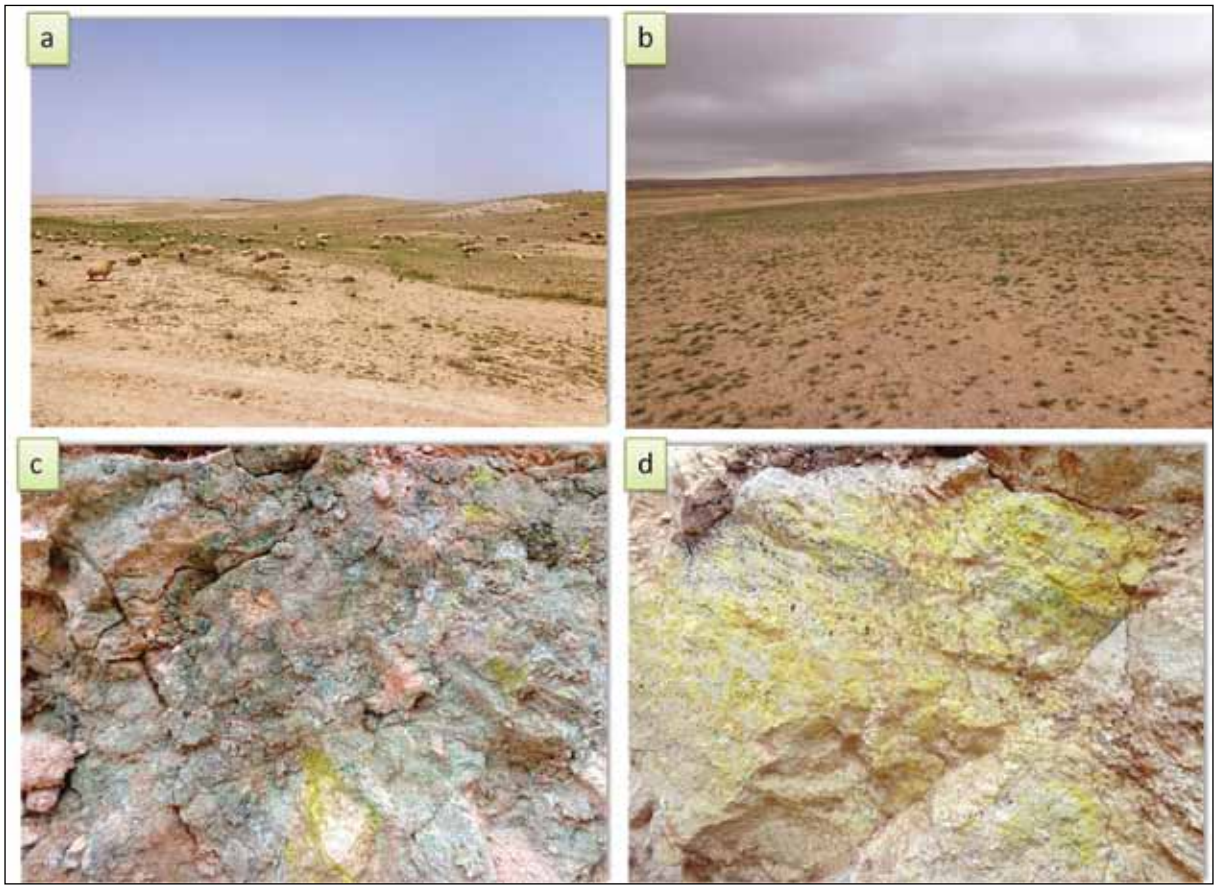

Figure 2. (a) Landscape of the study area showing grazing by herbavious animals.
(b) A Photograph showing a general view of the landscape indicating the scarcity of vegetation cover.
(c) A photograph illustrates the presence of secondary encrustations of uranium and Cr- rich smectites in the altered marble/top soil.
(d) A phtograph of yellow secondary uranium minerals filling porous rocks.

© 2017 Jordan Journal of Earth and Environmental Sciences . All rights reserved - Volume 8, (Number 1), (ISSN 1995-6681)

Figure 3. Photographs of wild plants **(a)** Ornithogalum trichophyllum **(b)** Malva sylvestris **(c)** Scorzonera papposa **(d)** Erodium hirtum **(e)** Astragalus sparsus **(f)** Gymnarrhena micranta **(g)** Astragalus sp. **(h)** Leopoldia longipes.

3. Result and Discussion

3.1. Mass Spectrometry Analysis (ICP- MS) Results

The mass spectrometry analysis (ICP- MS) results are given in Table 1. The table includes the concentration results of As, Cd, Cr, Se, Sr, V and U in the soil and plant samples. The calculated transfer factors TF are given in Table 2.

Table 1. Trace elements concentrations (mg/Kg) in soil and plant of Khan Al- Zabib area

Soils							
SAMPLE ID	As	Cd	Cr	Se	Sr	V	U
1	26.1	62.7	256	9.4	781	177	23
2	27.3	82.1	219	17.5	849	203	29.8
3	28.2	108.5	224	10	799	190.5	20.7
4	13.6	47.9	74.4	7.1	569	94.6	6.87
5	6.73	10.2	52.3	2.1	337	62.9	4.77
6	9.21	8.54	86.3	2.1	400	59.8	5.24
7	7.07	12.95	55.9	2.5	353	66.8	4.02
8	8.9	9.44	78	1.9	392	57.4	4.91
9	6.96	7.08	65.9	1.6	374	56.8	4.5
10	12.85	5.97	111.5	2.6	464	69.5	7.47
Mean	14.69	35.54	122.3	5.68	531.8	103.8	11.13
Std. Error of Mean	2.83	11.85	24.88	1.7	64.3	19.24	3.02
Minimum	6.73	5.97	52.3	1.6	337	56.8	4.02
Maximum	28.2	108.5	256	17.5	849	203	29.8
Number of values	10						
Plants							
Plant Name	As	Cd	Cr	Se	Sr	V	U
Erodium hirtum	1.9	4.21	24.3	3.18	274	14.6	1.645
Malva sylvestris	1.34	23.2	14.6	7.32	226	10.9	1.045
Astragalus sp.	2.7	6.87	34.2	5.9	230	21.8	1.84
Arthocnemum mucronatum	0.7	2.83	4.7	0.275	166.5	4.4	0.34
Gymnarrhena micrantha	1.01	4.03	7.3	0.601	142.5	6.8	1.025
Maresia pygmaea	1.82	2.3	19.4	0.407	404	10.7	1.76
Astragalus sparsus	1.21	2.77	8.3	0.544	134	7.8	0.809
Leopoldia longipes	0.82	1.135	9.34	0.206	152	7	1.16
Gynandriris sisyrinchium	1.14	1.42	17.75	0.247	178	7.5	0.662
Convolvulus arvensis	0.88	0.32	5.14	0.2	152	3.6	0.973
Mean	1.35	4.9	14.5	1.9	205.9	9.51	1.126
Std. Error of Mean	0.2	2.1	3.02	0.9	26.3	1.71	0.154
Minimum	0.7	0.32	4.7	0.2	134	3.6	0.34
Maximum	2.7	23.2	34.2	7.32	404	21.8	1.84
Number of values	10						

Table 2. Soil- Plant transfer factor (TF) of Trace elements concentrations (mg/Kg) Khan Al-Zabib area

TF							
SAMPLE ID	As	Cd	Cr	Se	Sr	V	U
Erodium hirtum	0.07	0.067	0.1	0.3	0.35	0.1	0.07
Malva sylvestris	0.05	0.3	0.06	0.4	0.26	0.05	0.04
Astragalus sp.	0.09	0.06	0.15	0.6	0.3	0.1	0.1
Arthocnemum mucronatum	0.05	0.06	0.06	0.04	0.3	0.05	0.1
Gymnarrhena micrantha	0.15	0.4	0.1	0.3	0.4	0.1	0.2
Maresia pygmaea	0.2	0.26	0.2	0.2	1.01	0.2	0.3
Astragalus sparsus	0.2	0.2	0.1	0.2	0.4	0.1	0.2
Leopoldia longipes	0.1	0.1	0.1	0.1	0.4	0.1	0.2
Gynandriris sisyrinchium	0.16	0.2	0.2	0.15	0.5	0.1	0.1
Convolvulus arvensis	0.07	0.05	0.04	0.07	0.3	0.05	0.1
Mean	0.114	0.2	0.111	0.24	0.422	0.141	0.1
Std. Error of Mean	0.02	0.04	0.02	0.054	0.07	0.03	0.014
Minimum	0.05	0.05	0.04	0.04	0.26	0.05	0.04
Maximum	0.2	0.4	0.2	0.6	1.01	0.2	0.3
Number of values	10						

3.1.1. Arsenic (As)

Arsenic (As) is a carcinogen and is associated with human skin, lung and bladder cancers (Ng et al., 2003; ATSDR, 2005). The permissible limit of As in soil which recommended by WHO (2007) and Pendias (2000) is 10 mg/kg As. The toxic limit of As in plant species is 0.1 recommended by WHO (2007). The concentrations of (As) in the soils of Khan Al-Zabib area ranged between 6.73 to 28.2 mg/kg with a mean value of 14.69 mg/kg. Six soil samples are above the permissible limit. The highest value of (As) in the plant species of the study area is 2.7 mg/kg and is recorded in Astragalus sp. The lowest value of (As) concentration is 0.7 mg/kg and is recorded in Arthocnemum mucronatum. The mean value is 1.35 mg/kg. Figure 4 illustrates the (As) concentrations in the plant species of the study area. The mean transfer factor from soil to plant of Khan Al-Zabib area is 0.114. The highest transfer factor is 0.2 in Astragalus sparsus and Maresia pygmaea. The lowest TF is 0.05 in Arthocnemum mucronatum.

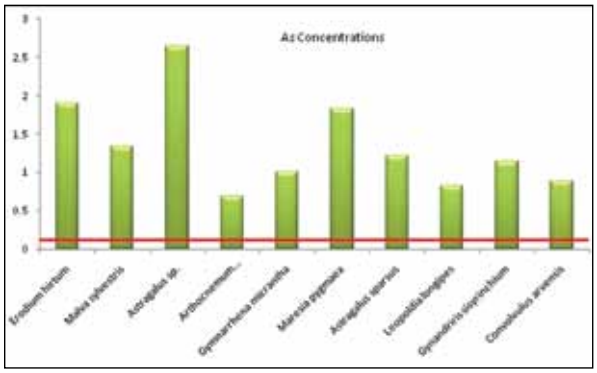

Figure 4. As concentrations in wild plant sp. in Khan Al- Zabib area

3.1.2. Cadmium (Cd)

Cadmium is an extremely toxic metal that has no known necessary function in the body. Cadmium toxicity contributes to a large number of health conditions, including the major killer diseases, such as heart disease, cancer and diabetes (Sheppard et al., 1985). The permissible limit of Cd in soil as recommended by WHO (2007) is 5 mg/kg. The toxic limit of Cd to the plant species recommended by WHO, 2007 is 0.02 mg/kg. The concentrations of Cd in soils of Khan Al-Zabib area ranged between 5.97 to 108.5 mg/kg with mean 35.54 mg/kg. All collected soil samples from this area are above the permissible limit. The highest value of Cd content is 23.2 mg/kg in plant species of Khan Al-Zabib area and is recorded in Malva sylvestris. The lowest value of Cd concentration is 0.32 mg/kg and is recorded in Convolvulus arvensis. The mean value is 4.9 mg/kg. According to WHO, 2007, all plant species of Khan Al-Zabib area are above the toxic limits. Figure 5 shows the Cd concentrations in the wild plant species of the study area. The mean transfer factor of Cd from soil to plant of Khan Al-Zabib area is 0.2. The highest transfer factor is 0.4 in Gymnarrhena micranta. The lowest TF is 0.05 in Convolvulus arvensis

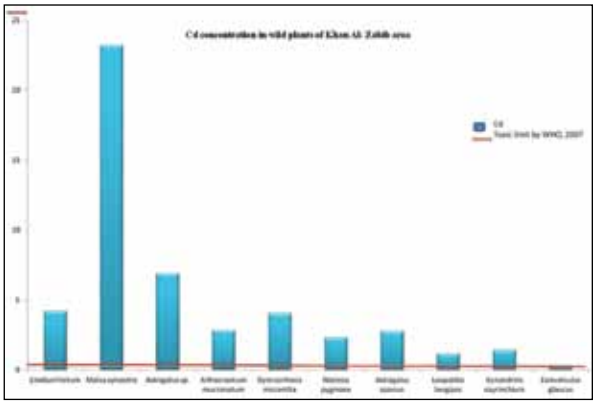

Figure 5. Cd concentrations in wild plant sp. in Khan Al- Zabib area

3.1.3. Chromium (Cr)

The abundance of Cr in the Earth's upper crust averages 100 mg/kg (Pendias, 2000). WHO (2007) and Pendias (2000) recommended that 75 mg. Kg-1 Cr in soil is critical concentration to be toxic and recommended that 1.3 mg/Kg is the toxic limit to plant species. The concentrations of Cr in the soils of Khan Al-Zabib area range between 52.3 to 256 mg/kg with a mean value of 122.3 mg/kg. Six soil samples in this area have Cr- values above the permissible limit as recommended by WHO (2007) and Pendias (2000). The highest value of Cr content in plant species of the study area is 34.2 mg/kg and is recorded in Astragalus sp. The lowest value of Cr content is 4.7 mg/kg and is recorded in Arthocnemum mucronatum. The mean value is 14.5 mg/kg. The Cr toxic limit as recommended by WHO, 2007 is below the all concentrations of Cr in all plant species collected from this area. Figure 6 shows the Cr concentrations in plant species of Khan Al-Zabib area. The mean transfer factor from soil to plant of the study area is 0.111; the highest transfer factor is 0.2 in Gynandriris sisyrinium and Maresia pygmaea. The lowest TF is 0.04 in Convolvulus arvensis.

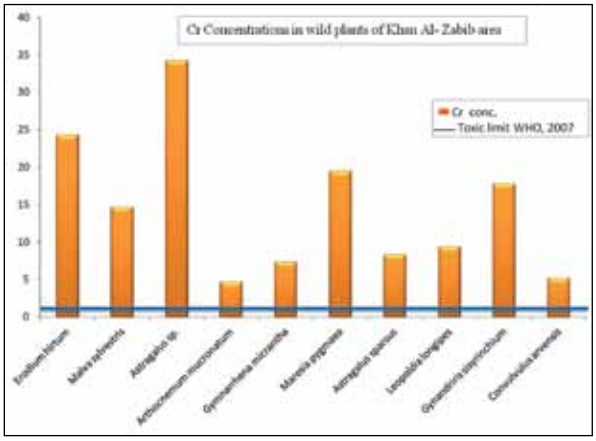

Figure 6. Cr concentrations in wild plant sp. in Khan Al-Zabib area

3.1.4. Selenium (Se)

The average content of selenium in the Earth's crust is estimated as 0.05 mg/kg (Pendias, 2000). Toxic Se concentration limit is 0.5 mg/kg soils (Pendias, 2000) and 0.05 in plants according to WHO (2007). The concentrations of Se in soils of Khan Al-Zabib area range between 1.6 to 17.5 mg/kg with a mean value of 5.68 mg/kg. All soil samples of Khan Al-Zabib area are above the permissible limit for Se as recommended by Pendias (2000). The highest value of Se content in plant species of Khan Al-Zabib area is 7.32 mg/kg and is recorded in Malva sylvestris. The lowest value of Se content is 0.2 mg/kg and is recorded in Convolvulus arvensis, the mean value is 1.9 mg/kg. Figure 7 indicates that all plant species recorded in the study area have exceeded the toxic limit as recommended by WHO. The mean value of transfer factor of Se from soil to plant of the study area is 0.24. The highest transfer factor is 0.6 and is found in Astragalus sp. The lowest TF value is 0.04 and is found in Arthocnemum mucronatum.

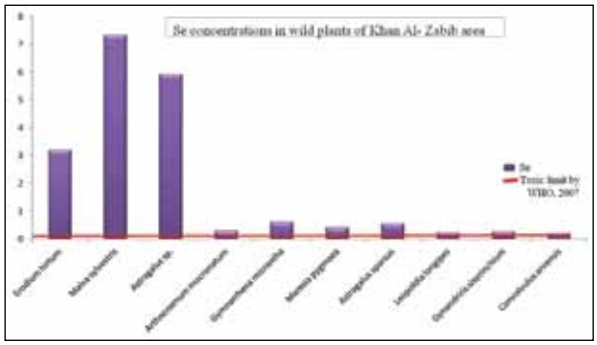

Figure 7. Se concentrations in wild plant species of Khan Al- Zabib area.

3.1.5. Strontium (Sr)

Strontium is a relatively common element in the Earth's crust and its contents range between 260 and 370 mg/kg (Pendias, 2000). According to Pendias (2000), 150 mg/kg concentration value of Sr in soils is toxic, and 50 mg/kg concentration value of Sr in plants is highly toxic referring to WHO (2007). The concentrations of Sr in the soils of Khan Al-Zabib area range between 337 to 849 mg/kg with a mean value of 531.8 mg/kg. All soil samples in this area are above the toxic limit as recommended by Pendias (2000). The highest value of Sr content in plant species of Khan Al-Zabib area is 404 mg/kg and is recorded in Maresia pygmaea. The lowest value of Sr content is 134 mg/kg and is recorded in Astragalus sparsus. The mean value is 205.9 mg/kg. The Sr toxic limit as recommended by WHO (2007) is below the all concentrations of Sr in all plant species collected from this area. Figure 8 shows the Sr concentrations in plant species of the study area. The mean transfer factor from soil to plant of the study area is 0.422. The highest transfer factor is 1.01 in Maresia pygmaea, and the lowest TF is 0.26 in Malva sylvestris.

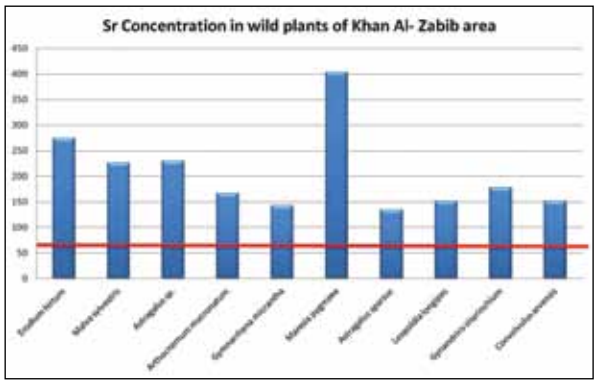

Figure 8. Sr concentrations in wild plant species of Khan Al- Zabib area.

3.1.6. Vanadium (V)

Levels of V in soils are closely related to the parent rock types. Its worldwide soil average is estimated at 129 mg/kg, within the range of 69–320 mg/kg (Pendias, 2000). WHO (2007) recommended that 2 mg/kg V concentration is toxic to plants. The concentrations of V in soils of Khan Al-Zabib area range between 56.8 to 203 mg/kg with a mean value of 103.8 mg/kg. The highest value of V content in plant species of Khan Al-Zabib area is 21.8 mg/kg and is recorded in Astragalus sp., and the lowest value of V content is 3.6 mg/kg and is recorded in Convolvulus arvensis. The mean value is 9.51 mg/kg. As shown in Figure 9, all plant species recorded in the study area are above the toxic limit according to WHO. The mean value of transfer factor of V from soil to plant of the study area is 0.1. The highest transfer factor is 0.2 in Maresia pygmaea, and the lowest TF is 0.05 in Arthocnemum mucronatum & Convolvulus arvensis.

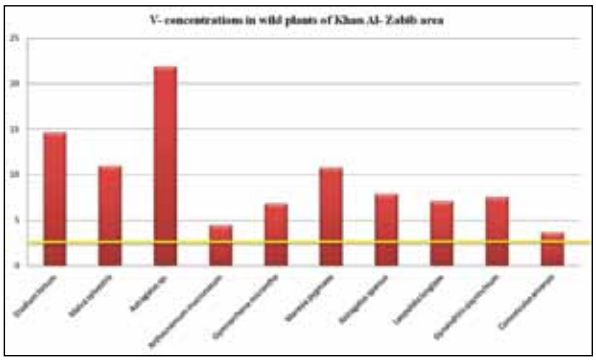

Figure 9. V concentrations in wild plant species of Khan Al- Zabib area.

3.1.7. Uranium (U)

The toxicity of U can be caused by breathing air containing uranium dusts or by eating substances containing uranium, which then enters the bloodstream. Once in the bloodstream, the uranium compounds are filtered by the kidneys, where they can cause damage to the kidney cells (ATSDR, 2005; Sheppard et al., 1985). The toxic limit for U concentrations in soils and plants are 1 & 0.3 mg/kg, respectively, recommended by WHO (2007). The concentrations of U in soils of Khan Al-Zabib area range between 4.02 to 29.8 mg/kg with a mean value of 11.13 mg/kg. All soil samples in this area are above the toxic limit as recommended by WHO (2007). The highest value of U content in plant species of Khan Al-Zabib area is 1.84 mg/kg and is recorded in Astragalus sp. The lowest value of U content is 0.34 mg/kg and is recorded in Arthocnemum mucronatum. The mean value is 1.126 mg/kg. The U toxic limit as recommended by WHO (2007) is below all the concentrations of U in all plant species collected from this area. Figure 10 shows the U concentrations in plant species of the study area. The mean transfer factor from soil to plant of the study area is 0.141. The highest transfer factor is 0.3 and is found in Maresia pygmaea. The lowest TF is 0.04 and is found in Malva sylvestris.

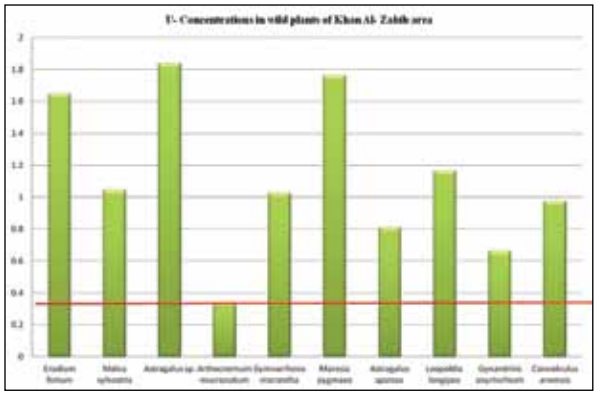

Figure 10. U concentrations in wild plant species of Khan Al- Zabib area.

Conclusions

The present work aims to characterize the soil and the ability of wild plant species in Khan Al-Zabib area/ Central Jordan to absorb different hazardous trace elements chemically and mineralogically. The behavior of toxic heavy metals and trace elements (As, Cd, Cr, Se, Sr, V and U) in soils and plants was investigated. The ability to assess of wild plant species in Khan Al-Zabib area/ Central Jordan for the absorption of different hazardous trace elements. The environmental geochemical survey has revealed variations of trace elements concentrations in soils and plant species. The sources of trace elements are related to the leaching processes from the parent rocks of the area. The potential mobilization of As, Cd, Cr, Se, Sr, V and U seems to decrease as follows: Sr > Cr >V> Cd > Se >As > U. The absorption of these elements in plants is variable from one species to another, but the majority of plants shows that the accumulation of metals followed this order: Sr > Se > Cd > V > As > Cr > U, indicating that the metal release in the soils correlates with their absorption by the plants. The concentration of these elements was depend on climatic geologic events in Central Jordan. Differences between trace elements TFs values for various plant species are related to the different characteristics and behavior of the wild plants. In general, the comparative uptake of trace elements is affected by numerous physical, chemical and biological conditions of the soil. The uptake of elements by plants depends on the plant species and the concentration of elements in the soil. The values are above the permissible limits according to world health organization (WHO). The information on the concentration level and transfer of (As, Cd, Cr, Se, Sr, V and U) from soil to plant will provide important information during the environment risk assessment that is expected to be carried out by JUMCO in the near future. Further studies and investigations are needed to assess and evaluate the ecotoxicity of heavy metals on plant species by the different RSE in the different soils of Central Jordan.

Acknowledgments

The financial help of the Deanship of Academic Research, University of Jordan, and the Jordanian Uranium Mining Company (JUMCO) is highly appreciated. Special thanks are due to Dr. Samer Kahook and Dr. Hussein Allaboun from JUMCO for their support during the progress of the present work.

References

[1] Abed, A. and Al- Eisawi, D. (1994). The geobotanical exploration for Copper and Manganese in north- eastern Wadi Araba, Jordan. Dirasat, 21 (3): 189- 201.

[2] Abed, A., Sadaqah, R., & Al Kuisi, M. (2008).Uranium and potentially toxic metals during the mining, beneficiation, and processing of phosphorite and their effects on ground water in Jordan. MINE WATER ENVIRON , 27(3), 171–182. DOI:10.1007/s10230-008-0039-3.

[3] Agency for Toxic Substances and Disease Registry (2005). Toxicological profile for Arsenic (Draft for public comment). Atlanta, GA: U. S. Department of public health and human services, Public health service.

[4] Al- Eisawi, D. M. (1996). Vegetation of Jordan. Book published By UNESCO (ROSTAS), Cairo Office. Cairo. pp. 284.

[5] Al- Eisawi, D. M. (1998). The field guide to wild flowers of Jordan and neighboring countries. Press foundation Al- Rai, pp 296.

[6] Barjous, M. (1986). The Geology of Siwaqa, Bull. 4, NRA, Amman–Jordan.

[7] Bender, F. (1968). Geologie von Jordanian. Beitrage zur Regionalen Geologie der Erde, Band 7. Borntraeger, Berlin.

[8] Blake, G., and Ionides, M. (1939). Report on the Water Resources of Transjodan and their Development. Crown Agents for Colonies, London.

[9] Buck, E. C., Brown, N. R. and Dietz, N. L. (1996). Contaminant uranium phases and leaching at the Fernald site in Ohio. Environ. Sci. Technol., 30:81–88. DOI: 10.1021/es9500825.

[10] Burdon, D. (1959). Handbook of the Geology of Jordan. Benham and Company Ltd., Colchester.

[11] Bzour, A. F., Khoury, H. N. and Oran, S. A. (2016). Assessment of Bioavailability of Chromium (Cr), Vanadium (V) and Uranium (U) in Wild Plants in Siwaqa Area, Central Jordan. International Journal of Current Research of Biosciences and plant Biology, 3(12),84- 94. doi: http://dx.doi.org/10.20546/ijcrbp.2016.312.010.

[12] Chen, S. B., Zhu, Y. G. and Hu, Q. H. (2005). Soil to plant transfer of 238U, 226Ra and 232Th on a uranium mining-impacted soil from southeastern China. J. Environ. Radioactivity, 82:223–236.

[13] Djingova, R. and Kuleff, I. (2000). Instrumental techniques for trace analysis. In: Trace elements: Their distribution and effects in the environment. Vernet, J. P. (ed.). Elsevier science Ltd., United Kingdom, pp. 146.

[14] Elie, M., Techer, I., Trotignon, L., Khoury, H., Salameh, E., Vandamme,D., Boulvais, P. and Fourcade, S. (2007): Cementationof kerogen-rich marls by alkaline fluids released during weathering of thermally metamorphosed marly sediments. Part II: Organic matter evolution, magnetic susceptibility and metals (Ti, Cr, Fe) at the Khushaym Matruck natural analogue (central Jordan). Applied Geochemistry, 22, 1311-1328. DOI.org/10.1016/j.apgeochem.2007.02.013

[15] Feinbrun, N. (1986). Flora Palaestina. Vol. III, IV. The Israel Academy of Sciences and Humanities. Jerusalem.

[16] Fourcade, S., Trotignon, L., Boulvais, P., Techer, I., Elie, M., Vandamme, D., Salameh, E., and Khoury, H. (2007): Cementation of kerogen-rich marls by alkaline fluids released during weathering of thermally metamorphosed marly sediments. Part I: Isotopic (C, O) study of the Khushaym Matruk natural analogue (central Jordan). Applied Geochemistry, 22, 1293-1310.

[17] Jaser, D. 1986. The geology of Khan Ez Zabib, Bull; Amman, Jordan,NRA, 3 p.

[18] Khoury, H. 2006. Industrial rocks and minerals in Jordan, second edition, Publications of the University of Jordan

[19] Khoury, H. and Nassir, S. (1982). A discussion on the origin of Daba – Siwaqa marble, Dirasat., 9, 55–56.

[20] Khoury, H., Mackenzie, R., Russell, J. and Tait, J. 1984. An iron-free volkonskoite, Clay Minerals, 19, 43–57.

[21] Khoury, H. N. and Abu-Jayyab, A. 1995. A short note on the mineral volkonskoite, Dirasat., 1, 189–198.

[22] Khoury, H. 2006. Industrial rocks and minerals in Jordan, second edition, Publications of the University of Jordan

[23] Khoury, H. N. (2012). Long-term analogue of carbonation in Travertine from Uleimat Quarries, Central Jordan, Environ Earth Sci , 65, 1906–1916. DOI: 10.1007/s12665-011-1173-y.

[24] Khoury, H., Salameh, E. and Clark, I. (2014). Mineralogy and origin of surficial uranium deposits hosted in travertine and calcrete from central Jordan. Applied Geochemistry, 43: 49- 65. DOI: 10.1016/j.apgeochem.2014.02.005.

[25] Khoury, H. (2014). Geochemistry of surficial uranium deposits from central Jordan. Jordan Journal of Earth and Environmental Sciences (JJEES), (6): 3, 11- 22.

[26] Khoury, H. N. (2015). Uranium Minerals of Central Jordan. Applied Earth Science (Trans. Inst. Min. Metall. B), 124 (2), 104-128. DOI: 10.1179/1743275815Y.0000000005.

[27] Khoury, H., Sokol, E. and Clark, I. (2015). Calcium uranium oxides from central Jordan: associations, chemistry, and alteration products, Canadian Mineralogist. 53, 61-82.

[28] Khoury, H., Kokh, S., Sokol, E., Likhacheva, A. Seryotkin, Y., Belogub, E. (2016): Ba- and Sr-mineralization of fossil fish bones from metamorphosed Belqa Group sediments, central Jordan, Arabian Journal of Geosciences, 9:461. DOI 10.1007/s12517-016-2503-x.

[29] Levy, D. B., Barbarick, K. A., Siemer, E. G. and Sommers, L. E. (1992). "Distribution and partitioning of trace metals in contaminated soils near Leadville, Colorado," J. Environ. Qual. , 21(2): 185–195. DOI:10.2134/jeq1992.00472425002100020006x..

[30] Nassir, S., and Khoury, H. N., (1982): Geology, Mineralogy and Petrology of Daba marble, Jordan. Dirasat, 9 (1), 107-140.

[31] Oran, S. A., and Abu Zahra, H. (2014). Impact of the cement dust emitted from the south cement factory in Tafila/ Jordan on plant diversity of the surrounding area. Int J Biodivers Conserv 6 (5): 400-414. DOI: 10.5897/IJBC2014.0694.

[32] Oran, S. A. and Al-Zo'ubi, E. 2016. The Impact of the Emitted Dust from Zarka (Jordan) Petroleum Refinery on Plant Biodiversity, Int. J. Curr. Res. Biosci. Plant Biol., 3(6): 1-13. DOI: 10.20546/ijcrbp.2016.306.001.

[33] Pendias AK, Pendias H. Trace elements in Soils and Plants. 3. FL, United States: CRC press; 2000. pp. 10–11.

[34] Pierzynski, G. M., Sims, J. T., and Vance, G. F. (2000). Soils and Environmental Quality, CRC Press, London, UK, 2nd edition.

[35] Powell, J. H. (1989). Stratigraphy and Sedimentology of the Phanerozoic Rocks in Central and Southern Jordan. Bull. 11, Geology Directorate, Natural Resources Authority (Ministry of Energy and Mineral resources) Amman, Part B: Kurnub, Ajlun and Belqa Group, 161P.

[36] Powell, J. H., Moh'd, B. K. (2011). Evolution of Cretaceous to Eocene alluvial and carbonate platform sequences in central and south Jordan. GeoArabia 16 (4): 29–82.

[37] Quennel, A. (1956). The structural and geomorphic evaluation of the Dead Sea Rift. Quart. J. Geol. Sci. Lond., 64, 1–24.

[38] Sheppard, M. I. and Sheppard, S. C. (1985). The plant concentration ratio concept as applied to natural U. Health Phys., 48: 494–500.

[39] Shiowatana, J., McLaren, R., Chanmekha, N., and Samphao, A. (2001). "Fractionation of arsenic in soil by a continuous-flow sequential extraction method," J. Environ. Qual. 30 (6): 1940–1949. DOI: 10.2134/jeq2001.1940.

[40] Tomé, V., Rodrigues, P. and Lozano, J. (2002). Distribution and mobilization of U, Th and 226Ra in the plant- soil compartments of a mineralized uranium area in South- west Spain. J. Environ. Radioactivity, 59: 223- 243. DOI: 10.1016/S0265-931X(01)00035-2.

[41] Techer, I., Khoury, H., Salameh, E., Rassineux, F., Claude, C., Clauer, N., Pagel, M., Lancelot, J., Hamelin, B., and Jacquot, E,. (2006). Propagation of high-alkaline fluids in an argillaceous formation: Case study of the Khushaym Matruk natural analogue (Central Jordan). Jour. Of Geoch. Exploration, 90, 53-67.

[42] Wilson, B. PyattB. (2007). Heavy metal dispersion, persistence and bioaccumulation around an ancient copper mine situated Anglesey, UK. Ecotoxicol Environ Saf., 66 :224- 231. DOI:10.1016/j.ecoenv.2006.02.015.

[43] Whicker, F.W., Hinton, T.G., Orlandini, K.A. and Clark, S.B., (1999). Uptake of natural and anthropogenic actinides in vegetable crops grown on a contaminated lake bed. J. Environ. Radioactivity, 45: 1-12. DOI: 10.1016/S0265-931X(98)00076-9.

[44] World Health Organization WHO. (2007). Joint FAO/WHO Expert standards program codex Alimentation Commission. Geneva, Switzerland. Available, onlinehttp://www.who.int[Accessed 10/09/2012].

[45] Yanagisawa, K., Muramatsu, Y. and Kamada, H., (1992). Tracer experiments on the transfer of technetium from soil to rice and wheat plants. Radioisotopes, 41: 397- 402. DOI: 10.3769/radioisotopes.41.8_397.

[46] Zohary, M. (1966). Flora Palaestina. Vol. I, II, III. The Israel Academy of Sciences and Humanities. Jerusalem.

المملكة الأردنية الهاشمية

صندوق دعم البحث العلمي

الجامعة الهاشمية

المجلة الأردنية
لعلوم الأرض والبيئة

JJEES

مجلة علمية عالمية محكمة

المجلد (٨) العدد (١)

http:// jjees.hu.edu.jo/

ISSN 1995-6681

المجلة الأردنية لعلوم الأرض والبيئة

مجلة علمية عالمية محكمة

المجلة الأردنية لعلوم الأرض والبيئة: مجلة علمية عالمية محكمة ومفهرسة ومصنفة، تصدر عن عمادة البحث العلمي في الجامعة الهاشمية وبدعم من صندوق البحث العلمي - وزارة التعليم العالي والبحث العلمي، الأردن.

هيئة التحرير:

رئيس التحرير:

- الأستاذ الدكتور عيسى مخلوف

الجامعة الهاشمية، الزرقاء، الأردن.

مساعد رئيس التحرير

- الأستاذ الدكتور نزار الحموري

الجامعة الهاشمية، الزرقاء، الأردن.

الأعضاء:

- الأستاذ الدكتور نجيب أبو كركي
الجامعة الأردنية

- الأستاذ الدكتور عاطف خرابشة
جامعة البلقاء التطبيقية

- الأستاذ الدكتور نزار أبو جابر
الجامعة الأردنية الألمانية

- الأستاذ الدكتور خالد الطراونة
جامعة الحسين بن طلال

- الأستاذ الدكتور محمد عطاالله
جامعة اليرموك

- الأستاذ الدكتور فايز أحمد
الجامعة الهاشمية

- الأستاذ الدكتور أنور جريس
جامعة مؤته

- الأستاذ الدكتور عبدالله ذيابات
جامعة آل البيت

فريق الدعم:

المحرر اللغوي

- الدكتور قصي الذبيان

تنفيذ وإخراج

- عبادة الصمادي

ترسل البحوث إلكترونيا إلى البريد الإلكتروني التالي:

رئيس تحرير المجلة الأردنية لعلوم الأرض والبيئة

jjees@hu.edu.jo

لمزيد من المعلومات والأعداد السابقة يرجى زيارة موقع المجلة على شبكة الانترنت على الرابط التالي:

www.jjees.hu.edu.jo

المملكة الأردنية الهاشمية

صندوق دعم البحث العلمي

الجامعة الهاشمية

المجلة الأردنية لعلوم الأرض والبيئة

JJEES

مجلة علمية عالمية محكمة

تصدر بدعم من صندوق دعم البحث العلمي

http://jjees.hu.edu.jo/

المجلد (٨) العدد (١)

ISSN 1995-6681

أيلول ٢٠١٧ / ذو الحجة ١٤٣٨